# Role of R-loops in chemotherapy-induced cell death in acute myeloid leukemia

Dissertation

zur Erlangung des Grades

Doktor der Naturwissenschaften

Am Fachbereich Biologie

der Johannes-Gutenberg-Universität Mainz

vorgelegt von

Moufida Taileb

geb. am 02.05.1989 in Annaba, Algerien

Mainz, 2025

Dekan:

1. Berichterstatter:

2. Berichterstatter:

Tag der mündlichen Prüfung: 07.08.2025

# Table of Contents

# Abbreviations

**Table 1: List of abbreviations**

| Abbreviation | Full Form |
|---|---|
| 53BP1 | p53 Binding Protein 1 |
| RPA | Replication Protein A |
| 7-AAD | 7-Aminoactinomycin D |
| A. dest | Distilled Water |
| NHEJ | Non-Homologous End Joining |
| AML | Acute Myeloid Leukemia |
| APS | Ammonium Persulfate |
| ATCC | American Type Culture Collection |
| BLISS | Bliss Independence Model |
| BM | Bone Marrow |
| BSA | Bovine Serum Albumin |
| COSMIC | Catalogue of Somatic Mutation in Cancer |
| DAPI | 4',6-Diamidino-2-Phenylindole |
| DMSO | Dimethylsulfoxide |
| DNA | Desoxyribonucleic Acid |
| DSB | Double Strand Break |
| DSMZ | German Cancer Cell Line Depository |
| ECL | Enhanced Chemiluminescence |
| EDTA | Ethylenediaminetetraacetic Acid |
| FLT3 | FMS-like Tyrosine Kinase 3 |
| FSC | Forward Scatter |
| g | Gram |

| | |
|---|---|
| HPC | Hematopoietic Progenitor Cell |
| HR | Homology-Based Recombination |
| hr | Hour |
| HSC | Hematopoietic Stem Cell |
| L-Glu | L-Glutamine |
| min | Minute |
| MTT | 3-(4,5-Dimethylthiazol-2-yl)-2,5-Diphenyltetrazolium Bromide |
| NPM1 | Nucleophosmin |
| p53depl | Depleted p53 |
| p53wt | Wild-Type p53 |
| PAGE | Polyacrylamide Gel Electrophoresis |
| PBS | Phosphate-Buffered Saline |
| PBST | PBS-Tween20 |
| PFA | Paraformaldehyde |
| pH | Potentia Hydrogenii |
| rpm | Rounds Per Minute |
| RT | Room Temperature |
| SDS | Sodium Dodecyl Sulfate |
| SSB | Single Strand Break |
| SSC | Side Scatter |
| TEMED | N,N,N',N'-Tetramethylethane-1,2-Diamine |
| Tris | Tris(Hydroxymethyl)Aminomethane |

| | |
|---|---|
| UV | Ultraviolet |
| ZIP | Zero Interaction Potency |
| γH2AX/gH2AX | Phospho-Histone 2AX |
| WHO | World Health Organization |
| ELN | European Leukemia Network |

# Summary

Acute myeloid leukemia (AML) is a clonal disorder of hematopoietic progenitor cells, characterized by excessive proliferation and aberrant self-renewal. Young AML patients are treated with the same induction therapy consisting of cytarabine (ARA-C) and daunorubicin (DNR), irrespective of the genetic background or expected long-term outcome. Identifying better biomarkers is crucial for stratifying patients into standard or experimental treatment approaches. To investigate the biological behavior of AML cells, we analyzed three AML cell lines (HL60, MOLM13 and OCI-AML3) upon treatment with ARA-C and DNR. We assessed proliferation, apoptosis, DNA damage and R-loop formation. Moreover, RNA-seq was performed to examine the expression of genes involved in R-loop regulation. Finally, we blocked the induction of R loop formation by overexpression of RNAseH1 to explore the role of R loops in treatment sensitivity. Our findings revealed differential drug sensitivity among the cell lines. HL60 cells exhibited the highest sensitivity to ARA-C, whereas MOLM13 cells responded best to DNR. DNA damage analysis, measured by *yH2AX* foci, revealed that DNR-induced DNA damage was lower in HL60 cells compared to MOLM13. Conversely, ARA-C treatment resulted in higher levels of *yH2AX* foci in HL60 than in MOLM13 cells. Co-localization studies with *RAD51* and *53BP1* foci indicated preferential activation of specific DNA repair pathways in response to damage. Furthermore, we quantified R-loop formation before and after DNR exposure. R-loop levels increased in MOLM13 but not HL60 cells, correlating with their sensitivity to DNR. Similarly, ARA-C treatment led to elevated R-loop formation in HL60 cells. Interestingly, RNA-seq analysis demonstrated downregulation of genes involved in R-loop prevention and removal upon treatment. The persistence of R-loops following genotoxic stress may induce replication stress and DNA damage, suggesting a potential link between R-loop accumulation and drug sensitivity. To validate this hypothesis, we utilized inducible RNAseH1 overexpression models, including wild type (WT), catalytically inactive (D210N), and catalytically inactive/mutant hybrid-binding domain (WKKD). Overexpression of RNAseH1 WT conferred increased resistance to chemotherapy, supporting the hypothesis that R-loop accumulation contributes to therapy-induced cell death. These findings provide new insights into the role of R-loops in AML chemotherapy response and suggest a potential therapeutic strategies targeting R-loop metabolism to improve AML therapy.

# Zusammenfassung

Die akute myeloischen Leukämie (AML) ist eine klonale Erkrankung der hämatopoetischen Vorläuferzellen, die durch unkontrollierte Proliferation und Selbsterneuerung charakterisiert ist. Junge AML-Patienten werden unabhängig vom genetischen Hintergrund der Leukämie oder der zu erwartenden Langzeitprognose mit der gleichen Induktionstherapie bestehend aus Cytarabin (ARA-C) und Daunorubicin (DNR) behandelt. Daher ist die Identifizierung von präziseren Biomarkern entscheidend, um Patienten für standardisierte oder experimentelle Behandlungsansätze stratifizieren zu können.

Um das biologische Verhalten von AML-Zellen zu untersuchen, analysierten wir drei AML-Zelllinien (HL60, MOLM13 und OCI-AML3) nach der Behandlung mit ARA-C und DNR. Wir untersuchten Proliferation, Apoptose, DNA-Schäden und die Bildung von R-loops. Darüber hinaus wurde eine RNA-Seq Analyse durchgeführt, um die Expression von Genen, die an der Regulation von R-loops beteiligt sind, zu ermitteln. Abschließend blockierten wir die Induktion der R-loop-Bildung durch Überexpression von RNAseH1, um die Rolle von R-loops bei der Behandlungssensitivität zu untersuchen.

Unsere Ergebnisse zeigten eine unterschiedliche Sensitivität der Zelllinien gegenüber der Behandlung. HL60-Zellen wiesen die höchste Empfindlichkeit gegenüber ARA-C auf, während MOLM13-Zellen am stärksten auf DNR ansprachen. Die Analyse der DNA-Schäden, die anhand von γH2AX-Foci bestimmt wurden, ergab, dass die DNR-induzierten DNA-Schäden in HL60-Zellen geringer waren als in MOLM13. Im Gegensatz dazu führte die Behandlung mit ARA-C in HL60-Zellen zu einer höheren Anzahl von γH2AX-Foci als in MOLM13-Zellen. Ko-Lokalisierungsexperimenten mit RAD51- und 53BP1-Foci deuteten auf eine bevorzugte Aktivierung spezifischer DNA-Reparaturwege als Reaktion auf eine Schädigung hin.

Darüber hinaus haben wir die Bildung von R-Loops vor und nach DNR-Exposition quantifiziert. Die R-Loop-Konzentration stieg in MOLM13-Zellen, jedoch nicht in HL60-Zellen an, was mit ihrer Sensitivität gegenüber DNR korreliert. In ähnlicher Weise führte die Behandlung mit ARA-C in HL60-Zellen zu einer erhöhten R-loop-Bildung. Interessanterweise zeigte die RNA-Seq-Analyse, dass die Expression von Genen, die an der Vermeidung und Entfernung von R-loops beteiligt sind, nach der Behandlung negativ reguliert wurden. Die Persistenz von R-loops nach genotoxischem

Stress könnte zu Replikationsstress und DNA-Schäden führen, was auf einen möglichen Zusammenhang zwischen der Akkumulation von R-loops und der Sensitivität gegenüber der Behandlung hindeutet. Um diese Hypothese zu überprüfen, verwendeten wir induzierbare RNAseH1-Überexpressionsmodelle, einschließlich einer Wildtyp (WT)-, einer katalytisch inaktiven (D210N) und einer katalytisch inaktiven/mutierten Hybrid-Bindungsdomäne (WKKD) Variante. Die Überexpression von RNAseH1 WT führte zu einer erhöhten Resistenz gegenüber Chemotherapie. Dies stützt unsere Hypothese, dass die Anhäufung von R-Loops zum therapieinduzierten Zelltod beiträgt.

Diese Ergebnisse liefern neue Erkenntnisse über die Rolle von R-loops beim Ansprechen auf eine AML-Chemotherapie und weisen auf potenzielle therapeutische Strategien hin, die auf den R-loop-Stoffwechsel abzielen, um die AML-Therapie zu verbessern.

# Aim of the project

The aim of this project is to investigate the role of R-loops in DNA damage response and drug sensitivity in acute myeloid leukemia (AML) cell lines. This study seeks to identify novel biomarkers, specifically focusing on R-loops, to predict patient responses to treatment. Additionally, the project aims to uncover new drug targets that can enhance cell death, potentially improving therapeutic strategies for AML.

# 1 Introduction

## 1.1 **Acute** myeloid leukemia

Acute myeloid leukemia (AML) is a disease of hematopoietic stem cells residing in the bone marrow. It is caused by genetic alterations in precursors of blood cells that lead to an excess of neoplastic clonal myeloid stem cells and results in increased proliferation, an arrest in differentiation and unlimited self-renewal[1].

AML is a heterogeneous disease characterized by various molecular abnormalities, which significantly influence its pathogenesis and prognosis. Currently, AML prognosis is stratified by co-existing chromosomal and genetic abnormalities[2], [3].

### 1.1.1 Mutations in AML and its impact on the treatment:

AML is a highly heterogeneous disease. While it can be classified into favorable, intermediate, and adverse-risk groups based on cytogenetic characteristics, outcomes within these categories can differ significantly. The discovery of recurrent genetic mutations, such as fms-like tyrosine kinase 3 (*FLT3)* internal tandem duplications *(ITD)* and in nucleophosmin 1 (*NPM1)*, has improved the ability to predict individual prognosis and tailor treatment strategies. The primary treatment approach continues to involve cytarabine- and anthracycline-based (such as daunorubicin) chemotherapy, with allogeneic stem cell transplantation as an option for eligible patients[4]. In this thesis, three different AML cell lines, MOLM13, OCI-AML3 and HL60 cell lines, expressing one of the above mentioned mutations, in addition to depletion of *TP53*, respectively, have been used.

AML classification considers genetic mutations such as *FLT3*, *NPM1*, and *TP53* to assess prognosis. Table 2 summarizes the impact of these mutations on AML risk categories[5]. *FLT3* mutations, particularly *FLT3-ITD*, are among the most common mutated oncogene in AML. These mutations are associated with a poor prognosis due to their role in promoting leukemic cell proliferation and resistance to apoptotic cell death[6], [7]. *NPM1* mutations are the most common genetic alteration and are found in about one-third of cases of AML that are diagnosed recently. With the 2022 World Health Organization (WHO 2022) and European Leukemia Network (ELN 2022) classification of myeloid neoplasms requiring >10 percent of

leukemic blasts for diagnosis, *NPM1*-mutated AML (*NPM1*$^{mut-}$AML) has been reclassified as a separate entity. *NPM1* mutation is commonly associated with other mutations, e.g. *FLT3-ITDs*[8], [9].

***Table 2: AML risk stratification by genetics. Modified from** [5].*

| Risk Category | Genetic Mutations | Notes |
|---|---|---|
| **Favorable** | - Mutated *NPM1* without *FLT3-ITD*<br>- Biallelic mutated *CEBPA* | Associated with good prognosis. |
| **Intermediate** | - Mutated *NPM1* with *FLT3-ITD* (low allelic ratio)<br>- Wild-type *NPM1* without *FLT3-ITD* or with *FLT3-ITD* (low allelic ratio) | Represents a standard risk profile. |
| **Adverse** | - *TP53* mutations<br>- *FLT3-ITD* (high allelic ratio)<br>- Complex karyotype | Linked to poor outcomes. |

Alterations in *TP53,* a tumor suppressor gene, are typically linked to unfavorable outcomes. Approximately 5–10% of patients with de novo AML have *TP53* mutations; these mutations are more common in older patients and those with therapy-related AML. The management of *TP53*-mutated AML is particularly difficult because it correlates with complex karyotypes and resistance to both traditional and innovative treatments[10]. In addition to being mutated, *TP53* gene can also be depleted in primary AML cells and cell lines such as HL60 (one of the cell lines studied in this thesis)[11].

In a recent study, Ali et al. classified AML patients based on the presence or absence of specific mutations in the above-mentioned genes (Figure1). This approach allowed for a more comprehensive characterization of the genetic landscape in AML patients, providing valuable insights into how these mutations influence disease progression, prognosis, and treatment response. By grouping patients according to their mutational profiles, the study was able to

identify distinct AML subtypes with varying clinical outcomes[12]. The study emphasized that incorporating genetic profiling into AML classification, enhances risk stratification and allows for more personalized treatment approaches.

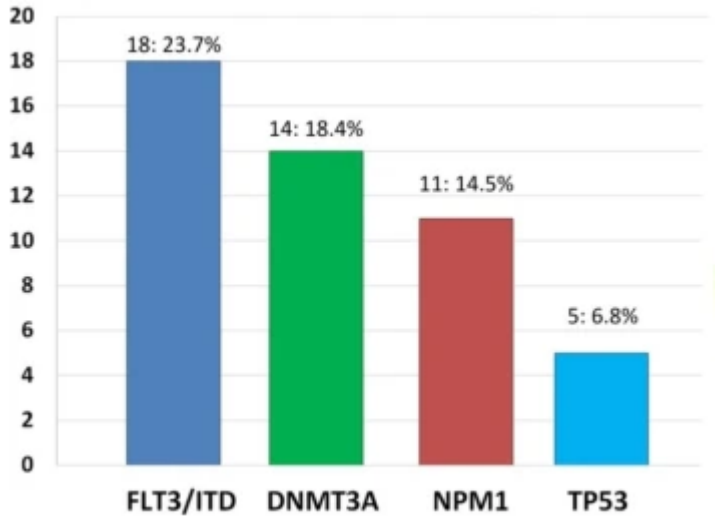


**Figure 1: Prevalence and distribution of AML patient subtypes.**

Estimated allelic frequencies of FLT3, DNMT3A, NPM1, and TP53 variants in a subset of de novo acute myeloid leukemia samples. Numbers preceding the percentages represent the number of patients in this study. Modified from[12].

### 1.1.2 Current AML treatment

AML is no longer considered as a single disease but rather as a collection of distinct subtypes, each defined by unique pathophysiological, clinical, cytogenetic, and molecular characteristics. These diverse AML sub-types respond to specific therapeutic approaches and exhibit significantly varied outcomes[13].

Since cytarabine (ARA-C) and anthracyclines (such as idarubicin or daunorubicin (DNR)) were identified as effective agents in AML, and their combination of both drugs in the 1970s (known as the 3+7 regimen; three days of an anthracyline plus seven days of ARA-C), it has remained the standard induction therapy. This regimen achieved long-term cure rates in 30–40% in younger AML patients[14], [15]. This regimen, referred to as induction therapy, is designed to achieve complete remission (CR), defined as less than 5% blasts in the bone marrow. Approximately 60–80% of patients with newly diagnosed AML attain CR following induction

treatment. However, if remission is not achieved, a second high-dose ARA-C and anthracycline is usually administered as a subsequent treatment approach. The optimal dose of DNR remains uncertain[4], [16][17]. Previous studies have shown conflicting results regarding the effectiveness of high versus low doses of DNR in induction chemotherapy for newly diagnosed AML[18].

## 1.2 DNA damage response

In this project, AML cell lines were treated with two widely used chemotherapeutic agents, ARA-C and DNR. These drugs are commonly employed in the standard treatment regimen for AML due to their potent cytotoxic effects on rapidly dividing cancer cells, which results in the accumulation of DNA double-strand breaks (DSBs), which are highly detrimental to cell survival[19], [20]. This study aims to assess the extent of DNA damage induced by these drugs and evaluate the cellular responses, including DNA repair mechanisms. In this study, three distinct DNA repair genes were analyzed to gain insight into the specific repair mechanisms utilized by the cells in response to DNA damage. These genes are as follow: *53BP1*, *RAD51* and *RPA*, they play a role in non-homologues-end-joining (NHEJ) and homologues recombination (HR) repair pathways, respectively[21], [22], [23]. DNA repair pathways play a crucial role in maintaining genomic stability by detecting and correcting damage caused by environmental stressors, chemotherapeutic agents, or intrinsic cellular processes. Understanding the involvement of these repair genes can provide valuable information about the cell's ability to recover from genotoxic stress and may also contribute to developing targeted therapeutic strategies that exploit DNA repair deficiencies in cancer treatment.

The accurate detection and repair of DNA damage are crucial for maintaining genome stability. Various DNA lesions can obstruct replication fork progression, leading to fork collapse and the formation of DSBs, which disrupt the genome's physical continuity[24], [25]. The mechanism of DNA repair involves several mechanisms two of which are mentioned in this study (NHEJ) and (HR) (Figure 2). The first repair mechanism that comes into action after DSBs is classical NHEJ (C-NHEJ), which repairs DSBs by directly ligating blunt DNA ends without the need for sequence homology. This process relies on several key proteins, including Ku70/80 and DNA-PKcs. While C-NHEJ operates throughout the cell cycle, it is most prevalent during the G0/G1 and G2 phases[24], [26][27].

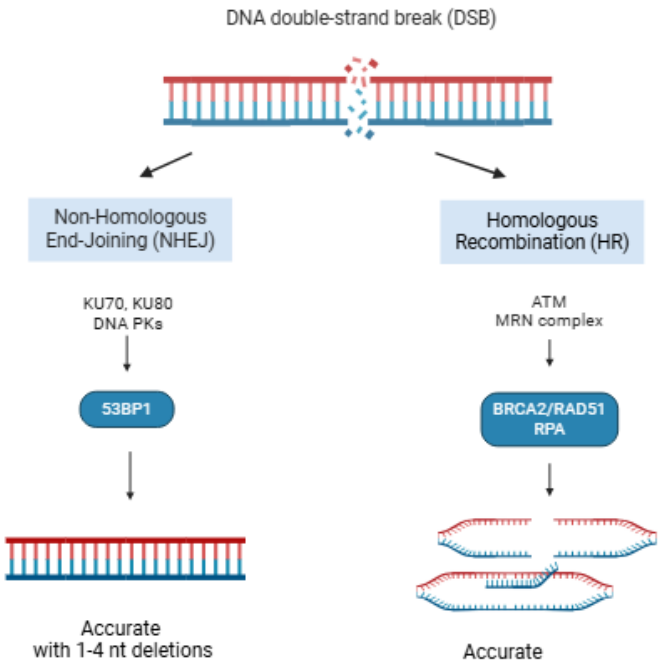


**Figure 2: Pathways for repairing DNA double-strand breaks (DSBs).**

The repair of DNA double-strand breaks (DSBs) largely depends on whether DNA end resection is initiated. If resection is inhibited, NHEJ pathway is preferred. Conversely, when DNA end resection occurs, HR pathway is activated. Modified from*[24]*. Created in BioRender.com

Alternatively, the ends of a DSB can undergo resection**,** generating 3' single-stranded DNA (ssDNA) overhangs**.** The resected DSB can then be repaired through various mechanisms such as HR being predominant during mid-S and mid-G2 phases of the cell cycle, when DNA replication is most active and a sister chromatid is available as a repair template[24], [26]. Since HR utilizes a homologous or sister chromatid**,** it requires strand invasion facilitated by the recombinase *RAD51***,** making the process largely error-free[24], [28]**.** In contrast, C-NHEJ repairs DSBs without the need for an intact DNA template. As a result, it is primarily active during the G1 phase, as already mentioned, of the cell cycle, when a homologous DNA template is unavailable [24].

## 1.3 R-**loops** in AML

### 1.3.1 R-loop formation and distribution

R-loops are known as three stranded nucleic acid structure of RNA:DNA hybrids with a displaced non-template DNA strand. These structures are known to be mainly formed during replication and transcription[29], [30], [31]. R-loops have been linked to ongoing transcription, but not exclusively, until recent studies suggested that R-loops can be considered as transcription by-products mainly in *cis* at the site of transcription[32]. It has also been shown in recent studies that effective formation of co-transcriptional R-loops depends on the presence of a free RNA-end and a GC skew, which can be referred to the asymmetric distribution of guanines and cytosines between the strands[32], [33]. The sequence specific accumulation of R-loops may be due to the thermodynamic stability of GC-rich RNA when binding to its complementary DNA strand[32][34], [35]. This property made RNA:DNA hybrids more stable than dsDNA[36], which may depend on the oligomeric length, the content of deoxypyrimidines/deoxypurines, and the A·T/U proportion[37]. As a result, elimination of an R-loop after its formation may be considered as an energy consuming process[30]. Moreover, R-loops can also form in trans, with *RAD51* being involved, at a distant site of transcription[32], [38]. Interestingly, in humans R-loops are also prevalent at promoter regions containing CpG islands (CpGIs)[32], [39], [40].

Several methodologies to detect RNA:DNA hybrids or R-loops have been established and considered as crucial to understand how R-loops are formed and when and where they are located within the genome. A study using the monoclonal hybrid specific S9.6 antibody to stain RNA:DNA hybrids showed that they form at different loci across the genome[32], [41]. The availability of different methods to detect R-loops led to divergences between studies to show where these hybrids accumulate due to the transient nature of R-loop. This was pointed out when the use of a hybrid sensor, a catalytic inactive version of RnaseH1 or the hybrid binding domain of RNaseH1 tagged to fluorescent protein, showed a nuclear staining of RNA:DNA hybrids[41]. In addition to its presence in the nucleus, R-loops also accumulate in the mitochondrial DNA (mtDNA), these are known as mitochondrial R-loops. This consists of heavy (H) and light (L) strand with different nucleotide composition[42], [43]. High levels of R-loops

lead to mtDNA instability. The accumulation of these pathologic R-loops in mitochondria can be prevented by the mitochondrial degradosome complex[43], [44]. To further study R-loops and localize them, a catalytically inactive RNaseH1 D210N (GFP–dRH) was used to visualize RNA:DNA hybrids through the cell. This was preceded by the knock down (KD) of two genes, *SETX* and *BRCA1*, that are known to affect R-loop levels by removal or prevention, respectively. This KD resulted in an increased GFP–dRH signal, not only in the nucleus but also in the cytoplasm[45], [46].

### 1.3.2 **Physiological** roles of R-loops

R-loops have been considered as accidental by-products and harmful to cellular physiology as well as source of genomic instability if they are not removed properly[32][29], [30]. Until recently, a new category of R-loops was identified known as regulatory R-loops, which play a crucial role in multiple physiological processes[32] (Figure 3).

#### **1.3.2.1 Chromatin accessibility** and transcription

It has been proven that regulatory R-loops are involved in chromatin and gene regulation by activating and silencing gene expression[32], [47]. Some genome-wide studies identified R-loops at 3' ends, which align with a well-established role of R-loops in promoting transcription termination by stalling RNA polymerase II (RNAP II)[32], [48], [49].

#### **1.3.2.2** DNA **damage** response and repair

Genome integrity is protected not only through the timely resolution of R-loops but also through the involvement of R-loops and RNA–DNA hybrids in DNA damage signaling and repair. R-loops contribute to DNA damage by stalling replication forks or facilitating the formation of DSBs, thereby activating the ATR and ATM protein kinases that coordinate the DNA damage response (DDR)[50], [51], [52]. Furthermore, similar to class switch recombination, R-loops function as intermediates in DNA repair by triggering a non-canonical ATM-induced DNA DDR, along with the backward translocation of RNAPII, which facilitates repair accessibility, even without the presence of DSBs[50], [53]. For instance, ssDNA binding proteins *RPA* and *RAD51* can facilitate the R-loop-induced DNA repair[50], [54].

### 1.3.2.3 Telomere and centromere maintenance

Centromeres are transcribed by RNAPII in long non-coding RNA, also known as Cen RNA, in a cell dependent manner at low levels[55], [56]. They can be found as single, double stranded or RNA:DNA hybrids at centromere ( Cen R-loops)[57], [58][59]. Cen R-loops facilitate the interaction of microtubules with the kinetochore during cell division, which is considered as the main function of centromeres, by recruiting RPA and ATP dependent activation of Aurora B[32], [60].

R-loops also from when telomeres are transcribed into telomere repeat-containing RNA (TERRA) either in *cis* or in *trans*. This formation promotes telomere maintenance by driving DNA repair. *TERRA* hybrids are removed by RNaseH during S phase to avoid replication conflicts[32], [50].

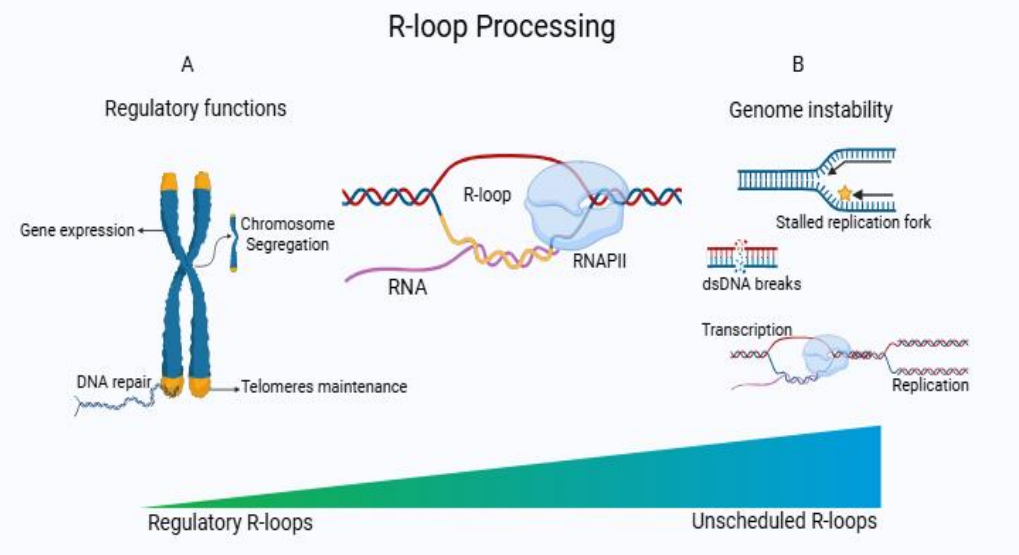


**Figure 3: Functions of regulatory and unscheduled R-loops.**

(A) Functions of regulatory R-loops: R-loops can recruit transcription factors or chromatin remodelers, change the histone/DNA methylation status, or form at promoters and transcription termination sites. By triggering the DNA damage response, enlisting repair-facilitating protein factors, or serving as repair intermediaries, R-loops encourage DNA repair. R-loops can promote chromosome segregation. Telomere repeat-containing RNA (TERRA), a G-rich repetitive long non-coding RNA with the tendency to form R-loops and essential for telomere maintenance, is produced when telomeres are transcribed. (B) Functions of unscheduled R-loops: R-loops, if left unresolved, can be processed into single-strand or double-strand breaks and contribute to genome instability. Replication forks are stalled which creates favorable conditions for R-loop constant formation/accumulation and DNA damage. Modified from[32], [50]

### 1.3.3 R-loops **involvement** in genomic instability

The exact ways in which R-loops contribute to DNA damage and genome instability remain under intense investigation, with various mechanisms being potentially involved depending on the context in which the R-loops or hybrids are formed.

R-loops are known to be beneficial in multiple physiological roles, as mentioned above. However the accumulation of these hybrids gives rise to the so-called unscheduled R-loops, which may be harmful to cells by causing DNA damage and ultimately genome instability[32], [61].

Normally, R-loops are prevented or removed promptly by several factors, including TOP1, SRSF1 or DDX9, DDX1, RNaseH1, respectively. A reason that can lead to R-loops accumulation and there conversion into unscheduled R-loops is the absence of one or more of R-loops regulating factors (Figure 4). R-loop accumulation was linked to replication stress and DNA damage as form of genome instability[32].

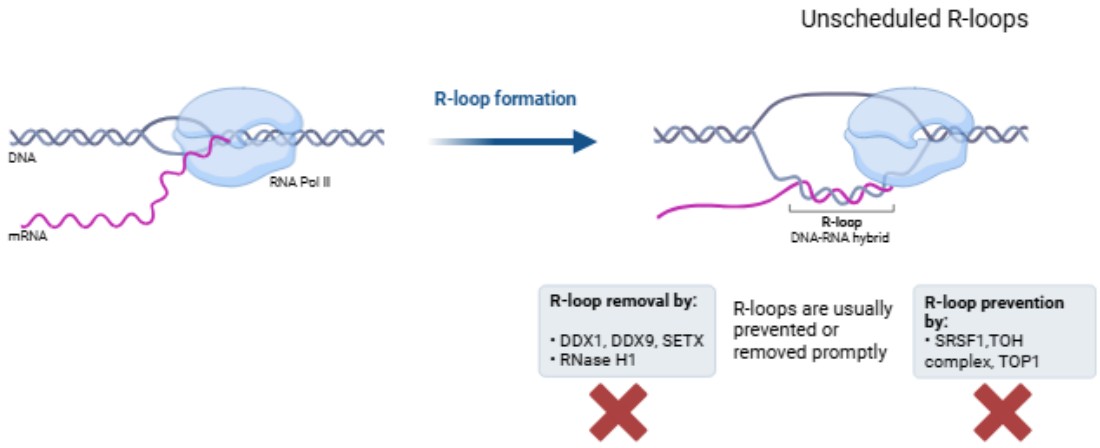


**Figure 4: A model of unscheduled R-loop formation.** R-loops are prevented or immediately removed, when formed, under the control of several factor as depicted. The absence of these factors leads to constant formation of R-loops and eventually accumulation, which can be harmful to the cell by causing DNA damage and replication stress. Modified from[32]. Created in BioRender.com

#### 1.3.3.1 The replication Stress response

In S phase, replication forks can encounter R-loops, resulting in replication stress and DNA damage. While there are mechanisms that separate transcription and replication both spatially and temporally, conflicts between these processes may still occur occasionally, as

they share the same DNA template[62], [63],[29],[64]. Several studies highlighting the influence of R-loops on replication stress responses support the idea that R-loops contribute to replication stress and genome instability[61], [65]. For this reason, R-loop formation is regulated by several DNA and RNA factors. Any dysfunction in these factors may result in R-loop accumulation and eventually cause replication stress[31].

#### 1.3.3.2 Replication fork stalling

The challenges associated with replication progression through transcribed chromatin have long been recognized as a source of genome instability. R-loops play a significant role in inducing genome instability in cycling S-G2 cells, primarily by stalling replication fork progression. R-loops, either alone or in conjunction with paused RNA polymerase, may contribute to replication fork blockage, further exacerbating replication stress.

During DNA replication, replication forks encounter various obstacles, and the presence of an R-loop can create a physical barrier, preventing the smooth progression of the replication machinery. This stalling can lead to replication stress, increasing the likelihood of replication fork collapse. If the stalled fork is not properly resolved, it may result in fork breakage[61], [63].

#### 1.3.3.3 DNA breaks

Growing evidence indicates that R-loop-mediated replication fork stalling plays a key role in transcription-replication conflicts and contributes significantly to R-loop-induced DNA damage[50], [61][31]. This may be due to DNA damage check point failure[31] or to the fact that the ssDNA displaced by the RNA:DNA hybrid is more vulnerable to mutagenic DNA damage than dsDNA[30]. Additionally, the exposed ssDNA in R-loops is highly susceptible to cytidine deaminases like APOBEC proteins or AID, which can result in DSBs if not properly resolved[66], [67]. These conflicts between transcription and replication are particularly detrimental to genome stability, as failure to repair DSBs can lead to mutations, chromosomal rearrangements, and genome instability, all of which are linked to cancer and other diseases. Proper regulation of R-loop formation and resolution is therefore essential for maintaining DNA integrity and preventing replication-associated damage.

#### 1.3.3.4 R-loops and cancer

Several studies on R-loops revealed a strong link between these hybrids and genetic and neurodegenerative diseases as well as cancer[30], [31]. In various cancers, R-loops are involved in tumorigenesis by causing DNA damage, genomic instability and alterations of genes expression especially when constantly formed and not regularly removed. This abnormal accumulation was observed in several cancer types including breast cancer and other solid tumors and hematological malignancies[68]. Yet, R-loops are less studied in hematological malignancies, especially AML.

It has been shown that R-loops exhibit a multifaceted interplay with tumor suppressor genes (TSGs) including modulation of their expression. The conversion into unscheduled R-loops when accumulating may lead to impairment or silencing of TSGs. This loss of function can hinder the mechanisms controlling cellular growth and division and eventually contribute to cancer development[68], [69]. Furthermore, oncogenes stimulate cells towards rapid division, which will lead to an increase in transcription activity as well as R-loop formation. The activation of oncogenes by R-loops causes changes in transcriptional activities and thus develop cancer hallmark[68], [70].

Unscheduled R-loops have been linked to cancer in several studied as already mentioned. Yet, what causes this accumulation cannot be linked to one specific factor/gene that regulates R-loops. Thus, exploring which of these factors/ genes is involved in R-loop accumulation can help us to understand the genome dynamics and function and the potential links of R-loops to cancer and more specifically to AML.

# 2 Material

## 2.1 Reagents for cell culture

**Table3: Reagents for cell culture**

| Media and Additives | Manufacturer |
|---|---|
| Dimethylsulfoxide | Sigma-Aldrich Corp. St. Louis, MO, USA |
| Fetal bovine serum (FBS) | Biochrome AG, Merck KGaA, Darmstadt |
| L-Glutamin (200mM) | GE Healthcare, PAA Laboratories GmbH, Pasching, Austria |

## 2.2 Chemicals

**Table 4: Chemicals**

| Chemical | Manufacturer |
|---|---|
| Ammoniumpersulfate (APS) | Sigma-Aldrich Corp., St. Louis, MO, USA |
| Annexin V Apoptosis Detection Kit PE | Invitrogen by Thermo Fisher Scientific, Waltham, MA, USA |
| BD Facst Clean Solution | Becton Dickinson Bioscience, Heidelberg |
| β-Mercaptoethanol | Sigma-Aldrich Corp., St. Louis, MO, USA |
| Bovine Serum Albumin | Sigma-Aldrich Corp., St. Louis, MO, USA |
| Bradford-Solution | BioRad, Munich |
| Cell Proliferation Kit I (MTT) | Roche Diagnsotics GmbH, Mannheim |
| 4',6-diamidino-2-phenylindole (DAPI) | CarlRoth GmbH & Co. KG, Karlsruhe |
| Ethanol | CarlRoth GmbH & Co. KG, Karlsruhe |
| Ethylenediaminetetraacetic acid (EDTA) | CarlRoth GmbH & Co. KG, Karlsruhe |
| FACSFlow™ | Becton Dickinson Bioscience, |

| | |
|---|---|
| | Heidelberg |
| Gelatin | Sigma-Aldrich Corp., St. Louis, MO, USA |
| Glycin | AppliChem GmbH, Darmstadt |
| Hoechst 33342 | Invitrogen, Life Technologies, Carlsbad, CA, USA |
| Hydrochloric acid | CarlRoth GmbH & Co. KG, Karlsruhe |
| Isopropanol | Hedinger Aug. GmbH & Co. KG, Stuttgart |
| Methanol | AppliChem GmbH, Darmstadt |
| N,N,N',N'-Tetramethylethane-1,2-diamine (TEMED) | Sigma-Aldrich Corp. St. Louis, MO, USA |
| PageRuler™ Prestained Protein Ladder | Thermo Scientific Waltham, MA, USA |
| Phosphate buffered saline (PBS) sterile | Sigma-Aldrich Corp. St. Louis, MO, USA |
| Poly-L-Lysine | Sigma-Aldrich Corp. St. Louis, MO, USA |
| Potassium chloride | Merck KGaA, Darmstadt |
| Potassium phospate | Merck KGaA, Darmstadt |
| Powdered milk | CarlRoth GmbH & Co. KG, Karlsruhe |
| Midori Green | Nippon Genetics Europe GmbH, Düren |
| Proteaseinhibitor | Roche Lifescience, Mannheim |
| Rinse Solution | Becton Dickinson Bioscience, Heidelberg |
| Shutdown Solution | Becton Dickinson Bioscience, Heidelberg |
| Sodium azide | CarlRoth GmbH & Co. KG, Karlsruhe |
| Sodium bicarbonate | Merck KGaA, Darmstadt |
| Sodium chloride | CarlRoth GmbH & Co. KG, Karlsruhe |
| Sodium citrate | Sigma-Aldrich Corp. St. Louis, Mo, USA |
| Sodium dihydrogen phosphate monohydrate | Merck KGaA, Darmstadt |
| Sodium dodecylsulfate (SDS) | CarlRoth GmbH & Co. KG, Karlsruhe |
| Sodium hydroxide | Merck KGaA, Darmstadt |

| | |
|---|---|
| Tris(hydroxymethyl)aminomethane (Tris) | CarlRoth GmbH & Co. KG, Karlsruhe |
| Triton-X-100 | Sigma-Aldrich Corp. St. Louis, MO, USA |
| Trypan blue | Sigma-Aldrich Corp. St. Louis, MO, USA |
| Tween®-20 | AppliChem GmbH, Darmstadt |

## 2.3 Solutions and buffers

**Table 5: Solutions and buffers**

| Name | Contents |
|---|---|
| Ammoniumpersulfate (APS) | 10% Ammoniumpersulfate in A. dest. |
| Blocking Solution (immunofluorescence) | 3% Bovine serum albumin (BSA) in PBS |
| Gel buffers (SDS-Page) | 1.5 M Tris (pH 8.8), Storage at 4 °C<br>1 M Tris (pH 6.8), Storage at 4 °C |
| Loading buffer 4x (laemmli buffer) | 250 mM Tris-HCl (pH 6.8)<br>8% (w/v) SDS<br>40 % (v/v) Glycerol<br>10 % (v/v) β-Mercaptoethanol<br>0.4 % (v/v) Bromphenol blue |
| Blocking buffer (Western blotting) | 5% (w/v) Milk powder in PBS |
| 10x Net-G | 0.5 M Tris<br>1.5 M NaCl<br>50 mM EDTA (pH 7,5)<br>0.4 % Gelantine<br>0.5 % Tween |
| 10x PBS | 1.37 M NaCl<br>27 mM KCl<br>100mM $Na_2HPO_4$<br>20mM $KH_2PO_4$ pH=7.8 |

| | |
|---|---|
| PBS/Tween (PBST) | PBS<br>0.1 % (v/v) Tween-20 |
| Complete™ Protease Inhibitor Cocktail (25x) | 1 Tablet (Roche) in 2 ml $H_2O$ |
| RIPA-Buffer – Protein lysis buffer | 50 mM Tris / HCl<br>150 mM NaCl<br>1% NP-40<br>0.1% Sodiumdesoxycholate<br>0.1 % SDS<br>1 mM EDTA<br>pH = 7.5 |
| Running buffer (SDS-Page) | 50 mM Tris<br>192 mM Glycerin<br>0.1 % (w/v) SDS |
| Transfer buffer (SDS-Page) | 50 mM Tris<br>192 mM Glycin<br>0.1 % (w/v) SDS<br>20 % (v/v) Methanol |
| Stripping solution (SDS-Page) | 62.5 mM Tris-HCl (pH 6.8)<br>2 % (w/v) SDS<br>100 mM β-Mercaptoethanol |
| Solubilization buffer (MTT) | 20 % (w/v) SDS<br>0.01 M HCl |
| Lysis Buffer | 2.5 M NaCl<br>100 nM EDTA<br>10 nM Tris<br>1% Na-Laurylsarcosinat |

## 2.4 Antibody list

### 2.4.1 Immunoblotting

**Table 6: Antibody list for Immunoblotting**

| Primary Antibody | Size (kDa) | Host | Dilution | Catalogue number | Manufacturer |
|---|---|---|---|---|---|
| RNaseH1 | 32 | Rabbit | 1:500 | 15606-1-AP | Proteintech |
| β actin | 42 | Mouse | 1:10000 | | Milipore |
| phospho-Histone H2A.X (Ser139) | 15 | Mouse | 1:5000 | 05-636 | Milipore |
| S9.6 | Na RNA:DNA hybrids | Mouse | 1:10000 | Ab234957 | abcam |
| dsDNA | Na dsDNA | Mouse | 1:10000 | MAB1293 | Milipore |

| Secondary Antibody | Host | Dilution | Catalogue number | Manufacturer |
|---|---|---|---|---|
| Anti-Mouse IgG HRP-conjugated | Goat | 1:2000 | 7076 | Cell Signaling. |
| IgG anti-rabbit (H+L) | Goat | 1:10000 | 074-1516 | KPL, Kirkegaard & Perry Laboratories Inc., Gaithersburg, MD, USA |
| Pierce™ ECL Western Blotting Substrate | Not applicable (na) | na | 32106 | Thermo Scientific™ |

### 2.4.2 Immunofluorescence

**Table 7: Antibody list for immunofluorescence**

| Primary Antibody | Host | Dilution | Catalogue number | Manufacturer |
|---|---|---|---|---|
| phospho-Histone H2A.X (Ser139) | Mouse | 1:5000 | 05-636 | Millipore |
| 53BP1 | Rabbit | 1:1000 | NB100-304 | Novusbio |
| Phosphor-RPA (S4/S8) | Rabbit | 1:1000 | A300-245A | Bethyl Laboratories |
| RAD51 | Rabbit | 1:10000 | Ab3801 | abcam |

| Secondary Antibody | Host | Dilution | Catalogue number | Manufacturer |
|---|---|---|---|---|
| Hoechst 33342 | Not applicable | 1:2000 | 11534886 | Invitrogen™ H3570 |
| Anti-Mouse Alexa 488 | Donkey | 1:1000 | A21202 | Invitrogen |
| Anti-Rabbit Alexa 568 | Goat | 1:1000 | A11011 | Invitrogen |

## 2.5 Primer list

**Table 8: qRT-PCR Primer list**

| | | |
|---|---|---|
| **SSRP1** | **Forward** | **TCACAGTGCCAGGCAACTTCCA** |
| | **Reverse** | **ACAGGTGGCTTGTGGACGTAGA** |
| **SRSF1** | Forward | TATCCGCGACATCGACCTCAAG |
| | Reverse | AAACTCCACCCGCAGACGGTAC |
| **TOP1** | Forward | AGTGCTAAGGCTGATGCCAAGG |
| | Reverse | GTCTGTGGCTTGAACTTCCAGC |
| **RNAseH1** | Forward | CCTCCAGTTAGCAGAGACACGT |
| | Reverse | CCAGTAAACGCCGATTCCTGCT |
| **RAD51** | Forward | CTGAGGCAGCTAAATTAGTTCCA |
| | Reverse | CACCCCGGTCAATGGGAAG |

**Table 9: RNaseH1 primer list**

| | |
|---|---|
| Forward | 5'-ggg gac aag ttt gta caa aaa agc agg ctt cac cat gcc caa gaa gaa gag gaa ggt-3' |
| Reverse | 5'-ggg gac cac ttt gta caa gaa agc tgg gtc tca cgt aga atc gag acc ga-3' |

## 2.6 Devices

**Table 10: Device list**

| **Device** | **Manufacturer** |
|---|---|
| Photometer | GE Healthcare „GeneQuant Pro |
| Cell irradiator | Buchler „CDCK 4905" |
| Incubator | Binder |
| Electrophoresis system | Biorad |
| Magnetic stirrer | Heidolph „MR3001" |
| Microscope | Olympus „CHT" |
| Microscope (Immunofluorescence | Leica Weidfield |

| | |
|---|---|
| imaging) | |
| pH meter | Hanna-Instruments „pH211“ |
| Pipets | Eppendorf, Gilson, Integra Biosciences „Pipetboy accu“ |
| Sterile bench | Thermo Scientific „HeraSafe KS18“ |
| Liquid nitrogen tank | Air Liquid, „Espace 151 Liquide” |
| Vortex | Neolab |
| Thermomixer (for reaction tubes) | Eppendorf |
| Waterbath | Köttermann |
| Scales | VWR International |
| Centrifuges | Roth, „Micro Centrifuge“<br>Thermo Scientific “Heraeus Fresco 17” |
| Chemiluminescence Imager | iBright Thermofischer |
| Flow Cytometer | Becton Dickinson (BD) FACS Canto,<br>Becton Dickinson (BD) FACS Canto II |

## 2.7 Disposables

**Table 11: Disposables**

| **Disposable** | **Manufacturer** |
|---|---|
| 6-, 12-, 24-, 96-well-plates | Greiner Bio-One GmbH, Kremsmünster, Austria |
| T-75 flasks, T-25 flasks | Greiner Bio-One GmbH, Kremsmünster, Austria |
| 6-, 12-, 24-, 96-well-plates | Greiner Bio-One GmbH, Kremsmünster, Austria |
| T-75 flasks, T-25 flasks | Greiner Bio-One GmbH, Kremsmünster, Austria |
| Serological Pipets 5 ml, 10 ml, 25 ml | Corning Inc., Corning, NY, USA |
| Desinfectant | Schülke & Mayr GmbH, Norderstedt |
| Cryo vials 1 ml | Greiner Bio-One GmbH, Kremsmünster, Austria |

| | |
|---|---|
| pH meter | Hanna-Instruments „pH211“ |
| 6-, 12-, 24-, 96-well-plates | Greiner Bio-One GmbH, Kremsmünster, Austria |
| T-75 flasks, T-25 flasks | Greiner Bio-One GmbH, Kremsmünster, Austria |
| 6-, 12-, 24-, 96-well-plates | Greiner Bio-One GmbH, Kremsmünster, Austria |
| T-75 flasks, T-25 flasks | Greiner Bio-One GmbH, Kremsmünster, Austria |
| Serological Pipets 5 ml, 10 ml, 25 ml | Corning Inc., Corning, NY, USA |
| Desinfectant | Schülke & Mayr GmbH, Norderstedt |
| Cryo vials 1 ml | Greiner Bio-One GmbH, Kremsmünster, Austria |
| Cryo vials | Nunc, Roskilde, Denmark |
| Cuvettes 1,6 ml | Ratiolab GmbH, Dreieich |
| Nitrocellulose membrane | GE Healthcare UK Limited, Amersham Place, Buckinghamshire, UK |
| Pasteur pipets | CarlRoth GmbH & Co. KG, Karlsruhe |
| Pipet tips 10 µl, 200 µl, 1000 µl | Starlab GmbH, Hamburg |
| Pipet tips 10 µl, 200 µl, 1000 µl | Greiner Bio-One GmbH, Kremsmünster, Austria |
| Reaction tubes 1,5 ml, 2 ml | Greiner Bio-One GmbH, Kremsmünster, Austria |
| Tubes 15 ml, 50 ml | Cellstar, Greiner Bio-One GmbH, Kremsmünster, Austria |

## 2.8 Software and databases

**Table 12: Software and databases**

| Software | Origin |
|---|---|
| Mendeley | Mendeley Reference Manager |
| ImageJ/Fiji | Wayne Rasband, National Institutes of Health, USA |
| FlowJo (version 10.6.1) | Tree Star Inc |
| Inkscape (1.0) | Inkscape.org |
| Harmony Software | |
| Graph Pad Prism (v8.4) | Graphpad Software, Inc. |
| FACS Diva | Becton-Dickinson |
| Microsoft Office 365 | Microsoft |

# 3 Methods

## 3.1 Cell lines and mutational background

We used different, well-characterized AML cell lines, established from AML patients[71][72], [73].These cell lines are freely available at online repositories such as, the ATCC. Each of these cell lines has different genetic background[11], [73][74]. The main goal to use these cell lines is to explore how they will react when treated with two drugs that are currently used in clinic The cell lines used in this project are shown in Table 13. All cell lines were obtained from DSMZ (German Cancer Cell Line Depository), and regularly monitored for mycoplasma contamination using the Vendor® GeM classic kit (Miverva Biolabs).

**Table 13: AML cell lines with mutational background**

| Cell lines | FLT3 | TP53 | NPM1 |
|---|---|---|---|
| HL-60 | wt | depleted | wt |
| MOLM13 | mut | wt | wt |
| OCI-AML3 | wt | wt | mut |

## 3.2 Cell culture conditions

### 3.2.1 Long term storage:

Cells were kept in liquid nitrogen in a freezing mix solution composed of fetal bovine serum (FBS) with 10% DMSO.

### 3.2.2 Thawing

Aliquots were thawed in a water bath at 37°C for 1-2 minutes and cells were transferred into 15 mL falcon tubes and diluted into fresh media. Cells were then spun down in a centrifuge at 1400 rpm (rotation per minute) for 5 minutes. Remaining supernatant was discarded and the pellet was re-suspended into 5 mL of fresh RPMI medium with 10% FBS.

### 3.2.3 Cell culture:

#### 3.2.3.1 Suspension cells:

Suspension cells were plated in 6-well plates at densities between 0.5 and 2 million/ml and placed in an incubator at 37 °C with 5% $CO_2$. All AML cell lines were split and expanded in 1:5 dilutions every 48 hours. Cell culture was maintained for maximal 8 weeks. HL-60, MOLM-13, OCI-AML-3 cell lines were cultured in Roswell Park Memorial Institute 1640 (RPMI-1640) medium supplemented with 10% FBS.

#### 3.2.3.2 Adherent cell lines

HEK-293T (293T) were cultured in 10 cm culture plates in DMEM with 10% FBS, 1% L- Glutamine, and 1% penicillin/streptomycin. Adherent cells were sub-cultured by decanting culture medium, washing with sterile PBS (phosphate-buffered saline) and incubated with 2 mL of Trypsin-EDTA solution for 3-5 minutes in the incubator. To stop the trypsin reaction 8 mL of fresh medium was added to the culture and cells were counted for re-plating. One million cells were then seeded per 10 cm culture plate and pipetted gently on the bottom of the plate to avoid cell aggregation and clumping. When the cells were 70-80 % confluent, they were sub-cultured at 1:5 dilution.

## 3.3 Cell line characterization

### 3.3.1 Cell proliferation using Trypan Blue dye exclusion assay

AML cell lines were seeded in a 6-well plate with a density of 10^6 cells per well in a final volume of 5 mL. Every 24 hr cells were re-suspended and consecutively 20 µL of cell suspension were mixed in a fresh sterilized reaction tube with 20 µL of Trypan Blue stain (0.04 % final concentration) to a dilution factor of 2. Ten µL of the mixed suspension was added between the cover glass and haemocytometer and all four corners chambers were counted. Trypan blue dye was used to measure proliferation rate, as this assay allows differentiating between live and dead cells; live cells with intact membranes do not absorb non-membrane permeable dyes (such as trypan blue), while dead cells absorb it. Counted average (avg.) number of cells was plugged into the Equation 1 to obtain the number of trypan blue unstained cells (viable cells) per mL of

solution. For longer time proliferation analysis, cells were split in 1:2 or 1:4 dilution every 3 days depending on doubling time of cells lines, which differ from each other.

$$\{Viable^{cells} = Avg.\ viable\ cells \times Dilution\ factor \times 10\text{^}4\}\ mL \quad (1)$$

### 3.3.2 Cellular toxicity assay using MTT based metabolic assay.

The MTT (3-(4,5-dimethylthiazol-2-yl)-2,5-diphenyltetrazolium bromide) tetrazolium reduction assay measures cellular metabolic activity in the presence of NADPH and reduces yellow tetrazolium salt MTT into purple formazan crystals (Prabst, Engelhardt, Ringgeler, & Hubner, 2017; Vega-Avila & Pugsley, 2011). These insoluble formazan crystals are dissolved using a solubilization buffer and are measured at 570 nanometer absorbance using a multi-well spectrophotometer. The number of viable and metabolically active cells is directly proportional to formation of formazan crystals.

In order to measure the effect of chemotherapeutic agents on the cellular metabolic activity and subsequently measure the cell viability, cells were seeded in density of 0.8x10^6 cells/mL (HL-60) and 0.5x10^6(MOLM13, OCI-AML3) in a final volume of 2mL in a 6-well plate. Cells were treated with appropriate concentration of cytotoxic agents and equivalent vehicle control (DMSO) (vehicle ctrl) to normalize the response and cell viability was measured for 24, 48 and 72 hour time points. For each point of time , 100 µL of seeded cells were transferred into a new F-bottom 96 well plate and supplemented with 10 µL of MTT reagent (buffer recipe as described in section 2.3) and incubated in an incubator maintained at 37 °C with 5% $CO_2$ for 4 hr. Formazan crystals formed during this incubation period were dissolved using 100 µL solubilization buffer and further incubated at 37 °C overnight and measured at 570 nm using multi-well spectrophotometer. Intensity responses from the treated samples were normalized to the vehicle. ctrl samples to obtain percent viable cells.

### 3.3.3 Combination treatment:

To reduce the toxic effects of either drugs alone and enhance the response compared to single inhibitor treatment, and explore whether the two used drugs are synergistic we performed a combination therapies. This necessitates the validation of combination strategies with respect to synergistic, additive or antagonistic response. To explore combinatorial responses, effective doses within the IC50 range for each of the inhibitors were used. Dose ranges for each chemotherapeutic agents were plated in a combination as shown in Figure5. Each experiment was performed in duplicates with a technical duplicate and measured at various time points ranging from 24 to 72 hours. To evaluate the potential synergy of combined drugs, the observed drug combination responses (e.g. dose-response matrix, see figure above) are usually compared with expected combination responses calculated by means of synergy scoring models (so-called reference or null models). Consequently, based on deviation of observed and expected responses one can classify the drug combination either as synergistic (i.e. combination effect is higher than expected) or antagonistic (i.e. combination effect is lower than expected).

The degree of combination synergy, or antagonism, is quantified by comparing the observed drug combination response against the expected response, calculated using a reference model that assumes no interaction between drugs.

The reference model I used to capture the drug interaction relationship is the Zero interaction potency (ZIP) model which captures the drug interaction relationships by comparing the change in the potency (effect at certain dose level) of the dose–response curves between individual drugs and their combinations. The expected response corresponding to the effect as if the single drugs did not affect the potency of each other (ZIP)[75], [76].

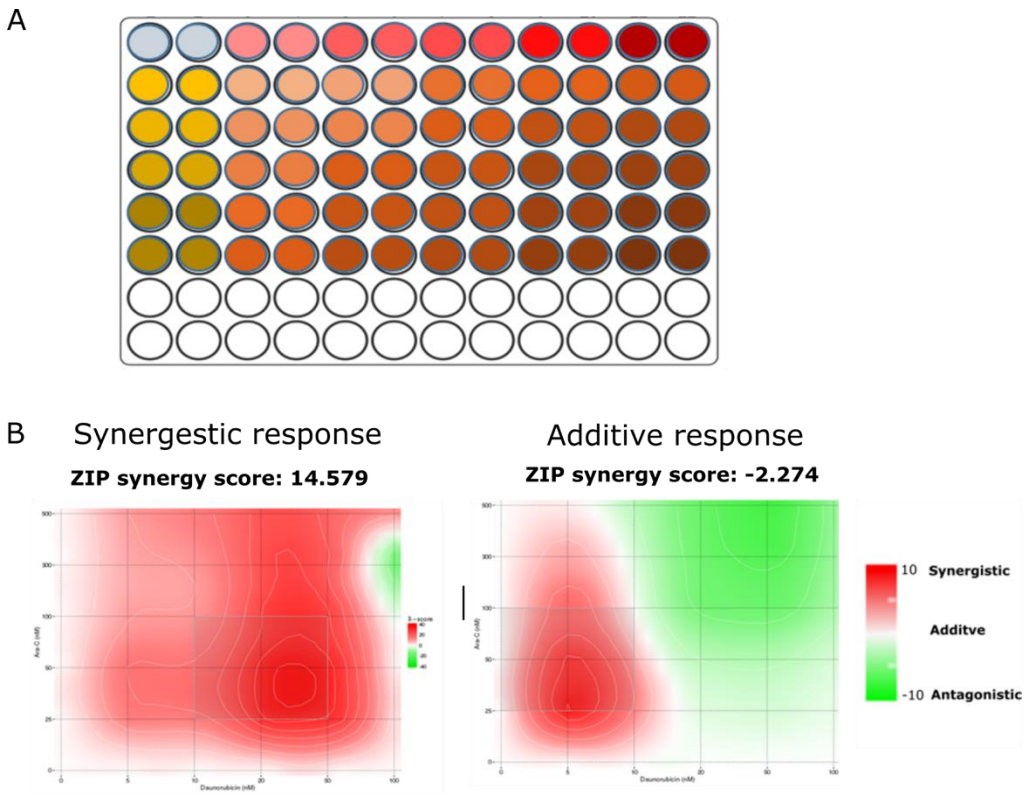


**Figure 5: Drug combination plating strategy and synergy evaluation.**

(A) Shown is a 96-well plating workflow with single dose response of Drug 1 (yellow) and Drug 2 (red) and combination dose matrix (Brown). Increase in color intensity corresponds to higher drug concentrations. Each of the responses was measured by using MTT assays. The response of single treatment and combinations were normalized to vehicle control (Blue; Veh. Ctrl.) to obtain viability or inhibition rates relative to controls. (B) Relative inhibition of growth was further utilized to compute three-dimensional surface plots to visualize overall synergy (red) or antagonistic effects upon drug combination using Zero interaction Potency (ZIP) statistical model.

## 3.4 Cell apoptosis

The efficacy of drug effects on cell lines was measured by cell viability and cytotoxicity assays as described in the earlier sections. These assays were extremely proficient in differentiating dead cells against viable cells. On the other hand, these assays lack detecting dying cells that can be caused by different cell death pathways such as apoptosis, necrosis, and autophagy. Since the two drugs, I am using to treat the cell lines I am working with, are known to both cause apoptotic cell death[20], [77] that can be mainly divided in two stages, early apoptotic and late apoptotic stages, I wanted to perform an an Annexin V assay. Early apoptotic cells flip their phosphatidylserine of the plasma membrane from the inner membrane to the outside and expose it to the surface. Annexin V protein that specifically binds to phosphatidylserine in presence on $Ca^{2+}$ can be used as a biomarker for cell in the early apoptotic stage. In order to measure the percentage of cells entering apoptosis, an EBioscience™ Annexin V Apoptosis-Detection kits (Invitrogen) was used. Co-staining with Annexin-V and 7-AAD was used to quantitatively measure the fraction of cells entering into early stage (Annexin-V positive, 7-AAD negative) versus late stage apoptotic cell death (Annexin-V positive, 7-AAD positive) cells as shown in Figure 6.

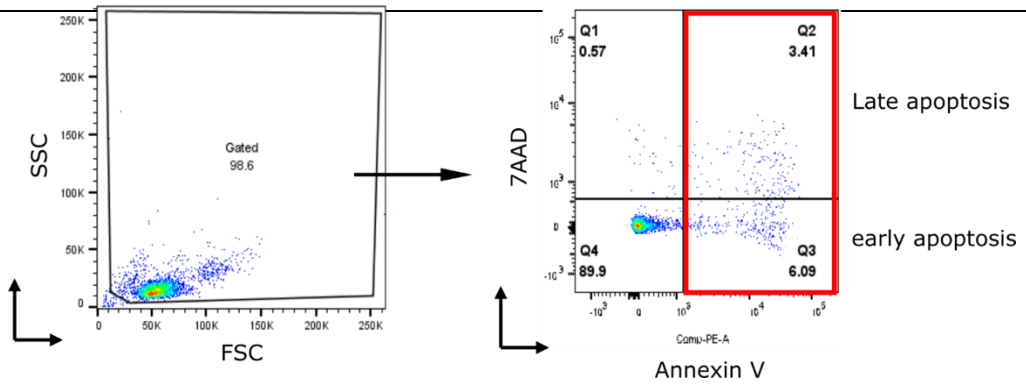


**Figure 6: Gating strategy for measuring apoptotic cells.**

Flow cytometry plots showing gating strategies for measuring Annexin-V expression and 7-AAD staining. Cells were gated using FCS against SSC. Upon exclusion of cell debris, Annexin-V conjugated with PE stain and 7AAD staining was analyzed. Cells positive for Annexin-V-PE were considered as early apoptotic cells and cells double positive for Annexin-V-PE and 7AAD as late apoptotic. Both fractions together (red box) were annotated as 'Apoptotic Fraction'. Percent of apoptotic cells was quantified and further compared to sample control using FlowJo software.

AML cell lines and primary samples were treated in 6-well plates with a final cell density of 8x10^5 cells/mL (HL-60) and 8x10^5 (MOLM13 and OCI-AML3). 600 µL of cell suspension was transferred into a FACS tube and washed once with PBS and once in 1x Binding buffer. Cells were than resuspended in 100 ul of 1x Binding buffer with fluorochrome-conjugated Annexin V (1:100 dilution) provided within the detection kit. Cells were gently vortexed and incubated at RT in dark for 15 min. After incubation, cells were washed in 2ml of 1x Binding buffer than resuspended in 200 µL of 1x Binding buffer with 2ul of 7-AAD viability staining solution and incubated for 10 min on ice or at 4 C until measured but not more than 4 hrs. Cells were not washed after the addition of 7-AAD.

## 3.5 DNA damage/ repair quantification

### 3.5.1 Immunofluorescence based DNA damage quantification

It is known that DRN and ARA-C are both leading to double strand break, this led us to think about exploring and quantifying the expression of the DSBs marker, γH2AX, along with identifying the DNA repair pathway that cells undergo by looking at the co-localized γH2AX foci with three different DNA repair genes, RAD51 involved in HR DNA repair pathway, 53BP1 involved in NHEJ DNA repair and RPA involved in multiple DNA repair pathway including HR repair. To be able to visualize the DNA damage as well as the DNA damage response (DDR) immunofluorescence is the fit method represented by the γH2AX foci and their co-localization with each of the DNA repair genes.

Prior to harvesting of treated and control cells, coverslips, slides and fixation reagents were prepared. After being treated for 24h with cytotoxic drugs, suspension cells were harvested and span down in epi tube for 5min at 800xg rpm. Cells were than washed once in PBS. In the meantime, using a hydrophobic pen, a square was drawn on Pol-L Lysine slides. Then cells were transferred onto the slide inside the square and let adhere for 30-45 min.

Primary antibodies directed against γH2AX 1:2000 (Cell Signaling, concentrations are shown in Appendix), was diluted in blocking buffer, and adjusted to 100 µL per slide/sample. Then 100 µL of primary antibody in blocking buffer was placed as a droplet on each slide. After overnight blocking, blocking buffer was discarded and the slides were incubated with primary antibody in a humidity chamber at RT. After 2 hr slides were washed 3X with PBST (PBS with 0.1% Tween-20) and incubated with Alexa 488 secondary antibody 1:1000 (Invitrogen, dilutions as shown in Appendix) along with Hoechst (1:5000 in blocking solution, Invitrogen, 33342) to counter stain the cell nucleus in the humidity chamber at RT for 1 hr in the dark. Slides were again washed 3X with PBST and prepared for mounting. A droplet/15 µL of ProLongTM Gold mounting medium (Thermo Scientific) was used to mount the slides with coverslips, incubated in dark for 5min. (Slides were stored in dark for 1 week in a slide storage box for later measurement). Mounted slides were sealed with nail polish before measurement. Images were acquired using Leica

microscope with a 63X oil objective. Acquired images were processed for foci quantification using Fiji software (modified protocol from Duke trinity college of arts and sciences, light microscopy core facility) and visualized using GraphPad Prism (version 8.01) with each column representing data from 200 cells (number of cells with more than 5 foci per cell).

Detailed foci count protocol :

1- Open the image of interest => split channels
2- Make sure to use DAPI channel to smooth image if needed, adjust Threshold and analyze particles. Set sized >200 to exclude little things that are not nuclei
3- Go to process, find maxima and adjust prominence until all foci are selected by the cross
4- a results window open up including max values of 255 and raw integrated density that will be divided by the max (255) to get the total number of foci.

### 3.5.2 Immunofluorescence based DNA repair pathway identification

Using the same slides prepared in section 5.1, we co-stained for yH2AX with 3 different DNA repair gene (one DNA repair gene per slide) *RAD51*, *53BP1* and *RPA*. Where *RAD51* is involved in homologues recombination (HR) DNA repair pathway, 53BP1 involved in non-homologues end joining (NHEJ) DNA repair and RPA involved in multiple DNA repair pathway including HR repair.

Slides were incubated with primary antibodies of the DNA repair gene along with yH2AX for 2hr at RT with the following dilutions: *RAD51* 1:10000 (abcam ab63801), *53BP1* 1: 1000 (Novusbio NB100-304), *RPA* 1:100 (Cell signaling 2267S) in blocking solution in a humidity chamber at RT. After incubation, slides were processed as mentioned in section 3.5.1.

To determine the DNA repair pathway, we quantified the co-localized yH2AX foci with each of the DNA repair genes using Fiji/ImageJ software as follow:

1- From the menu go to analyse then clolocalization and choose colocalization threshold
2- choose the 2 channel for which you want to quantify the co-localised foci
3- Go to process, find maxima and adjust prominence until all foci are selected by the cross

4- A results window open up including max values of 255 and raw integrated density that will be divided by the max (255) to get the total number of foci.

## 3.6 R-loops Quantification

### 3.6.1 Dot Blot:

#### 3.6.1.1 Purification of genomic DNA (which includes RNA-DNA hybrids)

R-loops are three stranded structures of RNA-DNA hybrid with a displaced non- template DNA strand that usually form during transcription. R-loops are located in the nucleus, cytoplasm, and mitochondria[32],[42], [78]. It has been shown that R-loops can be considered as source of genomic instability when not properly removed, this made curious to explore whether R-loops accumulation can be the source of chemotherapy-induced cell death as well as the DNA damage cause by DNR and ARA-C.

The genomic DNA was purified using Qiagen kit as per the manufacture's recommendations. DNA concentration was measured using NanoDrop™ after thawing on ice or freshly extracted and used immediately, but always placed on ice until used.

#### 3.6.1.2 Blotting DNA samples (which include RNA-DNA hybrids) onto nylon membranes

Dilutions of nucleic acids were prepared to desired concentrations in elution buffer from Qiagen kit (i.e., 50 ng/µL, 25 ng/µL, 12.5 ng/µL, 6.25 ng/µL). These samples with a range of concentrations (50, 25, 12.5, 6.25ng) ensure that there will be signals within the linear range. A positively charged nylon membrane was used to load samples. Spot 2 µL of each sample onto 2 membranes: one for the S9.6 antibody and the other for dsDNA antibody. The samples were allowed to saturate into the membrane for at least 2 min before crosslinking the membrane with UV light. The membrane was placed into the center of the UV device and crosslinked using the "Auto Crosslink" setting (1,200 µJ x 100).

#### 3.6.1.3 RNA-DNA hybrid detection with S9.6 antibody

Membranes were Incubated in blocking solution (5% milk in Tris-buffered saline with 0.05% Tween-20 (TBST) overnight at 4C on a shaker then Incubated overnight in primary antibody (in 1x NET-G) at 4 °C with shaking. Add anti-dsDNA antibody (1:10,000 dilution) to one membrane. Add 1µg/mL S9.6 antibody to the second membrane (1:1,000 dilution) in 1x NET-G. Membranes were then washed wash 3x with TBST. Perform each wash for 5-10 min with shaking at room temperature, followed by an Incubation with horseradish peroxidase (HRP) conjugated secondary antibody (anti-mouse, 1:5,000 dilution) in 1x NET-G with shaking at room temperature for 1hrt hen washed 3x with TBST for 5-10 min with shaking at room temperature.

To visualize the signal of both, S9.6 (R-loops) and dsDNA, membranes were developed with enhanced-chemiluminescence (ECL) reagents to acquire signals for imaging using iBright device.

#### 3.6.1.4 Quantification and normalization of S9.6 R-loop signal intensity using ImageJ.

Images of S9.6, dsDNA staining were saved in TIFF format, and analyzed using the ImageJ software Following steps from the protocol in[79].

#### 3.6.1.5 Ribonuclease treatments to evaluate signal specificity

NOTE: RNase treatment should be performed on the nucleic acid samples to demonstrate the specificity of S9.6 binding. Treatment with RNase H, but not RNase T1 or RNase III should result in a reduction in S9.6 immunostaining.

For digestion, samples containing RNA-DNA hybrids by preparing them in four separate tubes. each of the 4 samples was treated with either 5 U RNase H, 1000 U RNase T1, 0.5 U RNase III, or mock. Incubate samples at 37 °C for 15 min in 20 µL volumes then loaded 2 µL of each sample on a membrane.

### 3.6.1.6 Preparation of oligonucleotide controls to evaluate signal specificity

Oligonucleotide controls were used to demonstrate the specificity of S9.6 binding. S9.6 recognizes RNA-DNA hybrids, but not dsDNA or dsRNA controls, as has been previously reported.

oligonucleotides were dissolved in annealing buffer (10 mM Tris, pH 8.0; 50 mM NaCl, 1 mM EDTA) to 100 µM and prepared 4 reaction tubes as follow:

1. RNA-DNA hybrid #1: Mix 10 µL of ssRNA top strand with 10 µL of ssDNA bottom strand and 80 µL of annealing buffer.
2. RNA-DNA hybrid #2: Mix 10 µL of ssDNA top strand with 10 µL of ssRNA bottom strand and 80 µL of annealing buffer.
3. dsRNA: Mix 10 µL of ssRNA top strand with 10 µL of ssRNA bottom strand and 80 µL of annealing buffer.
4. dsDNA: Mix 10 µL of ssDNA top strand with 10 µL of ssDNA bottom strand and 80 µL of annealing buffer.

Samples were then heated at 95 °C for 10 min and allowed to cool down. Samples were Loaded 2 µL of each sample on 2 membranes, one for S9.6 antibody and one for dsDNA antibody.
Allow the samples to saturate into the membrane. Wait at least 2 min before crosslinking the membrane with UV light. Place the membrane into the center of the UV device and crosslink the membrane using a UV crosslinker using the "Auto Crosslink" setting (1,200 µJ x 100)[79].

### 3.6.1.7 Enzymatic treatment to evaluate the specificity of S9.6 (RNA-DNA) antibody.

Nucleotides of dsRNA, dsDNA, and RNA-DNA were prepared and blotted onto the nylon membrane. The results demonstrated that the S9.6 antibody binds exclusively to RNA-DNA hybrids(Figure 7A). Two µg of the samples were digested with RNase T1, RNase H, or RNase III for 15 min at 37 °C. A mock sample was also analyzed for comparison to the RNase-treated samples. Samples (50ng) were blotted onto two different membranes as described previously. The membranes were crosslinked, blocked and one of them was probed with S9.6 antibody **(**Figure7B). The results showed that the S9.6 signal correlates with the abundance of the loaded

sample. Treatment with RNase H, but not RNase T1 or RNase III results in a reduction in S9.6 staining. A second membrane was probed with a dsDNA antibody (Figure 7B) for the normalization. Image J was used to analyze the signal intensities. The 50 ng samples were selected for quantification as the signal intensities from the S9.6 and dsDNA antibodies were within the dynamic range. Signal intensities were normalized to those in mock samples.

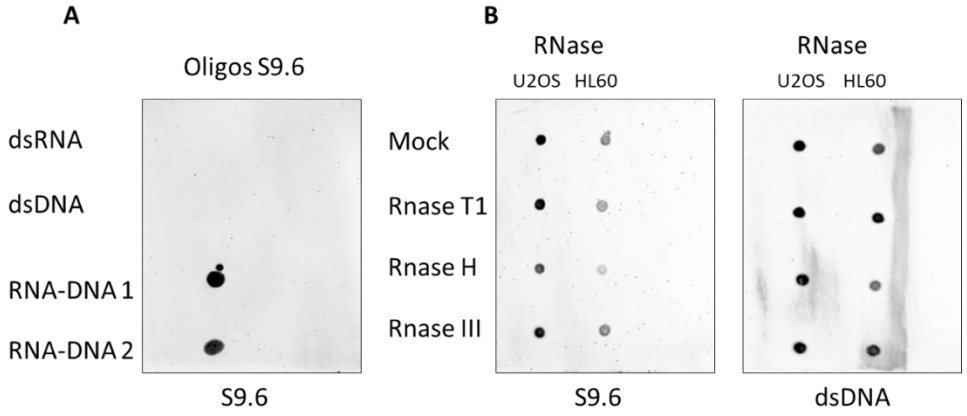


**Figure 7: Evaluation of the S9.6 antibody specificity by enzymatic treatment**

**(**A) S9.6 antibody dot-blot against a dilution series of synthetic oligonucleotides as dsRNA, dsDNA, or RNA-DNA hybrid. S9.6 binds specifically to RNA-DNA hybrids in a dose-dependent manner. (B) Nucleic acid samples from U2Os and HL60 cells were either mock treated or treated with RNase T1, RNase H, or RNase III and then loaded onto nylon membranes 50 ng per 2 µL dot. Membranes were then probed with S9.6 antibody or dsDNA antibody.

### 3.6.2 Immunofluorescence staining

we carried out an immunofluorescence analysis using the hybrid binding domain (HBD) of RNase H1 tagged to fluorochrome (Alexa 647), (that we got from Petri Beli lab at the IMB-Mainz) as illustrated in figure 8 that created in Biorender, in order to further confirm the expression of R-loops. Slides were prepared as mentioned in step 3.5.1, I added 100ul of HBD probe with a concentration of 150nM and yH2AX at a concentration of 1:5000 and incubated overnight at 4 degrees. slides were washed 3X with PBST (PBS with 0.1% Tween-20) and incubated with Alexa 488 secondary antibody 1:1000 (Invitrogen, dilutions as shown in Appendix) along with Hoechst (1:5000 in blocking solution, Invitrogen, 33342) to counter stain the cell nucleus in the humidity

chamber at RT for 1 hr in the dark. Slides were again washed 3X with PBST and prepared for mounting. A droplet/15 µL of ProLongTM Gold mounting medium (Thermo Scientific) was used to mount the slides with coverslips, incubated in dark for 5min. (Slides were stored in dark for 1 week in a slide storage box for later measurement). Mounted slides were sealed with nail polish before measurement. Images were acquired using Leica microscope with a 63X oil objective. Next, the nuclear mean intensity of the Alexa 647 channel was used to quantify R-loops usin imageJ softwar as follow:

1- Open the image of interest => split channels

2- Make sure to use DAPI channel to adjust Threshold and analyze particles.

3- A window of region of interest (ROI) opens up. Choose the Alexa 647 channel (R-loops) and check the show all box.

4- Make sure to set measurments and include mean, integrated density, raw integrated density

4- Click measure on the ROI window.

5- A result window opens up including the measurement of the mean

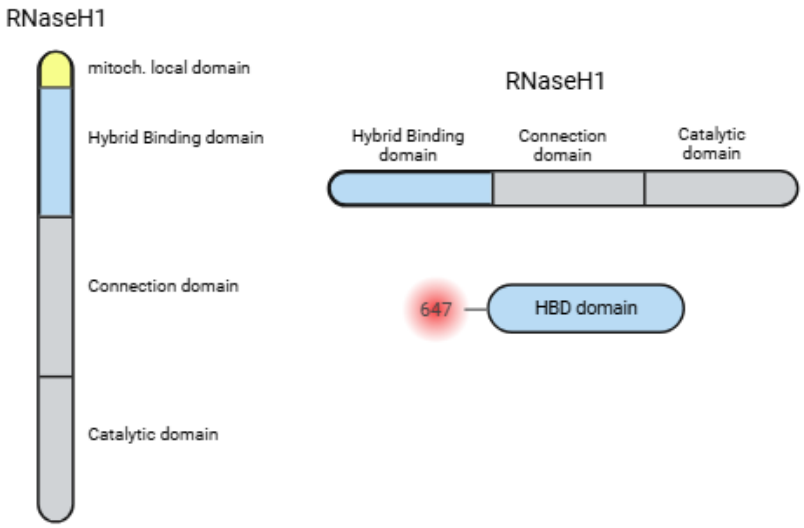


**Figure 8: Hybrid binding domain of RNaseH1 tagged to Alex647.**

The hybrid-binding domain of RNAseH1 was purified at the protein core facility at the IMB Mainz then tagged to Alexa 647 Fluorochrome. Created in Biorender.com.

## 3.7 Real time quantitative polymerase chain reaction (RT-qPCR)

Total RNA from cells was collected using High Pure RNA Isolation kit™ (Roche) as per the manufacture's recommendations. Concentration of extracted RNA was measured using NanoDrop™ after thawing on ice or freshly extracted and used immediately, but always placed on ice until used.

Forward and reverse primer sequences, for the gene of interest, as shown in the table 8 and are also available at OriGene company website. Sequences were then sent to be ordered from Biomers.net company. Luna® Universal One-Step RT-qPCR Kit was used with the RNA extracted and reactions were prepared as described in the table (13)

**Table 14: Components for RT-qPCR reaction**

| COMPONENT | Volume |
|---|---|
| Luna Universal One-Step Reaction Mix (2X | 10 ul |
| LUNA WARMSTART® RT ENZYME MIX (20X) | 1 ul |
| Forward primer (10 µM) | 0.8 ul |
| Reverse primer (10 µM) | 0.8 ul |
| Template RNA | Variable (≤ 1ug) |
| Nuclease-free Water | to 20ul |

GAPDH was used as reference gene and normalization of expression levels of the gene of interest amongst the treated samples or control samples. The fold change of expression of the gene of interest compared to the reference gene was evaluated based on the threshold cycle (CT) value obtained and normalized using Equation (2)[80].

$R$ = **2** $\Delta Ct$ = **2^-** ($CTSample – CTreference\ gene$) **(2)**

## 3.8 Stable cell line generations and validation

### 3.8.1 RNaseH1 preparation

The RNase H enzymes (RNase H1 and RNase H2) remove RNA-DNA hybrids through the endonucleolytic cleavage of an RNA moiety that is engaged in the hybrid molecule. R-loops are a form of RNA-DNA hybrids that arise when an RNA transcript base pairs to its DNA template, resulting in the displacement of the non-coding DNA strand . Defective R-loop removal results in a loss of genome integrity, likely due to DNA replication conflicts. RNase H1, coded by the RNH1 gene in yeast, is able to degrade RNA engaged in R-loops, and its overexpression is frequently used as a tool to promote their removal. RNase H1 consists of an N-terminal hybrid binding domain (HBD) and a C-terminal endonuclease motif[81].

Three different types of RNaseH1 were used to transduce AML cell lines. RNaseH1 Wild Type (WT) which resolves R-loops binding to the RNA moiety of the RNA-DNA hybrids and cleave it. RNaseH1 D210N, which is catalytically inactive due the mutation. Changed D (Aspartic acid) 210 to N (Aspargine), that makes able to bind to R-loops without resolving them and RNAseH1 WKKD which lacks the ability to bind R-loops due the mutations: Changed D 210 to N, W43 (Tryptophan) to A (Alanine), K 59 (Lysine)to A, K 60 to A, D274 to N and thus do not resolve them.

As Template, I used RNaseH1 (WT, D210N, WKKD) from addgene along with the primer shown in table 8.

The PCR kit used to amplify the RNaseH1 from addgene plasmid is Q5 High-Fidelity DNA Polymerase with an annealing temperature of 72˚C.

PCR mix in table 15:

**Table 15: Components for PCR reaction**

| COMPONENT | Volume (total V= 25ul) |
|---|---|
| 2x Mix NEB Q5 Tag | 12.5 µl |
| Forward primer (50 µM) | 0.5 µl |
| Reverse primer (50 µM) | 0.5 µl |
| Template DNA | 0.5 µl |
| Nuclease-free Water | to 11 µl |

Different annealing temperatures from 62-68°C were used to for the PCR reaction and then pick the one were the annealing was optimal

The optimal temperature chosen is 67°C were the DNA was run in agarose gel and then extracted using QIAquick Gel Extraction Kit from Qiagen as shown in the following steps:

1. Excise the DNA fragment from the agarose gel with a clean, sharp scalpel.

2. Weigh the gel slice in a colorless tube. Add 3 volumes Buffer QG to 1 volume gel (100 mg gel ~100 µl). The maximum amount of gel per spin column is 400 mg.

For >2% agarose gels, add 6 volumes Buffer QG.

3. Incubate at 50°C for 10 min (or until the gel slice has completely dissolved). Vortex the tube every 2–3 min to help dissolve gel. After the gel slice has dissolved completely, check that the color of the mixture is yellow (similar to Buffer QG without dissolved agarose). If the color of the mixture is orange or violet, add 10 µl 3 M sodium acetate, pH 5.0, and mix. The mixture turns yellow.

4. Add 1 gel volume isopropanol to the sample and mix.

5. Place a QIAquick spin column in a provided 2 ml collection tube or into a vacuum manifold. To bind DNA, apply the sample to the QIAquick column and centrifuge for 1 min or apply vacuum to the manifold until all the samples have passed through the column. Discard flow-through and place the QIAquick column back into the same tube. For sample volumes >800 µl, load and spin/apply vacuum again.

6. If DNA will subsequently be used for sequencing, in vitro transcription, or microinjection, add 500 µl Buffer QG to the QIAquick column and centrifuge for 1 min or apply vacuum. Discard flow-through and place the QIAquick column back into the same tube.
7. To wash, add 750 µl Buffer PE to QIAquick column and centrifuge for 1 min or apply vacuum. Discard flow-through and place the QIAquick column back into the same tube. Centrifuge the QIAquick column in the provided 2 ml collection tube for 1 min to remove residual wash buffer.
8. Place QIAquick column into a clean 1.5 ml microcentrifuge tube.
9. To elute DNA, add 50 µl Buffer EB (10 mM Tris·Cl, pH 8.5) or water to the center of the QIAquick membrane and centrifuge the column for 1 min.

### 3.8.2 Plasmid preparation

The RNASEH1 sequences were cloned in pLKO-TET-ON vector**,** which is a doxycycline (DOX)-inducible vector system and along with packaging and envelop vectors stable lentiviral particles can be produced (as described in Transfection and transduction section).
As a start, RNaseH1 were cloned into Entry/Donor vector (pDONR221) using the Gateway system that includes BP and LR reactions.

#### 3.8.2.1 Gateway BP Clonase Reaction:

For BP reaction I used as donor vector pDONR 221.
In 1.5ml Eppi tube:
7 µl of the attB-PCR-Product extracted from the gel was mixed with 1 ul of Donor vector with a concentration of 150ng/µl.
2µl of BP-Clonase Enzyme-Mix was added to the mix and incubated overnight at 4°C. After overnight incubation, 1µl of proteinase K was added to the mix, vortex and incubated for 10 min at 37°C.
Transform 1-2 µl of the BP recombination reaction into suitable Competent cells (E. coli host= and select for entry clones using Kanamycin antibiotic.
Note: You may store the BP reaction at −20°C for up to 1 week before transformation.

#### 3.8.2.2 Gateway LR Clonase Reaction:

After I have generated an entry clone, I performed the LR recombination reaction to transfer RNaseH1 into an attR-containing destination vector to create an attB-containing expression clone.
In 1.5ml Eppi tube:
7 ul Entry clone (RNaseH1 in pDONR221 50-150ng) was mixed with 1 ul destination vector (pLenti4/TO/V5-DEST 150 ng/ul) and 8ul TE Buffer, pH8
Next 2ul LR-clonase Enzym-Mix was added and incubat overnight at 25°C
After overnight incubation, 1 ul of proteinase K was added and incatbated for 10 min at 37°C after vortexing.
Transform 1-2 µL of the BP recombination reaction into suitable Competent cells (Stable 3)and select for entry clones using ampicillin antibiotic.

### 3.8.3 Transfection and transduction

Stable overexpression of RNaseH1 types were carried out using Tet on system. This system is known to allow the activation of gene expression by doxycycline (DOX) (DOX inducible system)[82].

#### 3.8.3.1 Transfection with TetR vector

In order to produce virus supernatants for an efficient and stable expression of Tet-R vector (pLenti6/TR ) in AML cell lines, 293T cells were transfected using TransIL-LT1 reagent (Mirus). 293T were seeded in 10 cm petri-plates with a seeding density of $10^5$ cells/mL, 30 hours prior transfection to achieve 60-70% confluence. Four hours prior transfection, the culture medium was gently removed from the plate and carefully replenish with 6 mL of fresh culturing medium without antibiotics (penicillin/streptomycin). For transfection, TransIL-LT1 transfection reagent was diluted in OptiMEM™ (GIBCO) and 20 µL of reagent was added to 280 µL of OptiMEM per 10 cm culture plate in an eppendorf tube and incubated at RT for 5 min. In the meantime, the plasmid mixture was prepared in a new eppendorf tube as shown in Table16.

**Table 16: Plasmid mixture for transfecting 293T cells TET-ON vector**

| Reagents | concentration per 10 cm plate |
|---|---|
| Packaging plasmid (pSPAX.2) | 1.8 µg |
| Envelope plasmid (pMD2.G) | 300 ng |
| Expression vector (pLenti6/TR) | 3 µg |
| OptiMEM™ | 20 µL |

After 5 min incubation, the plasmid mixture was added to the transfection reagent mixture and incubated at RT for 20 min. The whole mixture pipetted into the 10 cm plate with 293T cells, gently shaken and placed back into the incubator for 16 hr. After 16 hr/overnight incubation, the medium was carefully removed from the plates and replenished with 4 mL of fresh medium with 30% FCS without antibiotics and incubated in the incubator for 30 hr. After 30 hr incubation, the supernatant was collected from the plates in a 15 mL falcon and cells were discarded. After spinning down the supernatant, the virus supernatants were used immediately for AML cell transduction. Alternatively, supernatants were aliquoted in 1 mL tubes and stored at -80°C for later use.

#### 3.8.3.2 Lentiviral transduction of AML cell lines

Prior initiating transduction, AML cell lines were split 1-2 days before in a 1:2 to 1:5 dilution to get them in proliferating phase. On the day of transduction, 10^6 cells were seeded in a 6-well plate (Starstedt) with a final volume of 3 mL. One milliliter of frozen or freshly collected virus supernatant was added to the respective wells along with polybrene (Sigma) at a final concentration of 1 µl /mL. 6-well plates were sealed with micro-permeable membrane tape to avoid contamination and placed in the centrifuge for spinfection at 2000 rpm for 1 hr 30 min. After the spin down, plates were placed back in the incubator and maintained at 37°C for 4h and added 2 ml of fresh media and the maintained overnight. After overnight incubation with virus supernatant, cells were spun down in a 15 mL falcon at 1,400 rpm for 5min and the supernatant was replaced with fresh medium supplemented with Blasticidin (invivogen, 5ul/mL final concentration) and placed back in the incubator for 5 days for selection of positively transduced

cells. Fresh media with fresh Blasticidin was added every 2 days. Non-transduced cells served as a positive control for selection efficacy. Selection time for the positive population was based on complete cell death of control cells. Depending on the time of selection and efficiency of positive clones, virus titer for dilution was determined and optimized for each of the cell lines.
After selection, cells were aliquoated and stored in N2 liquid nitrogen until further transduction with pLenti4 pLenti4/TO/V5/DEST vector expressing RNaseH1.

#### 3.8.3.3 Transfection with pLenti4/TO/V5/DEST vector

In order to produce virus supernatants for an efficient and stable expression of RNaseH1 in AML cell lines, 293T cells were transfected using TransIL-LT1 reagent (Mirus). 293T were manipulated, using pLenti4/TO/V5/DEST vector the same way as with the TET-ON vector as explained in section 3.8.3.1 . The plasmid mixture was prepared as shown in Table 17.

**Table 17: Plasmid mixture for transfecting 293T cells with pLenti4/TO/V5/DEST vector**

| Reagents | concentration per 10 cm plate |
|---|---|
| Packaging plasmid (pSPAX.2) | 1.8 µg |
| Envelope plasmid (pMD2.G) | 300 ng |
| Expression vector (pLenti4/TO/V5-DEST) | 3 µg |
| OptiMEM™ | 20 µL |

#### 3.8.3.4 Lentiviral transduction of AML cell lines (Already transduced with TET-ON vector)

Prior initiating transduction, AML cell lines, already transduced with pLenti6 TETR-ON vector were thawed one week before to get them in proliferating phase. Transduction was performed as described in section 3.8.3.2 Fresh media with fresh Zeocin was added every 2 days. Non-transduced cells served as a positive control for selection efficacy. Selection time for the positive population was based on complete cell death of control cells. Depending on the time of selection and efficiency of positive clones, virus titer for dilution was determined and optimized for each of the cell lines.

## 3.9 Immunoblotting

Immunoblotting (Western Blot) is a widely used laboratory technique for detecting specific proteins in a sample using antibody-based recognition. It combines protein separation (SDS-PAGE) with antibody detection, allowing for qualitative and semi-quantitative protein analysis. This technique was first established in 1979[83] and the term western blot was not used until 1981[84].

### 3.9.1 Preparation of whole cell lysates

For validation of RNaseH1 overexpression efficiency upon exposure to doxycycline (DOX) for three days, 1-5x10^6 cells from each condition were collected, washed twice with cold PBS and re-suspended in 100 µL of RIPA buffer (recipe as shown in Material)**.** Cells were transferred into a 1.5 mL reaction tube and placed on ice to lyse cells for 15-20 min. RIPA buffer was supplemented with a cocktail of protease and phosphatase inhibitors (1:25 of Complete™ protease inhibitor, 1mM of Na3VO4, 5 mM of NaF and 2 mM of ß-glycerophosphate). After incubation, whole cell lysates were collected by spinning down the cell debris in a benchtop centrifuge maintained at 4°C at 13,000 rpm for 20 min and the supernatants were transferred into a new eppendorf . Whole cell lysates were directly used for immunoblots.

### 3.9.2 Bradford assay for protein concentration measurement

Protein concentration was measured prior to loading the samples on the SDS polyacrylamide gel and separating them according to their molecular weight. Bradford assay was used to measure colorimetric changes when protein molecules in whole cell lysates bind to Comassie Brilliant Blue stain under an acidic condition, converting red colored stain into blue. A colorimetric photometer was used to measure absorbance at 595 nm. One microliter of lysate was added to 800 µL of ddH2O and 200 µL of Bradford solution in a cuvette, gently vortexed and incubated at RT for 10 min. The absorbance measured was normalized against a standard curve to obtain protein concentration in µg of total protein per µL of protein lysate.

### 3.9.3 SDS-PAGE gel preparation, running and transferring

SDS-PAGE (Sodium Dodecyl Sulfate - Polyacrylamide Gel Electrophoresis) a widely used technique in molecular biology and biochemistry for separating proteins based on their molecular weight that was first described in 1970[85].

SDS-PAGE gels were generated in two stages with the bottom section representing the resolving gel and the top section the stacking gel. The difference in the gel composition allows to initially condense the lysates at the start of the gel run and once the proteins enter the resolving gel, they are further separated based on the charge and size/molecular weight of the proteins . The pore size of the resolving gel was adjusted to optimize segregation of the protein of interest (POI): 6-8% of SDS gels for segregating heavier proteins, e.g. 150-300 kDa (kilodalton) and 12-15% gels for lighter proteins, e.g. 10-30 kDa. As a standard a 10% resolving gels was used unless mentioned otherwise.

Once the concentration of proteins was adjusted amongst the samples of interest using the Bradford assay, sample volumes equating to 60 µg were heated in 4xLaemili buffer supplemented with ß-mercaptoethanol (10%) at 95°C for 5min. Samples were loaded on a 10% SDS gel, placed into the electrophoresis unit filled with running buffer and run at 100-150 V for 1-1.5hr.

After the electrophoresis, the gel was removed from the glass cassette and transferred to turboblot device on 1 layers of whatman filter paper, a nitrocellulose membrane was placed on top of the gel, followed by a similar layer of 1 whatman filter paper at the top, making sure to avoid bubble formation at each step. The gel, membrane and the whatman paper were all previously soaked in transfer buffer This whole construction was then placed in and run at 1.5gel program for 10min.

### 3.9.4 Membrane blocking and development

After transfer the nitrocellulose membrane was washed in 1xPBS on a membrane shaker unit at 50 rpm for 5 min at RT, in order to remove any traces of methanol of the transfer buffer. To check for equal loading and to stabilize the membrane-protein binding, the membrane was stained with Ponceau solution Ponceau stained membranes were washed with ddH2O until the

staining solution was removed. Then the membrane was blocked with 5% milk in PBS-T (Tween20™ reagent 0.05% and milk 5% weight/volume) on the shaker for 1 hr or overnight at 4°C, washed trice with PBS-T on a shaker for 5 min each round. After membrane blocking, the membrane was incubated with primary antibody directed against the RNaseH1 either overnight at 4°C on a shaker 70rpm. Primary antibodies were diluted in NET-G buffer as per the manufacture's recommended dilutions unless mentioned otherwise. Membranes were washed trice with PBS-T on a shaker and incubated with a secondary antibody conjugated with horseradish peroxidase, diluted in PBS-T for 1hr at RT. After incubation, the membrane was washed trice with PBS-T to remove the excess of unspecifically bound secondary antibody and briefly treated with enhanced chemiluminescence (ECL™, ThermoFischer Scienfitic) substrate solution followed by measuring the signal using a chemiluminescence Imager. The signal of the RNaseH1 was normalized to the signal of the housekeeping proteins such as GAPDH or ß-Actin.

# 4 Results

## 4.1 Exploration of genotoxic effects of daunorubicin and Cytarabin in AML cells

### 4.1.1 Analysis of cell growth upon treatment with DNR and ARA-C

We initially investigated the sensitivity of three different AML cell lines to standard of care drugs, which are currently used clinically: Daunorobicin (DNR) and Cytarabin (ARA-C). DNR and ARA-C are used as standard induction chemotherapy for patients with AML (ARA-C 100 mg/$m^2$ per day continuous intravenous infusion for 7 days plus intravenous DNR 60 mg/$m^2$ on days 1, 2, and 3 [7+3][86]. Each of these cell lines has a different genetic background as shown in table 1 (material and methods section). The main goal of using these cell lines is to study how they respond to treatment with the above mentioned drugs, that is, whether they respond differently or similarly in the context of their genetic profile. DNR belongs to a group of drugs known as anthracyclines, which are a type of antibiotic. This drug works by inserting itself between the base pairs of DNA, a process known as intercalation. By intercalating, DNR disrupts the normal function of the topoisomerase II enzyme. This enzyme is crucial for managing the structure of DNA during replication. When DNR inhibits this enzyme, it leads to the induction of both single and double-strand DNA breaks. As a result, this action halts the processes of DNA and RNA synthesis, affecting cell division and growth leading to apoptotic cell death[20] (Figure 9 A and B)

ARA-C is a synthetic drug that resembles naturally occurring pyrimidines, essential components of DNA. Once inside the cell, ARA-C is converted into its active triphosphate form. This active form competes with cytidine, a natural nucleotide, to incorporate itself into the growing DNA strand during replication. Because of this competition, the process of DNA replication comes to a stop, particularly during the S phase of the cell cycle, making ARA-C a highly effective drug against rapidly dividing cells, such as cancer cells that proliferate quickly [19]. The inability to continue DNA replication caused by ARA-C can lead to programmed cell death[77]. Both DNR and ARA-C play significant roles in cancer treatment by targeting the mechanisms of cell division at different stages.

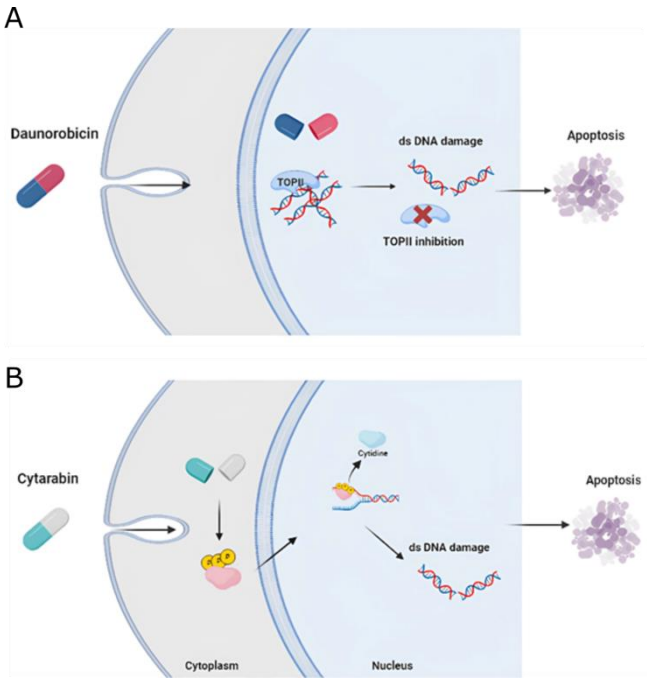


**Figure 9:Mode of action of daunorubicin (A) and cytarbine (B).**

(A) Daunorubicin stops cancer cells from growing by working inside their nucleus when it intercalates between DNA base pairs and disrupts DNA and RNA creation. It also stops topoisomerase II, an enzyme that helps DNA to unwind for replication. By stopping topoisomerase II, the drug causes DNA breaks and eventually leads to apoptotic cell death. (B) Cytarabine is a pyrimidine nucleoside analog that once inside the cells is converted into triphosphate form to be able to incorporate itself into the DNA leading to double strands breaks and apoptosis.

In order to analyze proliferation upon treatment with DNR and AraC, we performed an MTT assay measuring metabolic activity as a surrogate for proliferation. AML cell lines were treated with ARA-C and DNR either alone (Figure 10A and B) or in combination (Figure 10A). In single-agent treatments, MOLM13 cells exhibited the highest sensitivity to DNR, with an $IC_{50}$ of 53.14 nM, while HL60 cells were the least sensitive, with an $IC_{50}$ of 69.40 nM (Table 17). HL60 cells showed the best response to ARA-C treatment, whereas MOLM13 cells were the least responsive (Figure 10 and Table 18). OCI-AML3 cells demonstrated an intermediate response to both drugs (Figure 10).

**Table 18: Cytarabine and daunorubicin IC50 values for each of the three AML cell lines, HL60, MOLM13 and OCI-AML3.**

| IC50 | ARA-C | DNR |
|---|---|---|
| **HL60** | 26.63 | 69.40 |
| **MOLM13** | 184.2 | 42.20 |
| **OCI-AML3** | 55.85 | 53.14 |

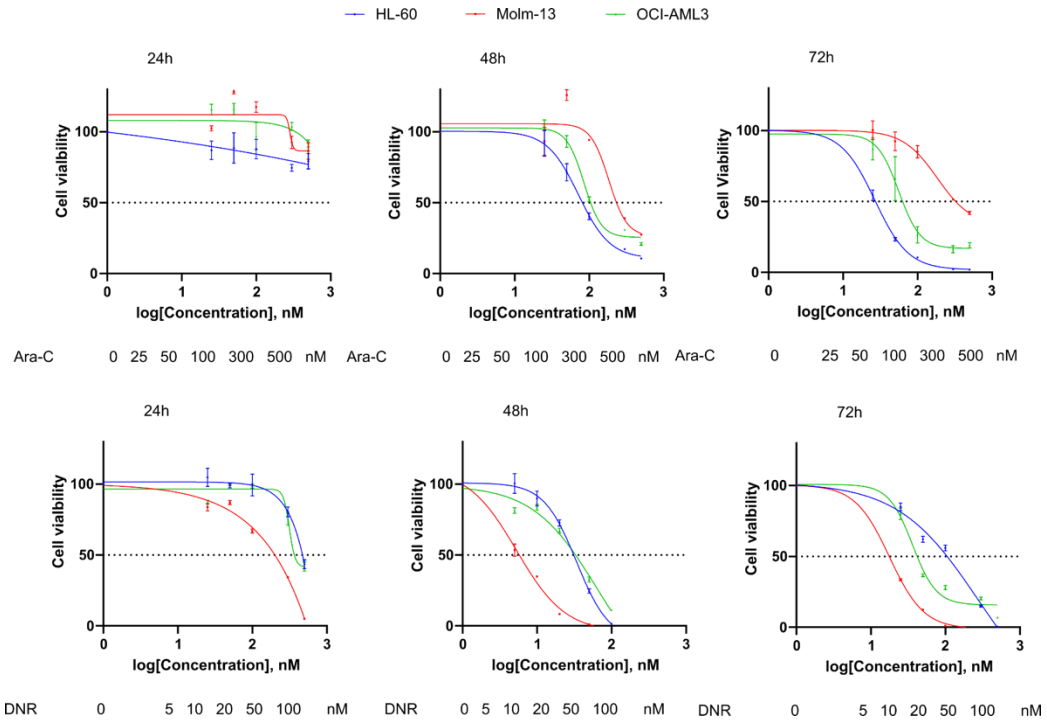


**Figure 10: Chemotherapy response in different AML cell lines.**

Dose response curves of three AML cell lines upon treatment with DNR (A) or ARA-C (B) at different concentrations for 24, 48 and 72 hours. MTT assay was performed upon treatment with DNR or ARA-C with increased concentration. Data are shown as mean ±SD of 3 independent experiments.

To evaluate potential synergism between the two drugs, a combination treatment was performed. These combination treatments overcame resistance observed with single-agent therapies in all three AML cell lines as shown in Figure 11A. For instance, the HL60 cell line demonstrated only minor response upon treatment with DNR alone and vice versa, MOLM13 cell line responded poorly to ARA-C treatment. The combination of ARA-C and DNR led to an almost 100% cell death in both cell lines (Figure 11A). This shows the power of combination therapy, which can overcome resistance mechanisms. To define whether DNR and ARA-C are synergistic, we applied the Zero Interaction Potency (ZIP) model, which captures the drug interaction relationships by comparing the change in the potency (effect at certain dose level) of the dose–response curves between individual drugs and their combinations. ZIP assumes that two non-interacting drugs are expected to incur minimal changes in their dose–response curves. The formulation of the model can be found in [75], [76], [87]. ZIP scores below -10 and above 10 indicate that the two drugs exhibit antagonistic and synergistic effects, respectively. However, ZIP scores between 10 and -10 exhibit additive effects, which is the case for ARA-C and DNR.(Figure 11B).

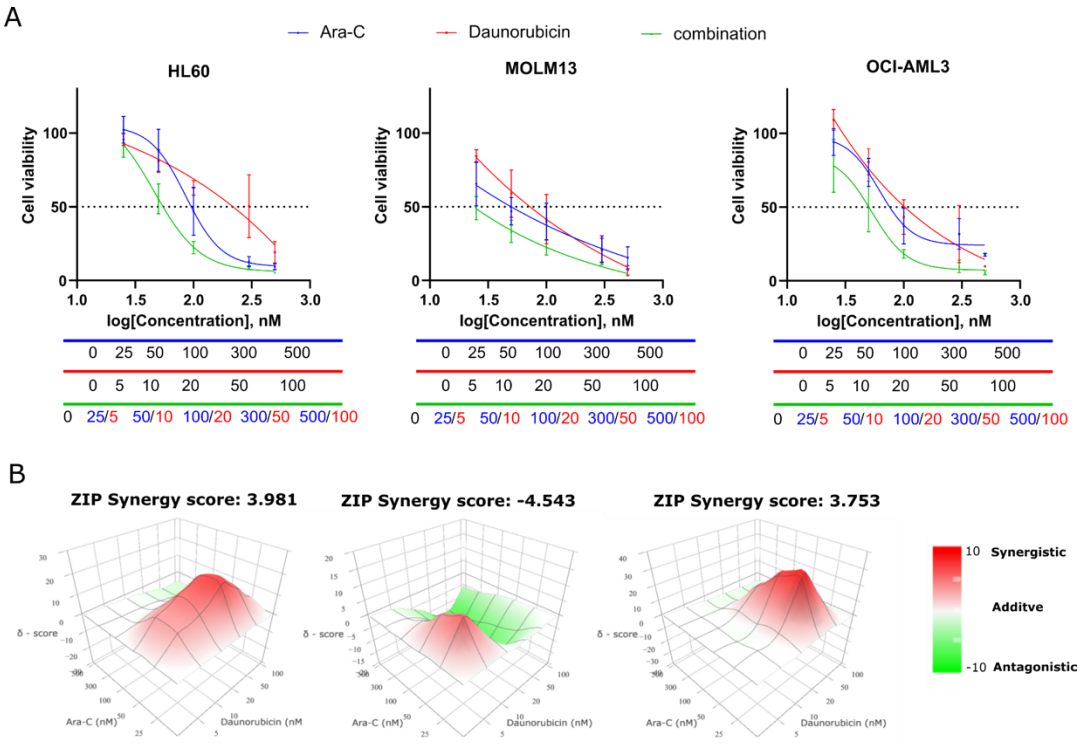


**Figure 11: Effect of combination treatment on different AML cell lines.**

(A) Shown are dose response curves upon treatment with AraC, DNR or in combination. Combination treatments effectively overcomes resistance observed with single-agent therapies in all three AML cell lines.The blue and red lines represent ARA-C and DNR concentrations respectively. The green line represent the combination treatment with blue and red numbers representing concentrations for ARA-C and DNR respectivly.Data are shown as mean ±SD of 2 independent experiments. (B) Panel displays ZIP synergy scores calculated using SynergyFinder software.

### 4.1.2 Analysis of cell death upon treatment with DNR and ARA-C

Both drugs are known to lead to apoptotic cell death, as described in their mechanisms of action, referenced in the earlier section 1.1 (Figure 10)[20], [77].

To confirm if apoptotic cell death occurs in the AML cells we are studying, we conducted experiments treating these cells with each drug separately. Initially, we treated all cell lines with either DNR or ARA-C at a range of increasing concentrations. The concentrations used were 5 nM, 20 nM, and 50 nM for DNR, and 300 nM, 500 nM, and 1 µM for ARA-C, across three different time points specified in the experimental design (Figure 12A).

After treatment, we measured the percentage of apoptotic cell death using Annexin V-PE staining, which identifies cells undergoing apoptosis. Our results showed that the MOLM13 cell line

exhibited a significantly higher level of programmed cell death when treated with DNR, reaching 80%, as illustrated in Figure 12B, compared to HL60 cells. In contrast, the HL60 cell line displayed the highest rate of apoptotic cell death when exposed to ARA-C, reaching nearly 80% (Figure 12B). Unlike the HL60 and MOLM13 cell lines, which exhibited varying levels of apoptosis in response to the same treatments, OCI-AML3 cells demonstrated a moderate level of programmed cell death when treated with each drug (Figure 12B). These observations Tomicgn with previous findings from the MTT assay, where HL-60 was identified as the least sensitive cell line to DNR but showed the greatest sensitivity to ARA-C treatment and vice versa for MOLM13. This emphasizes the differential sensitivity of the AML cell lines to the two drugs, highlighting important considerations for treatment strategies in combating AML.

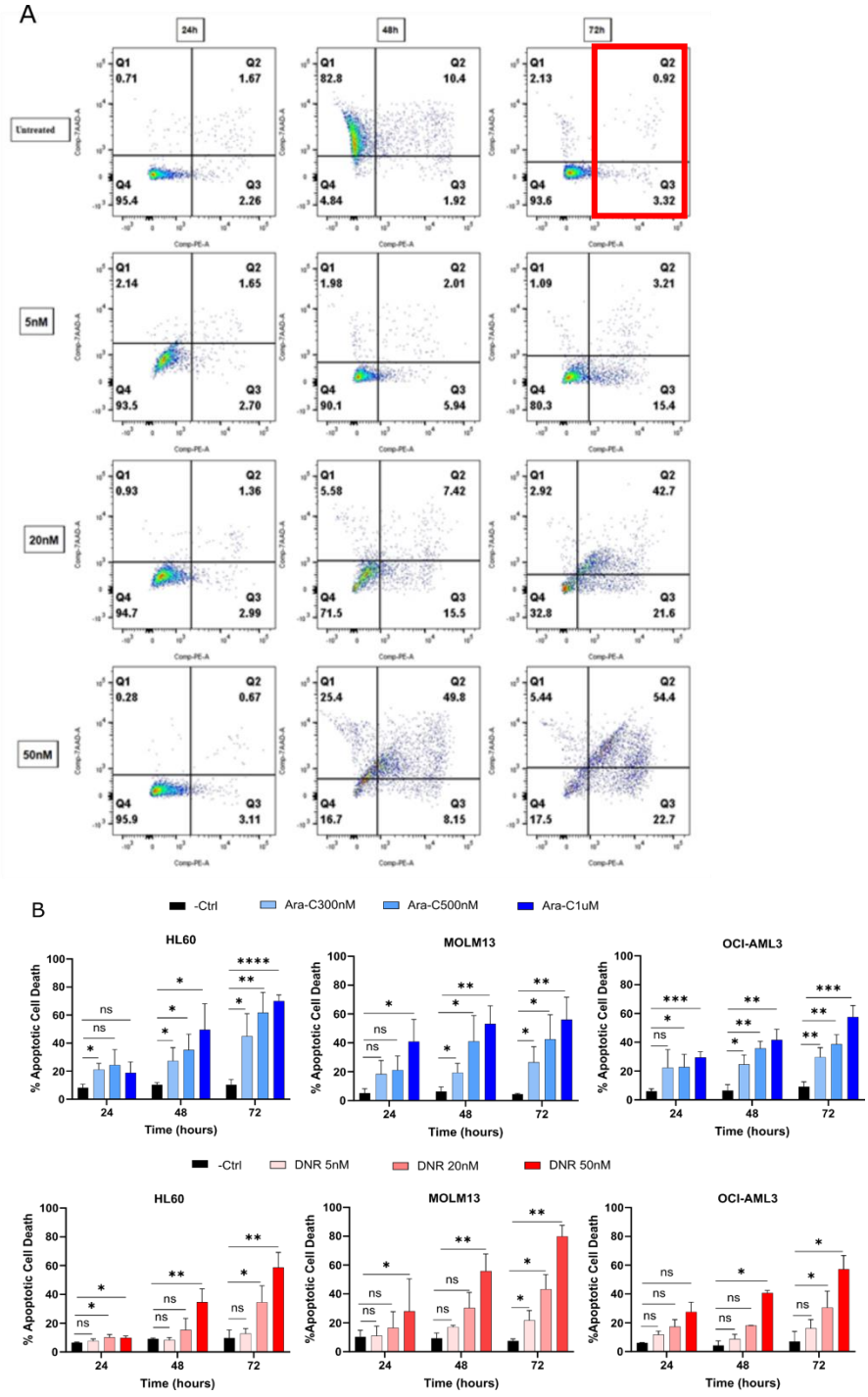


**Figure 12: Apoptotic cell death upon treatment with ARA-C and DNR.**

(A) Quantification of apoptotic cell death by summing up early and late apoptotic cells as shown in the red box. (B) All AML cell lines were treated with ARA-C or DNR with three different concentrations for each drug as indicated. Shown are graph bars representing the percentage of apoptotic cell death for each cell line upon treatment with each drug. Data are shown as mean ±SD of 3 independent experiments. Significances were calculated using unpaired t-test *<0.05, **<0.01, ***<0.001, ****<0.0001, ns: not significant.

## 4.2 Analysis of DNA damage response upon treatment with DNR and ARA-C

DNR and ARA-C are both chemotherapy agents that act by damaging DNA in cancer cells[19], [88]. This DNA damage is mainly studied by looking at the expression of *yH2AX*, which is known by the phosphorylation of the Ser-139 residue of the histone variant *H2AX*, a well-established marker for DNA double-strand breaks (DSBs) and is crucial in preserving genomic integrity by signaling and facilitating the repair of DNA DSBs[89], [90]. This was done by conducting an intracellular staining of *yH2AX* and DAPI by flow cytometry, allowing to differentiate the cell cycle phases in which DNA damage occurs. For example, cells in S phase might show higher *yH2AX* levels simply due to the fact, that DSBs occur during replication. Understanding when damage occurs within the cell cycle is vital and reveals repair process timing.

AML cell lines were treated with ARA-C and DNR with increasing concentrations, 25nM, 50nM and 2nM, 5nM, and 10 nM, respectively, for 48hrs. Then intracellular staining of yH2AX and DAPI was performed and analyzed by flow cytometry.

We observed an increase in DNA damage represented by *yH2AX* percentages upon treatment with both drugs. For instance, HL60 showed an increase of almost 50% in yH2AX, as shown in Figure 13, with the bivariate dot plots, and 14A, when treated with ARA-C at a concentration of 50nM. When looking at the histogram plot we observe an increase in S phase of the cell cycle in a dose dependent manner, suggesting that the DNA damage is occurring during S phase as ARA-C is mainly active in this phase. In contrast, when treated with DNR, only around 20% HL60 cells stained positive for of yH2AX this was mainly during G2 phase (sown in histogram plot) as it was increasing with increased drug concentration, suggesting that the DNA damage occurs during G2 phase as DNR is active during G2/M phases of the cell cycle. In MOLM13 cells, treatment with DNR resulted in 20% positive yH2AX cells, when treated with ARA-C only 15% of cells were positive (Supplementary figures 39 and 14B). In contrast to HL60 cells, we observed an arrest in G1 phase with constant increase when treated with ARA-C, in a dose dependent manner, and decrease when treated with DNR and increase in sub G1 as MOLM13 is the most sensitive cell line to it. OCI-AML3 cells, which showed a moderate response to both drugs in the MTT assay as mention above, had around 10% of yH2AX-positive cells upon treatment with ARA-C and 5% when treated with DNR (Supplementary Figure 40 and Figure 14C). Similarly to MOLM13, we observed

G1 arrest with a constant increase in a dose dependent manner when treated with both drugs. Suggesting that the DNA damage in MOLM13 and OCI-AML3 cells occurs in G1 phase of the cell cycle.

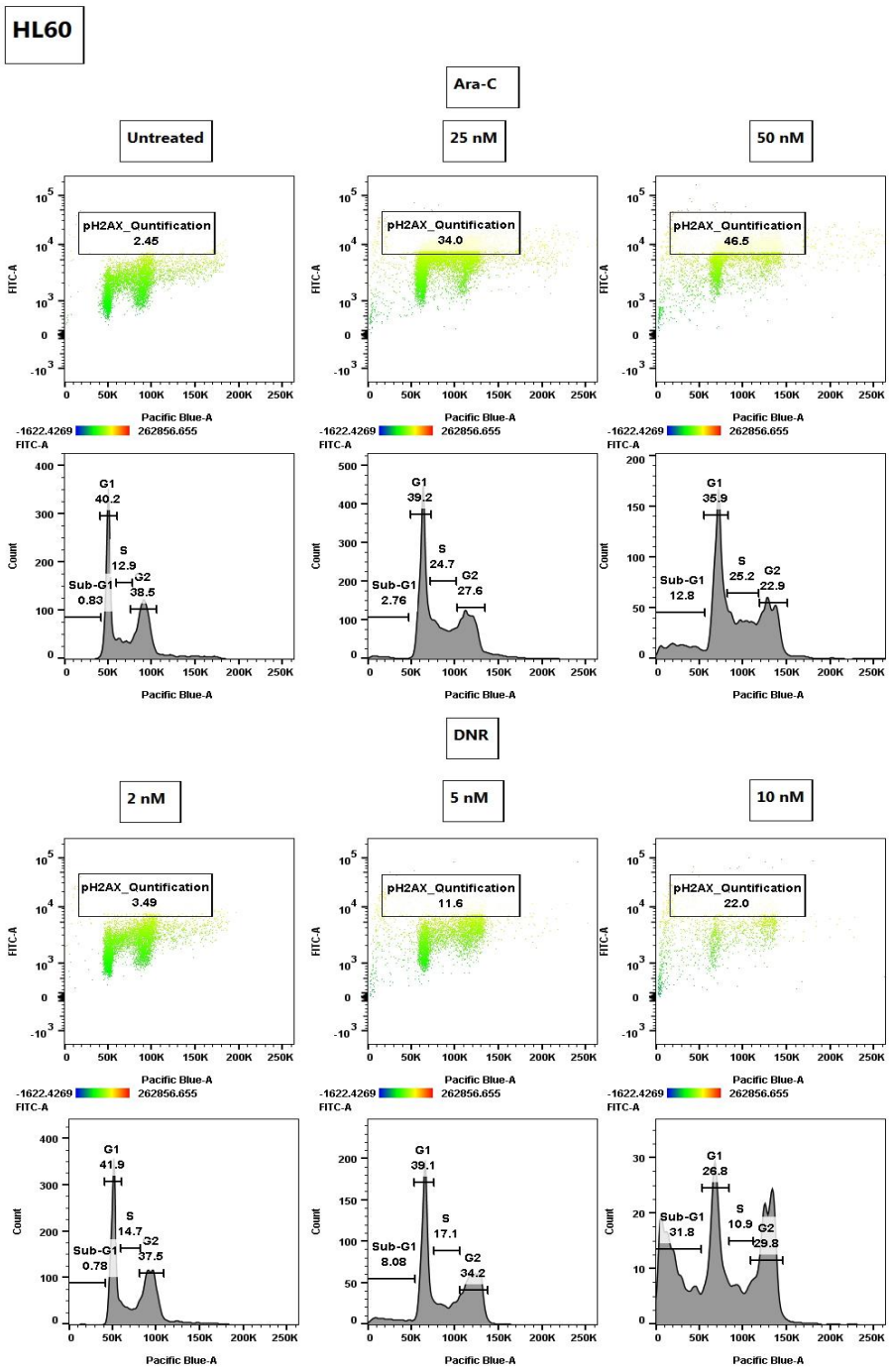


**Figure 13:DNA damage increases in dose dependent manner in HL60 cells.**

Flow cytometry analysis of yH2AX and cell cycle in HL60 cells, upon treatment with ARA-C and DNR with different concentrations as indicated for 48 hrs. Bivariate dot plots (upper panel for ARA-C and DNR) representing the changes in percentage of yH2AX before and upon treatment. Histogram plots (DAPI, lower panels for ARA-C and DNR) showing the distribution of cells in the phases (G1, S, G2) of the cell cycle.

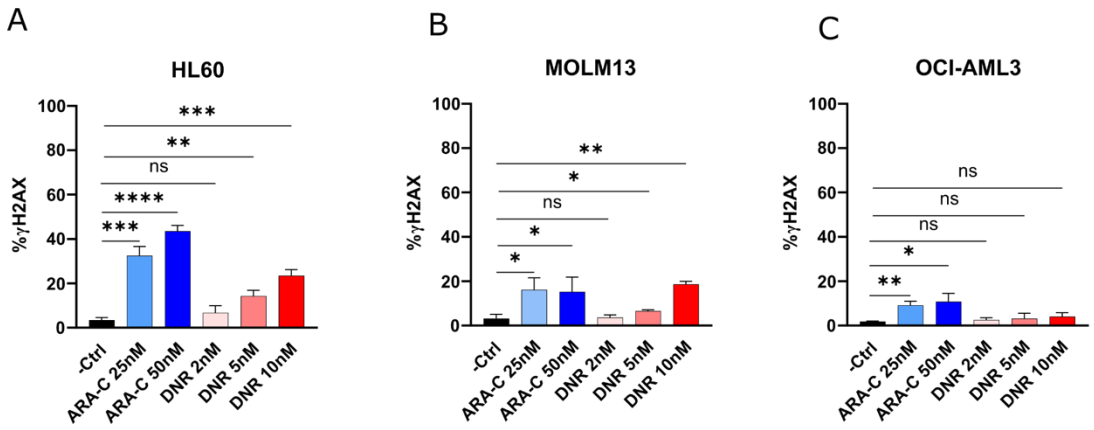


**Figure 14: Treatment with genotoxic drugs causes an increase in of yH2AX in a dose dependent manner.**

AML cell were treated with ARA-C (blue) and DNR (red) for 48 hours. Graph bars representing the percentage of *yH2AX* before and after treatment. Data are shown as mean ±SD of 3 independent experiments. Significances were calculated using unpaired t-test *<0.05, **<0.01, ***<0.001, ****<0.0001, ns: not significant.

Understanding how these drugs finally induce DNA damage has important implications for treatment and might have impact on treatment optimization and the development of new therapeutic strategies in AML. By studying how these cells respond to DNA damage induced by DNR and ARA-C, we can gain insights into the mechanisms of resistance and sensitivity in AML. Analyzing DNA damage repair pathways will help to better understand the described differential response of the cell lines.

HL-60, MOLM13 and OCI-AML3 cells were treated with either DNR or ARA-C for 24 hours (Figures 18, 19 and 20A). Next, we performed staining for yH2AX and simultaneously for several key DNA repair proteins that play vital roles in maintaining genomic integrity. First, we focused on RAD51. This protein is highly conserved across different species and is crucial for DNA repair through a process known as homologous recombination (HR)[21]. RAD51 not only facilitates the repair of damaged DNA but also influences how cells respond to treatments that cause DNA damage.

Second, we investigated 53BP1 expression and localization upon genotoxic treatment, an essential factor in the signaling and repairing of DNA DSBs. This protein is particularly active during the G1 phase of the cell cycle and is a key component of the non-homologous end joining

(NHEJ) pathway[22]. NHEJ is one of the primary mechanisms through which cells repair DSBs, ensuring that broken DNA ends are joined together efficiently.

Lastly, we analyzed RPA, a protein that binds to single-stranded DNA (ssDNA). RPA is involved in several important DNA repair mechanisms, including nucleotide excision repair (NER) and base excision repair (BER), as well as HR. RPA plays a critical role in stabilizing ssDNA, which is necessary for various DNA repair processes to occur effectively[23]. By immunofluorescence analysis for yH2AX and these DNA repair genes, we aimed to better understand the complex network of DNA damage responses and repair pathways within the cell (Figures 17, 18 and 19A).

To evaluate the DNA repair pathways activated in various cell lines, we measured the levels of yH2AX foci. These foci were examined both in relation to the previously mentioned DNA repair genes and on their own (Figures 17, 18 and 19B). Our results indicated that HL60 cells displayed the most significant DNA damage, as evidenced by the presence of yH2AX foci, particularly when subjected to treatment with ARA-C (Figures 15 and 17A). This level of damage was substantially higher than that observed in MOLM13 and OCI-AML3 cells in similar conditions (Figures 15 and 18A and 19A). Conversely, when we treated MOLM13 cells with DNR, the cells showed higher levels of DNA damage as compared to ARA-C treatment (Figure 15 and 18A).

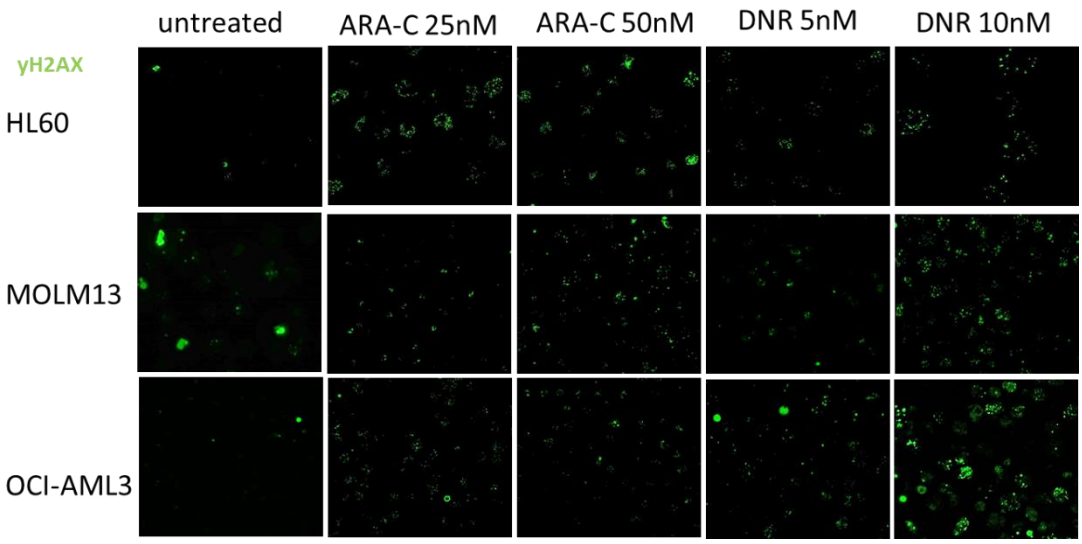


**Figure 15: DNA damage increases upon treatment with genotoxic drugs.**

Representative immunofluorescence images of γH2AX in HL60, MOLM13 and OCI-AML3 before and upon treatment with ARA-C and DNR at indicated concentrations for24 hrs.

To be able to determine the DNA repair pathway that is primarily used in the different AML cell lines, we analyzed the number of co-localized γH2AX foci (in 200 cells with > 5 foci) with each of the DNA repair genes. Representative examples of co-localization of γH2AX with the DNA repair protein 53BP1 in HL60 and MOLM13 cells is shown in Figure 16. Additional data showing the co-localization of γH2AX with each of the above-mentioned DNA repair proteins can be found in Supplementary Figures 41-43.

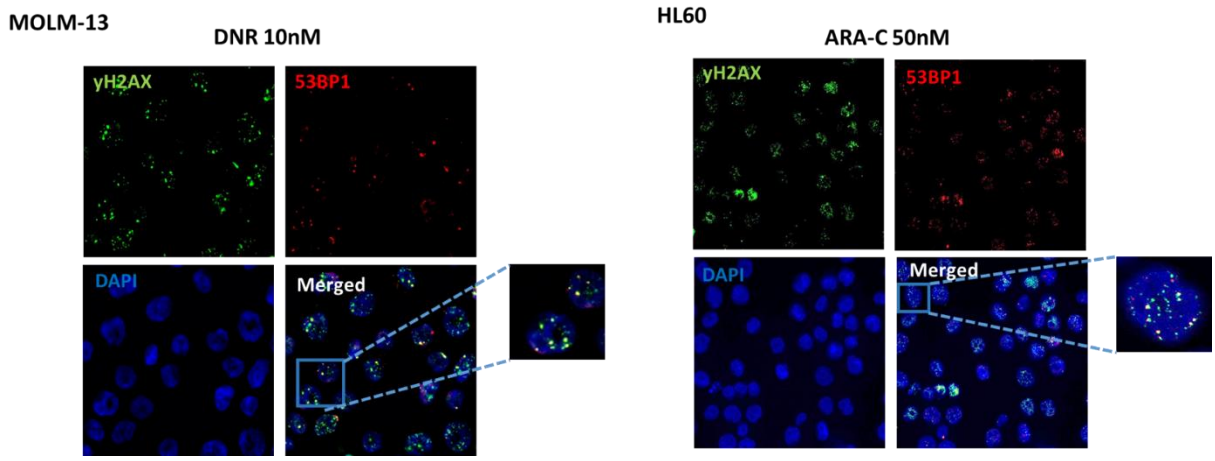


***Figure 16: 53BP1 co-localizes with γH2AX.***

Representative immunofluorescence images of HL60 and MOLM13 cells stained with DAPI (blue), γH2AX (green) and 53BP1 (red) upon treatment with DNR and ARA-C with indicated concentrations for 24 hrs, respectively.

In HL60 cells, foci with co-localization of γH2AX with RAD51 or 53BP1 was around 70% of all γH2AX foci upon treatment with ARA-C. In contrast, repair of DNR-mediated DSBs was strongly linked to NHEJ, as almost all γH2AX-foci showed co-localization with 53BP1. Co-localization with RPA was only detected in a minority of treated cells (Figure 17B).

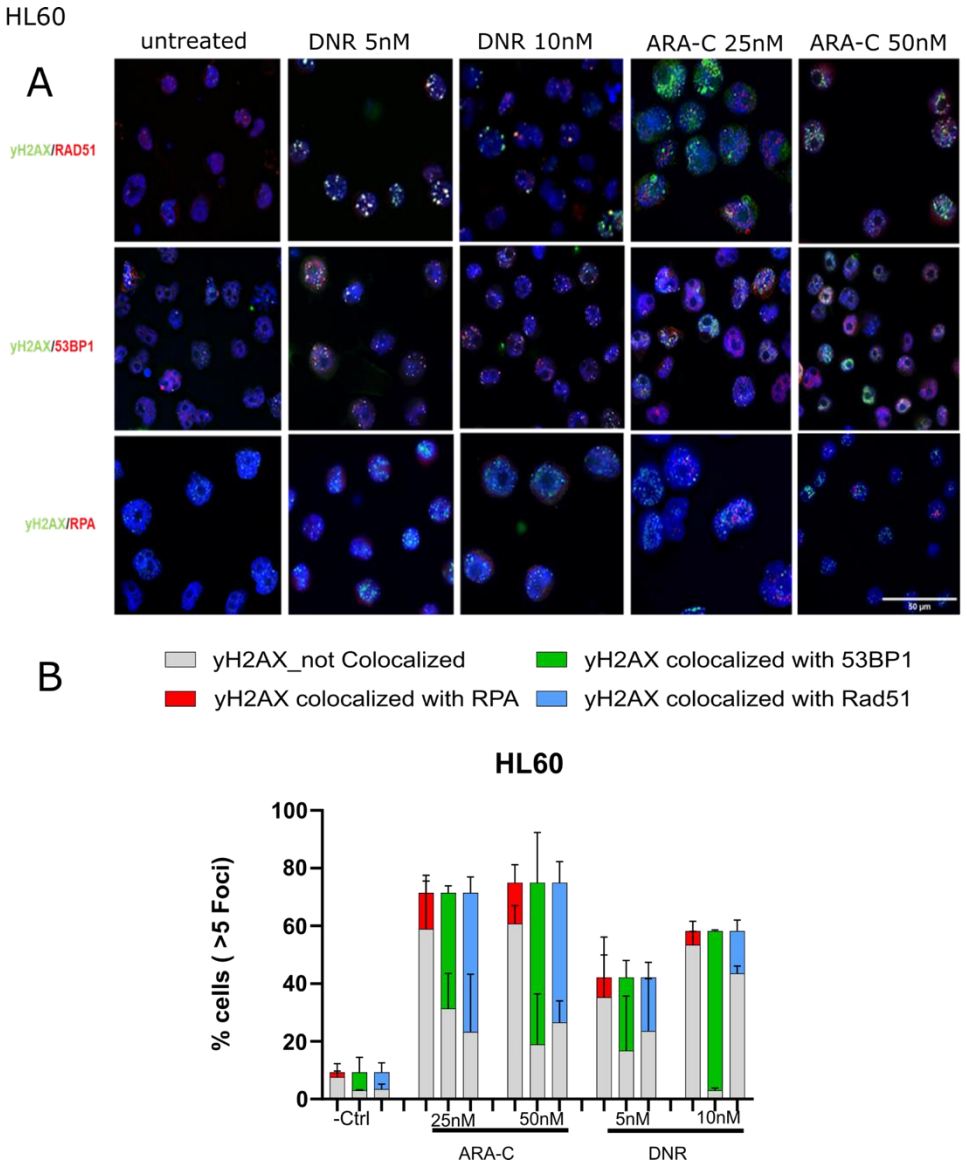


**Figure 17: DNA damage response in HL60 cell line upon treatment with genotoxic drugs.**

(A) Immunofluorescence analysis of γH2AX and RAD51, 53BP1 and RPA foci upon treatment of HL60 cells with DNR and ARA-C as indicated for 24 hours. (B) Quantification of chemotherapy induced foci and co-localization of γH2AX with indicated proteins. 200 cells that have more than five γH2AX foci were considered as positive. Shown is the mean ±SD of 2 independent experiments.

In MOLM13 cells, *RAD51* was co-localized in 50% of all *γH2AX* foci and *53BP1* in 40% upon treatment with ARA-C. In contrast to HL60 cells, co-localization of *53BP1* with *γH2AX* foci was diminished upon DNR treatment, indicating that NHEJ is required to repair DNA damage in MOLM13 cells (Figure 18B).

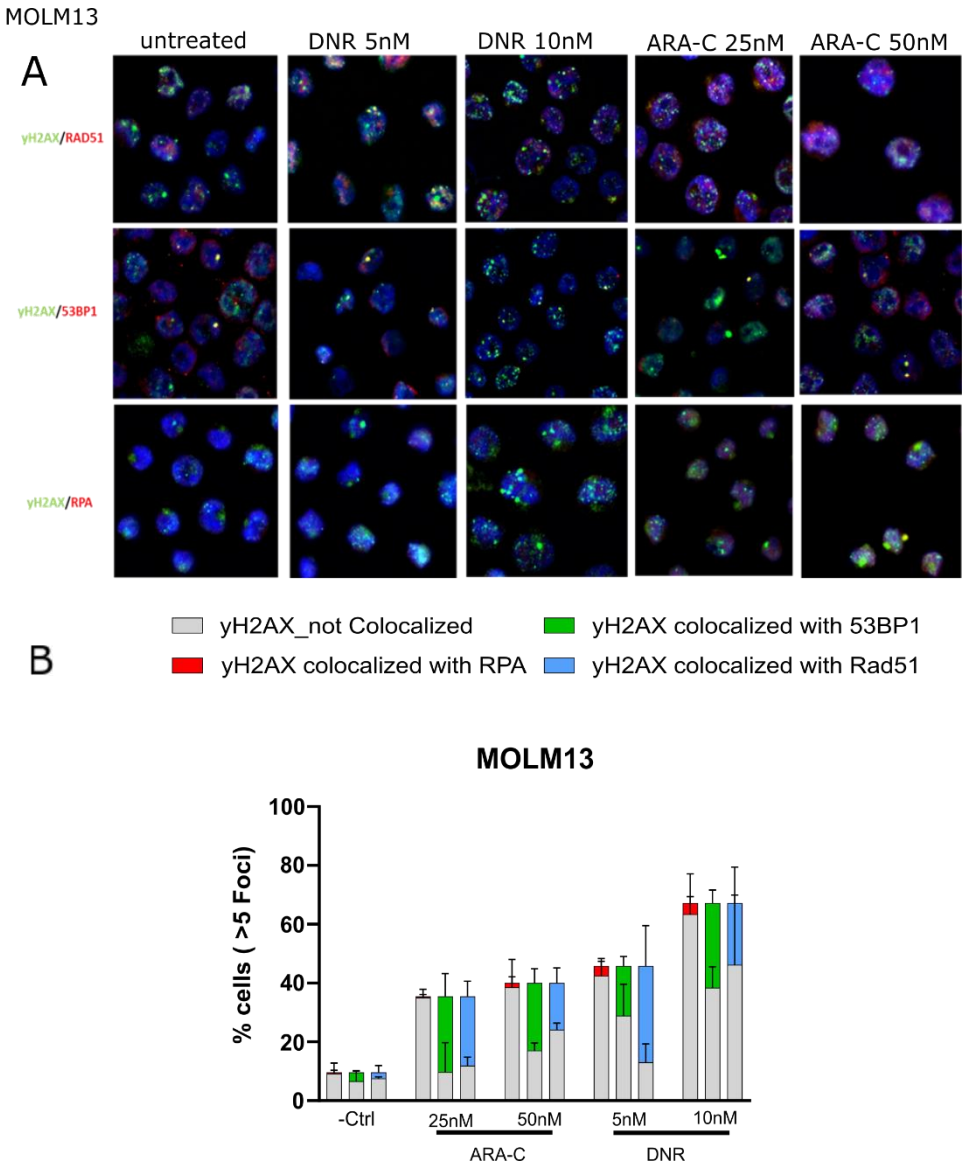


**Figure 18: DNA damage response in MOLM13 cell line upon treatment with genotoxic drugs.**

(A) Immunofluorescence analysis of γH2AX and RAD51, 53BP1 and RPA foci upon treatment of MOLM13 cells with DNR and ARA-C as indicated for 24 hours. (B) Quantification of chemotherapy induced foci and co-localization of γH2AX with indicated proteins. 200 cells that have more than five γH2AX foci were considered as positive. Shown is the mean ±SD of 2 independent experiments.

In OCI-AML3 cells, 53BP1 was co-localized with 50% of all γH2AX foci upon treatment with ARA-C (25nM), and RAD51 was co-localized with only 30%. Similarly, when treated with DNR, co-localization of 53BP1 with γH2AX was higher than for RAD51 with 53BP1 being co-localized with

50% of γH2AX (10nM) and RAD51 40% of all γH2AX, suggesting that NHEJ is taking place to repair the damaged DNA in OCI-AML3 cells which may explain the moderate response of these cells to both drugs (Figure 19B).

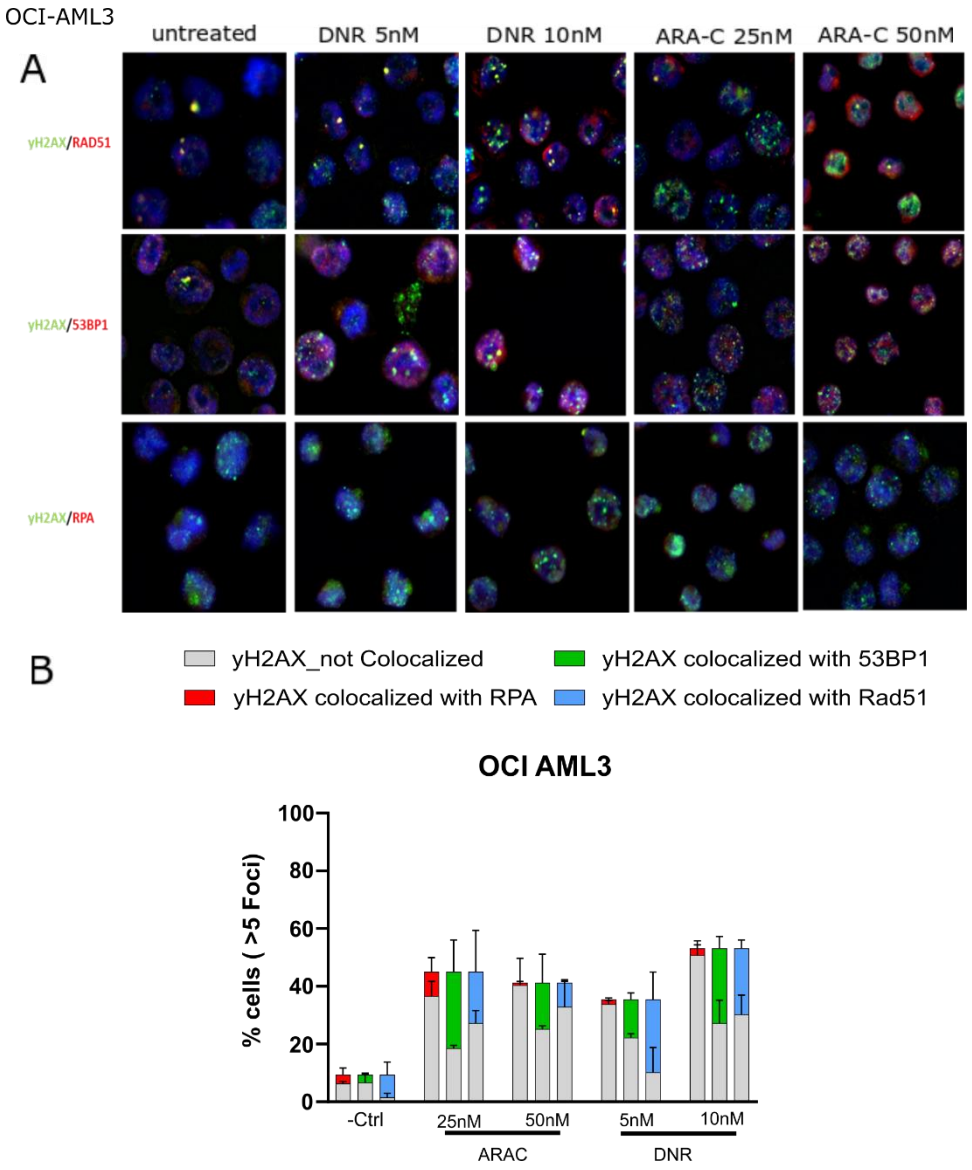


**Figure 19: DNA damage response in OCI-AML3 cell line upon treatment with genotoxic drugs.**

(A) Immunofluorescence analysis of γH2AX and RAD51, 53BP1 and RPA foci upon treatment of OCI-AML3 cells with DNR and ARA-C as indicated for 24 hours. (B) Quantification of chemotherapy induced foci and co-localization of γH2AX with indicated proteins. 200 cells that have more than five γH2AX foci were considered as positive. Shown is the mean ±SD of 2 independent experiments.

Next, we quantified the number of co-localized RAD51 and 53BP1 foci compared to the total number of all foci for each protein in HL60 cells (Figure 20 A and C). . Interestingly, the number of RAD51 foci was greater than both 53BP1 and RPA foci. This observation suggests either a potentially stronger role for RAD51 in the DNA repair process within these cell lines or being just present during S phase of the cell cycle[91]. However, it is important to note that from the total number of 53BP1 foci, around 60% were found to co-localize with yH2AX foci. In contrast, the co-localization between RAD51 and yH2AX was less consistent, with 30% of the RAD51 foci showing co-localization with yH2AX foci, except when treated with ARA-C with a concentration of 50 nM that was slightly higher (60%) (Figure 20 B and D). This distinction may highlight differences in the functional roles of these repair proteins in response to DNA damage in HL60. Suggesting that the cells prefer NHEJ repair pathway over HR, in HL60 cells (Figure 20).

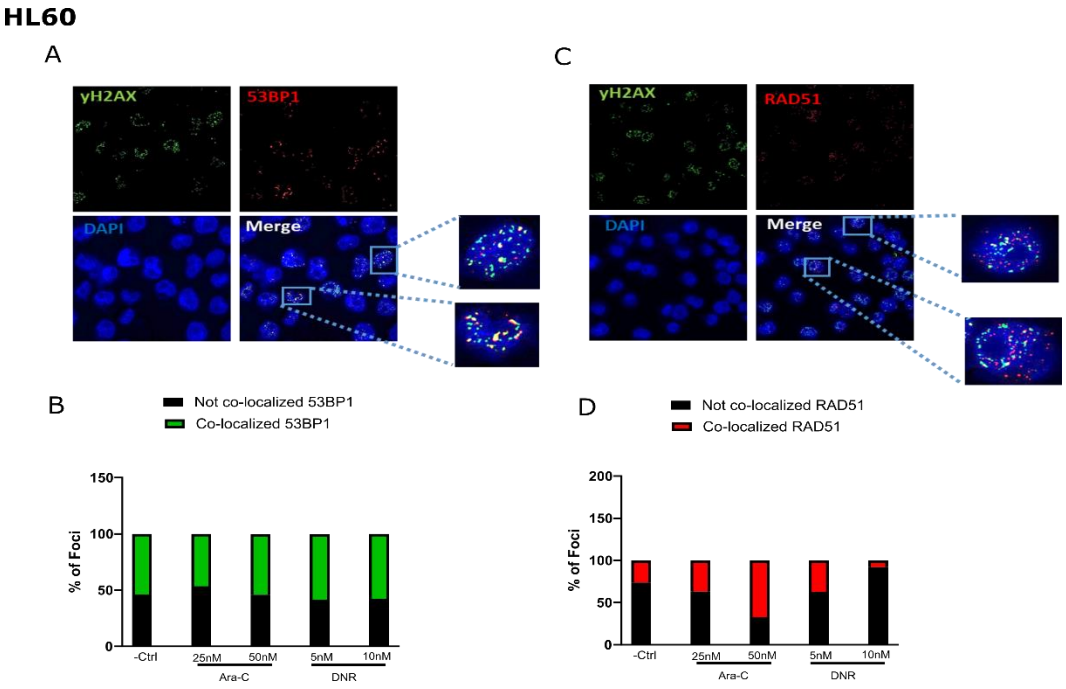


**Figure 20: Involvement of DNA repair genes in DNA repair.**

(A) and (C) Representative immunofluorescence staining of γH2AX (Ser 139) and 53BP1 and RAD51 foci upon ARA-C treatment showing the co-localization of γH2AX foci with 53BP1 foci (A) and with RAD51 foci (C) in HL60 cells. (B) and (D) show graph bars representing the number of co-localized 53BP1 and RAD51 foci with γH2AX foci. 200 cells that have more than five γH2AX foci were considered as positive. Shown is data of one experiment.

## 4.3 R-**Loops** in AML cell lines

### 4.3.1 R-loop formation **and** quantification in AML cells applying dot blot analysis

To measure the levels of R-loops in AML cell lines, we conducted experiments before and after treatment with DNR and ARA-C. We utilized the S9.6 antibody, which specifically binds to RNA:DNA hybrids, for our analysis. This was performed using a dot blot assay, which allowed us to visualize the presence of R-loops (Figures 21, 22, 23A).

Upon treatment with ARA-C, HL-60 cells demonstrated the highest levels of R-loops among the three tested cell lines, showing a steady increase over time, as illustrated in Figure 21B. In comparison, MOLM13 and OCI-AML3 cell lines exhibited significantly lower levels of R-loops upon treatment with ARA-C at the same time points (Figures 22B-C and 23B-C).

Conversely, when we treated the cells with DNR, the results differed. MOLM13 cells showed the highest R-loop levels, particularly after longer treatment durations (Figure 22B). In contrast, HL60 and OCI-AML3 cells formed fewer R-loops following DNR treatment (Figures 21B-C and 23B-C). These findings suggest that the R-loop dynamics in AML cell lines can be linked to the drug-induced cytotoxicity and sensitivity.

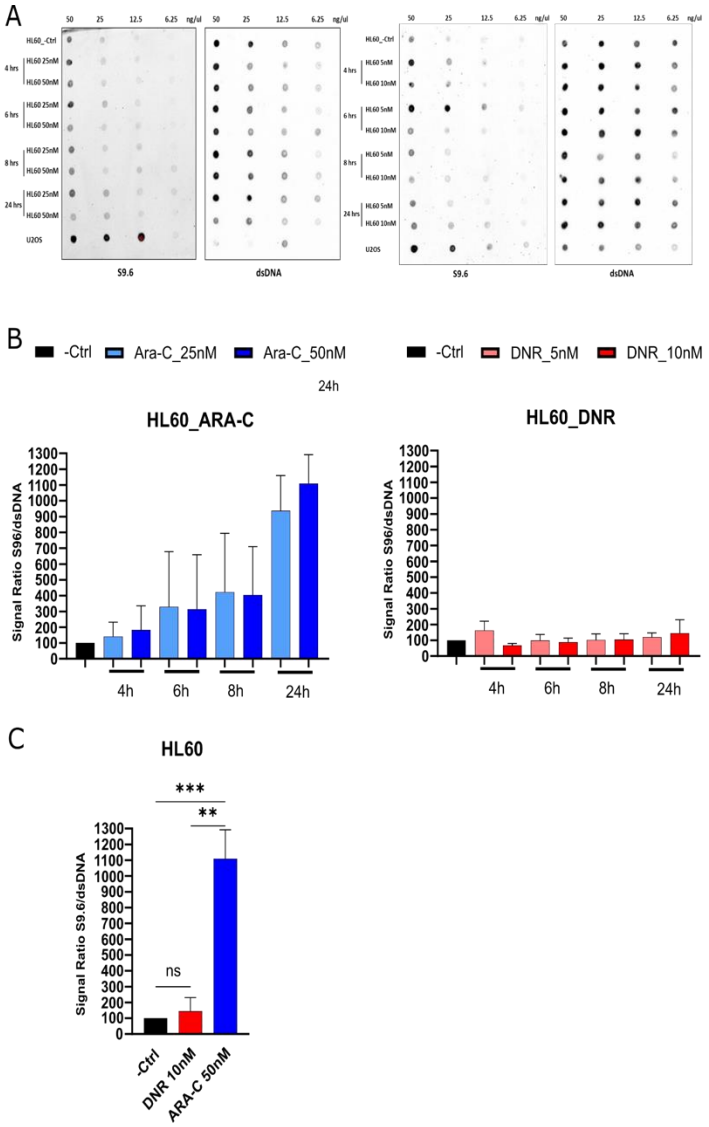


**Figure 21: R-loop levels increase in dose and time dependent manner in HL60 cells.**

(A) Dot Blot assay demonstrating R-loop formation upon treatment of HL60 cells with DNR and ARA-C for different concentrations and time points as indicated using the S9.6 antibody that specifically binds to RNA-DNA hybrids (left panel). The dsDNA membrane was incubated with an antibody directed against dsDNA (right panel). (B) R-loop quantification was performed by calculating the signal ratio of S9.6/dsDNA. Graph bars show R-loops level quantification before and after treatment as indicated. (C) Graph bars showing comparison between R-loop levels after treatment with ARA-C and DNR after 24hrs. Shown is the mean ±SD of 3 independent experiments. Significances were calculated using unpaired t-test ns: not significant (p= 0.4148), *** p=0.0007.

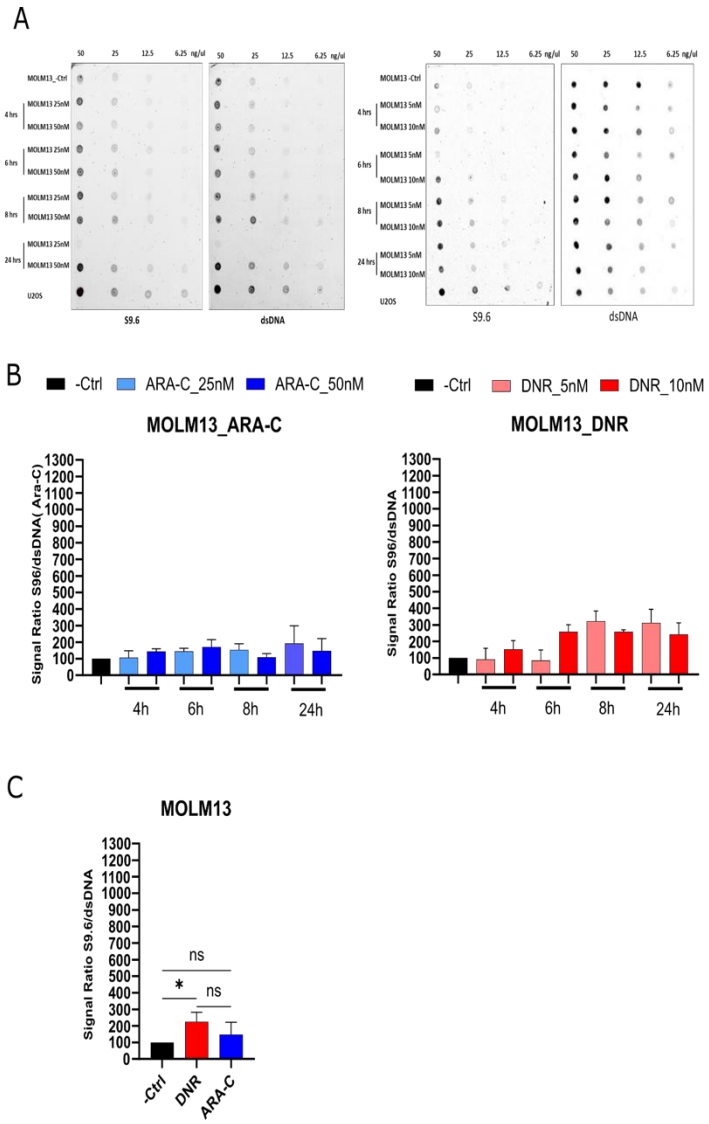


**Figure 22: R-loop levels increase in dose and time dependent manner in MOLM13 cells.**

(A) Dot Blot assay demonstrating R-loop formation upon treatment of MOLM13 cells with DNR and ARA-C for different concentrations and time points as indicated using the S9.6 antibody that specifically binds to RNA-DNA hybrids (left panel). The dsDNA membrane was incubated with an antibody directed against dsDNA (right panel). (B) R-loop quantification was performed by calculating the signal ratio of S9.6/dsDNA. Graph bars show R-loops level quantification before and after treatment as indicated. (C) Graph bars showing comparison between R-loop levels after treatment with ARA-C and DNR after 24hrs. Shown is the mean ±SD of 3 independent experiments. Significances were calculated using unpaired t-test. ns: not significant p=0.3265, * p=0.0199.

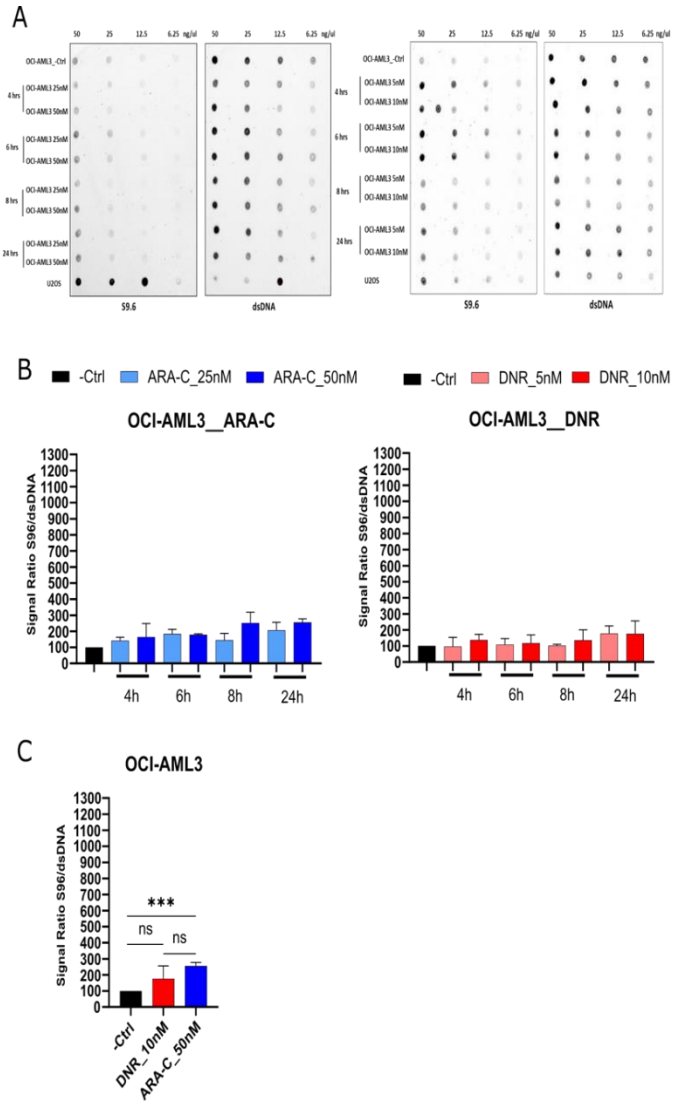


**Figure 23: R-loop levels increase in dose and time dependent manner.**

(A) Dot
Blot assay demonstrating R-loop formation upon treatment of OCI-AML3 cells with DNR and ARA-C for different concentrations and time points as indicated using the S9.6 antibody that specifically binds to RNA-DNA hybrids (left panel). The dsDNA membrane was incubated with an antibody directed against dsDNA (right panel). (B) R-loop quantification was performed by calculating the signal ratio of S9.6/dsDNA. Graph bars show R-loops level quantification before and after treatment as indicated. (C) Graph bars showing comparison between R-loop levels after treatment with ARA-C and DNR after 24hrs. Shown is the mean ±SD of 3 independent experiments. Significances were calculated using unpaired t-test. ns: not significant (p=0.1747), *** p=0.0003.

### 4.3.2 R-loop formation and quantification in AML cells applying immunofluorescence analysis

To better understand the role of R-loops related to cell sensitivity to genotoxic therapy and to further confirm our dot blot results, we performed an immunofluorescence (IF) analysis . For this, we used a probe consisting of the hybrid binding domain (HBD) purified from RNaseH1 and tagged

with the Alexa 647 fluorochrome. This probe was generously provided by the Beli Lab at the IMB (Figure 24).

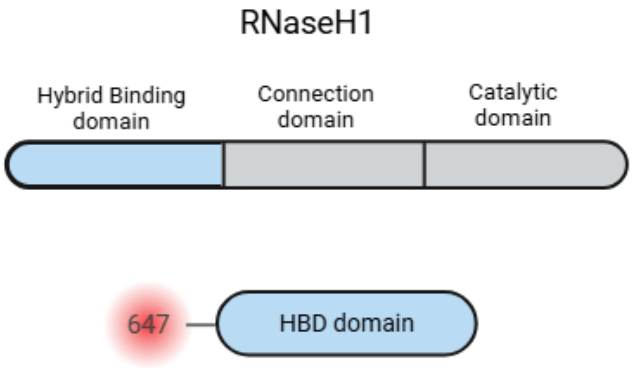


**Figure 24: RNaseH1 HBD probe for immunofluorescence (IF) staining of R-loop.** Created in BioRender.com

To assess the efficiency of the RNaseH1 HBD probe, we conducted an immunofluorescence (IF) staining assay in AML cells. This was done both prior to treatment with DNR and ARA-C, which served as a negative control and after a 24-hour treatment period with these drugs. The purpose of this approach was to measure the nuclear mean intensity, which is expected to indicate the presence of R-loops within the cells.

In addition, as a more reliable control, we utilized AML cells that overexpressed RNaseH1. The overexpression of this enzyme was intended to eliminate R-loops, which should result in a significant reduction or complete disappearance of the R-loop signal in the stained samples. In addition to this, we also included a mutant version of RNaseH1, referred to as WKKD. This mutant lacks the ability to bind to R-loops, allowing the R-loops to remain intact. By comparing these different setups, we aimed to gain insights into the detection and role of R-loops in the context of AML treatment (Figure 25A). A quantification of R-loops in all conditions mentioned above was done (Figure 25B).

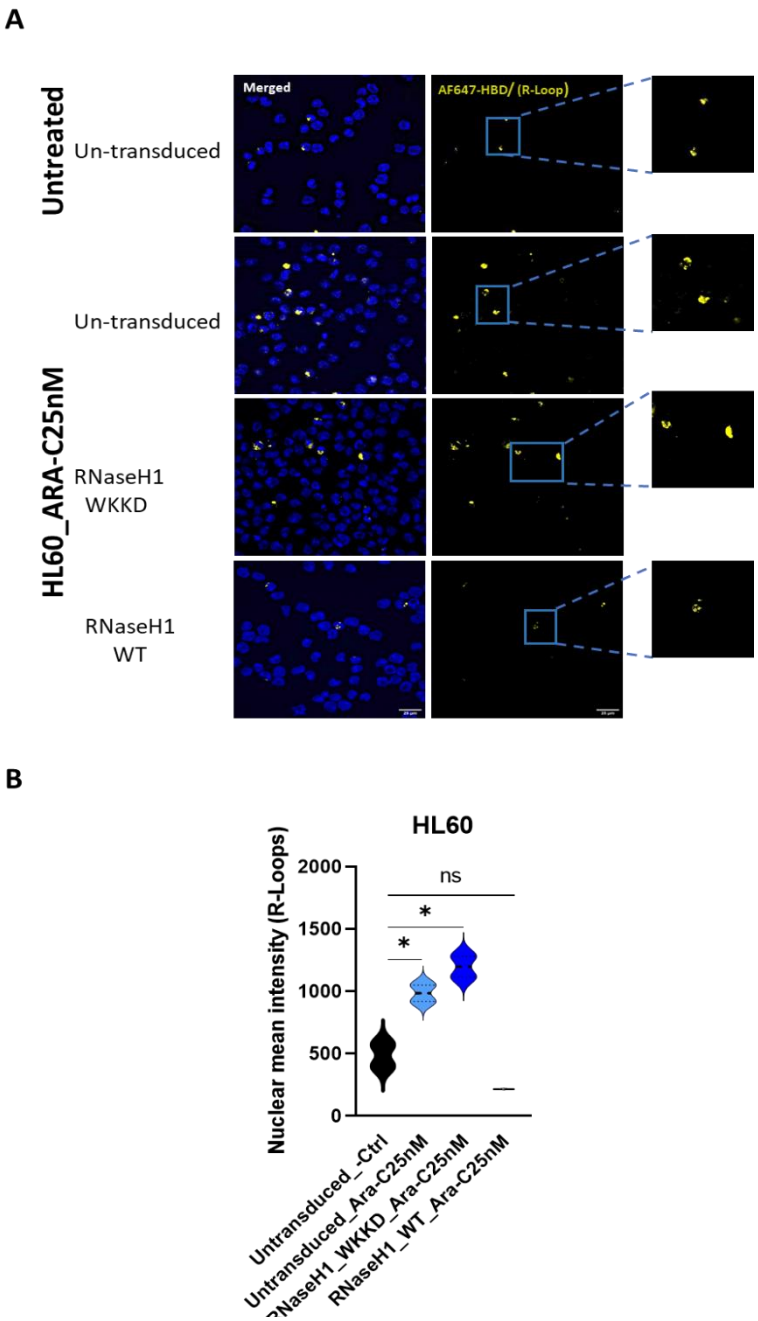


**Figure 25: Immunofluorescence analyses of R-loops to check the efficiency of HBD-RNaseH1 probe.**

(A) R-loop signal represented by the mean nuclear intensity increased after treatment with ARA-C in un-transduced HL60 cells. However, significant signal reduction was observed following the removal of R-loops by RNaseH1-WT but not mutant RNaseH1-WKKD after ARA-C treatment. (B) Violin plot representing R-loop signal quantification before and after removal of R-loops upon treatment with ARA-C. Shown is the mean ±SD of two independent experiments. Significances were calculated using unpaired t-test ns: not significant, * $p < 0.05$; ns: not significant. Scale bar 25µm.

After testing and confirming the efficiency of the RNaseH1 HBD probe, we proceeded to conduct experiments treating HL60 and MOLM13 cells with ARA-C and DNR for 24hrs. Upon treatment,

we stained HL60 and MOLM13 cells to visualize R-loops and DAPI as shown in Figures 26 and 27, respectively. We observed a notable increase in the R-loop signal in HL60 cells, in particular when treated with ARA-C at a concentration of 50 nM with a mean nuclear intensity (MNI) of around 3.000 as shown in Figure 28A. In contrast, MOLM13 cells exhibited the highest R-loop MNI exceeding 3.000 when treated with DNR (Figure 28B). These data confirm our findings of the dot blot assays and reinforce the correlation between treatment-mediated cytotoxicity and R-loop formation.

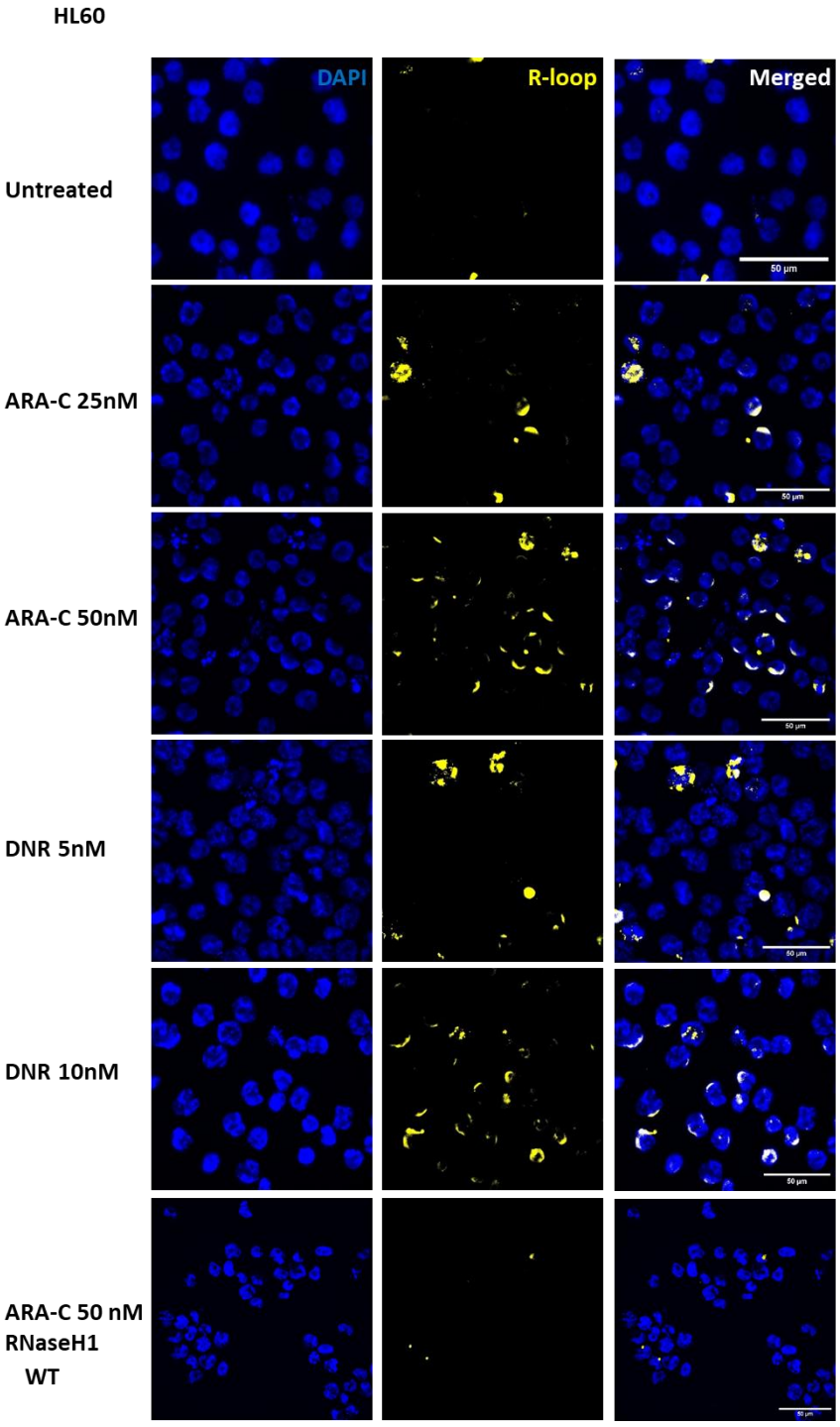


**Figure 26: Cytarabine induces more R-loop formation in HL60 cells.**

Representative immunofluorescence images of HL60 cells stained with DAPI (blue) and RNaseH1 HBD probe (yellow) upon ARA-C and DNR treatment as indicated for 24 hours. Scale bar 50µm.

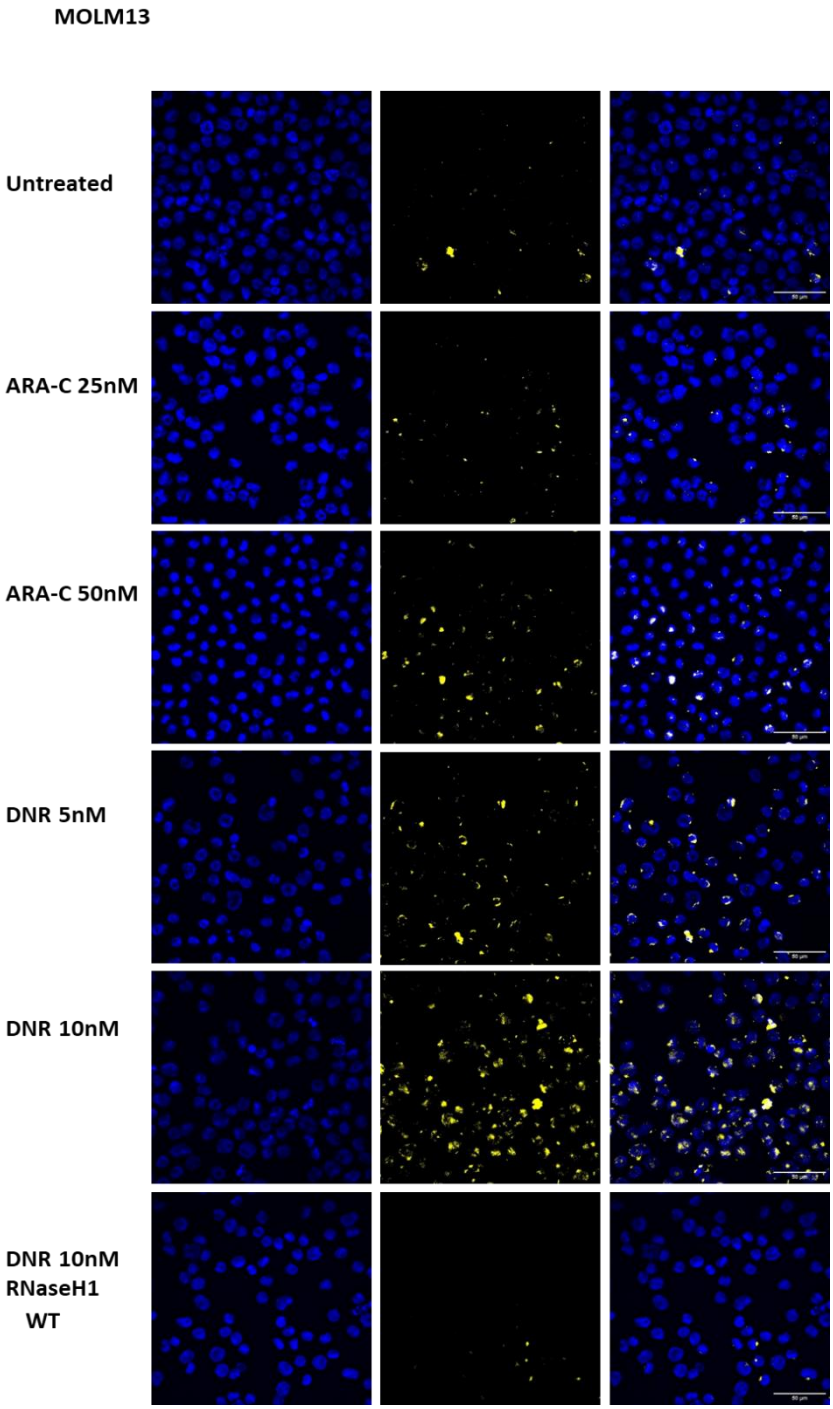


**Figure 27: Daunorubicin induces more R-loop formation in MOLM13 cells.**

Representative immunofluorescence images of MOLM13 cells stained with DAPI (blue) and RNaseH1 HBD probe. (yellow) upon ARA-C and DNR treatment as indicated for 24 hours. Scale bar 50µm.

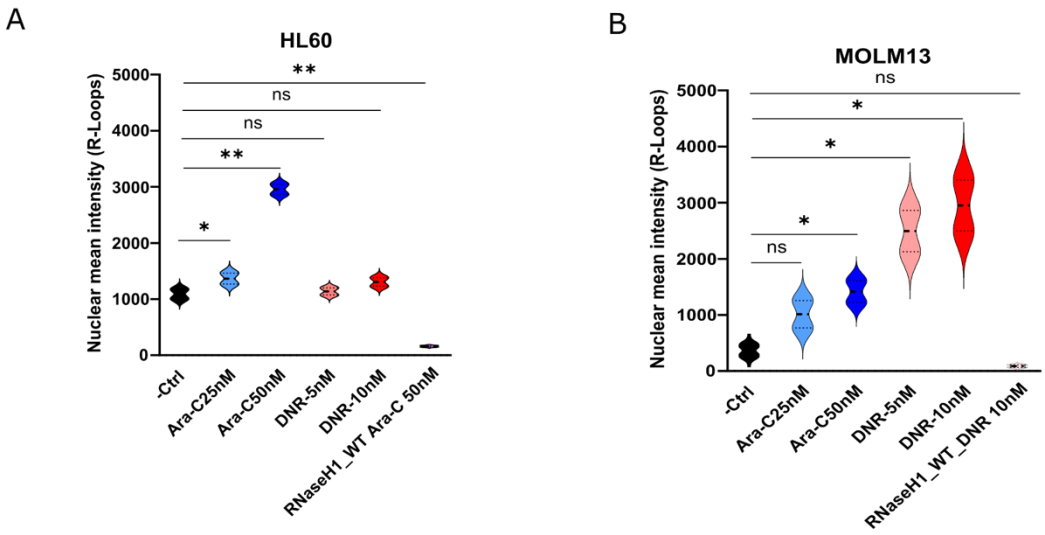


***Figure 28: R-loop levels upon treatment with ARA-C and DNR in HL60 and MOLM13 cells.***

HL60 cells (left panel) and MOLM13 cells (right panel) were treated with ARA-C or DNR at indicated concentrations for 24 hours. Shown is the mean nuclear intensity of R-loop staining using the RNaseH1 HBD probe. As a negative control, cells were transduced with RNaseH1-wild type (WT) and treated with ARA-C (blue) or DNR (red). Shown is the mean ±SD of 2 independent experiments. Significances were calculated using unpaired t-test *<0.05, **<0.01, ns: not significant.

### 4.3.3 Analysis of gene expression upon treatment with DNR and ARA-C

To understand how chemotherapy-mediated R-loop formation is regulated at the transcriptional level and the relationship between the constant formation and accumulation of R-loops upon drug-induced cell damage, we sought to investigate the expression of specific factors and genes that regulate R-loops.

First, we took advantage of already existing RNA-seq data-sets of HL60, MOLM13 and OCI-AML3 cells before and after treatment with ARA-C, DNR or both drugs, which was performed by our collaboration partner Piyush More in the Woinowsky laboratory. Here, we focused our analysis on selected genes playing important roles in in R-loop regulation: *RAD51* is involved in the formation of R-loops[32], *SSRP1*, *SRSF1*, and *TOP1* help to prevent R-loop formation[92], and RNaseH1 is responsible for removing them[92]. Further we investigated the expression of levels of *SETX, DDX1 and DDX9*, which are involved in R-loop removal.

Our results indicated a significant upregulation of RAD51 expression (Figure 29A) in HL-60 cells upon treatment with both drugs, while no similar increase was observed in the other two cell lines. Moreover, we found downregulation of *DDX1*, *DDX9* and RNaseH1 (Figures 29B, C, D) and upregulation of *STEX* (Figure 29E), all of which play crucial roles in the removal of R-loops[92]. There was also a decrease in the expression of the prevention genes *TOP1*, *SRSF1*, and *SSRP1* (Figure 29F, G, H) in HL-60 cells[92]. This observed effects occurred independently of ARA-C or DNR drug treatment. In contrast, in MOLM13 cells most genes were primarily regulated by DNR treatment compared to ARA-C. The regulation of R-loop genes was less pronounced in the OCI-AML3 cell line and in most cases was likely induced by DNR and not ARA-C similar to MOLM13. These observations are in line with the persistent presence of R-loops in cells undergoing cytotoxic therapy and support the hypothesis, that formation and persistence of R-loops play a role in cytotoxic effects in AML treatment.

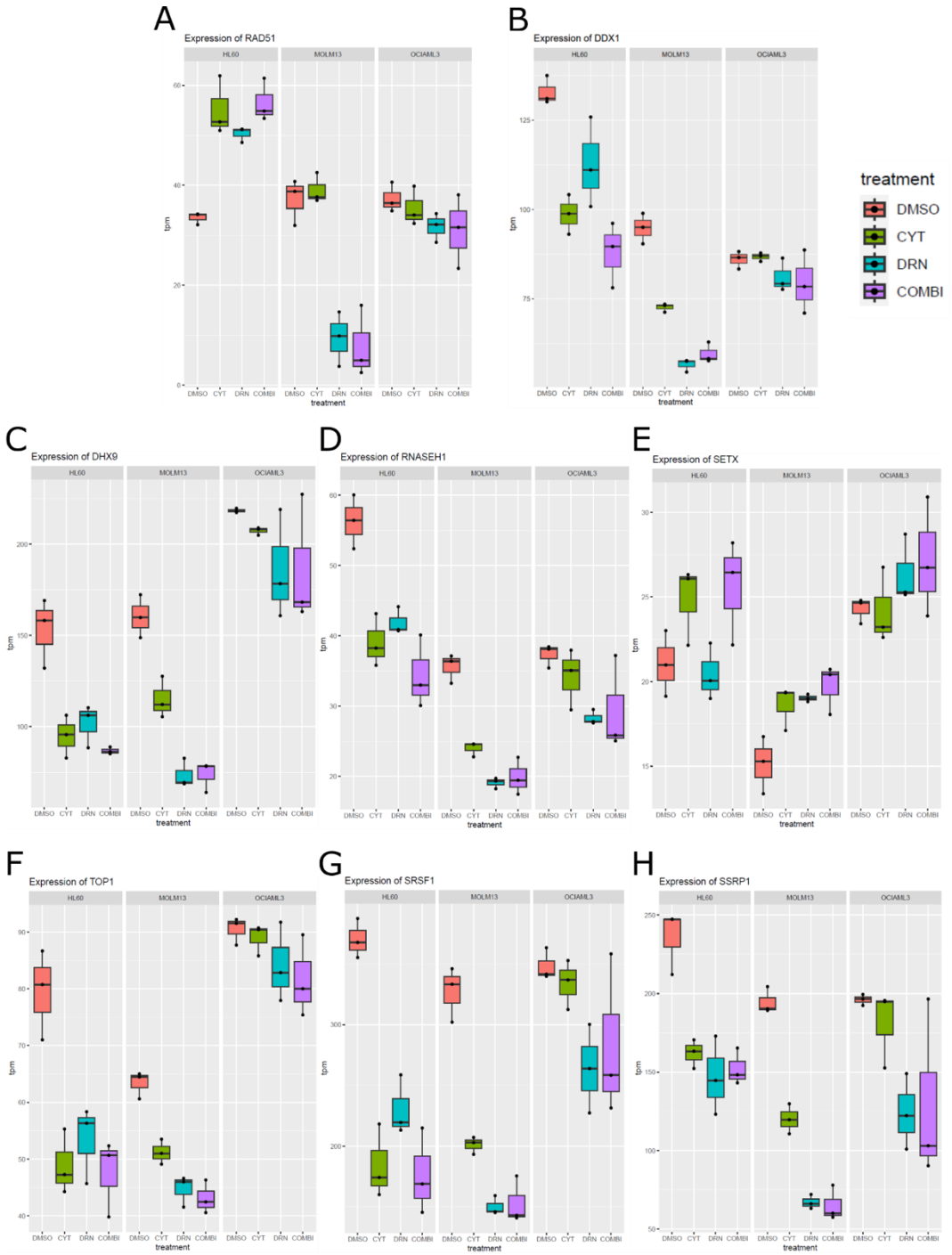


**Figure 29: Genes regulating R-loops exhibit altered expression after chemotherapy in AML cell lines.**.

RNA-seq analysis representing the expression of genes involved in R-loop regulation in absence and upon treatment with DNR and Ara-C with concentrations 0.02 µM and 0.1 µM respectively, either alone or in combination for 24 hour, in AML cell lines. Shown are transcripts per million (tpm) for each gene

To investigate time kinetics of expression of R-loop genes upon treatment, we conducted quantitative reverse transcription polymerase chain reaction (qRT-PCR). In the HL60 cells, we observed a 2-fold increase of the *RAD51* expression following treatment with DNR and ARA-C (Figure 30). Expression of RAD51 persisted over time upon treatment with ARA-C, but declined over time upon treatment with DNR, which is in line with the observed increase in the number of R-loops upon ARA-C treatment (Figure 30). Moreover, we noted a decrease in the expression of *SSPR1*, *SRSF1* and *TOP1* and only minor changes in RNaseH1 expression (Figure 30) independent of the used drugs.

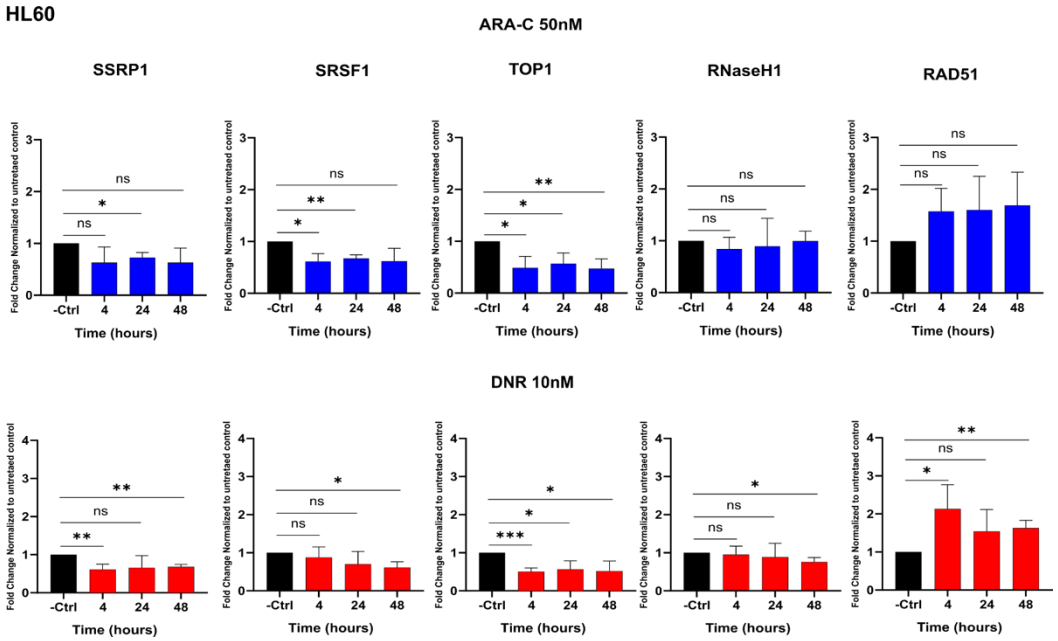


**Figure 30: Expression of genes regulating R-loops formation upon chemotherapy in HL60 cell line.**

qRT-PCR analysis of gene expression of R-loop-regulating genes before and after treatment with ARA-C (blue, upper panel) and DNR (red, lower panel) in HL60 cells for indicated time points and concentrations. Shown is the mean of 3 independent biological replicates. Significances were calculated using unpaired t-test *<0.05, **<0.01, ***<0.001, ns: not significant.

In the MOLM13 cell line, the pattern of gene expression was different. We observed a decrease in the expression levels of all examined genes when treated with both drugs (Figure 31). This downregulation was notably more pronounced upon DNR, highlighting the varying cellular responses to this specific chemotherapeutic agent by MOLM13 cell line. Interestingly, RAD51 was not up-regulated in MOLM13 cells, neither by ARA-C nor DNR. These findings point to a complex interaction between R-loop regulation and chemotherapy, leading to distinct responses in different cell lines.

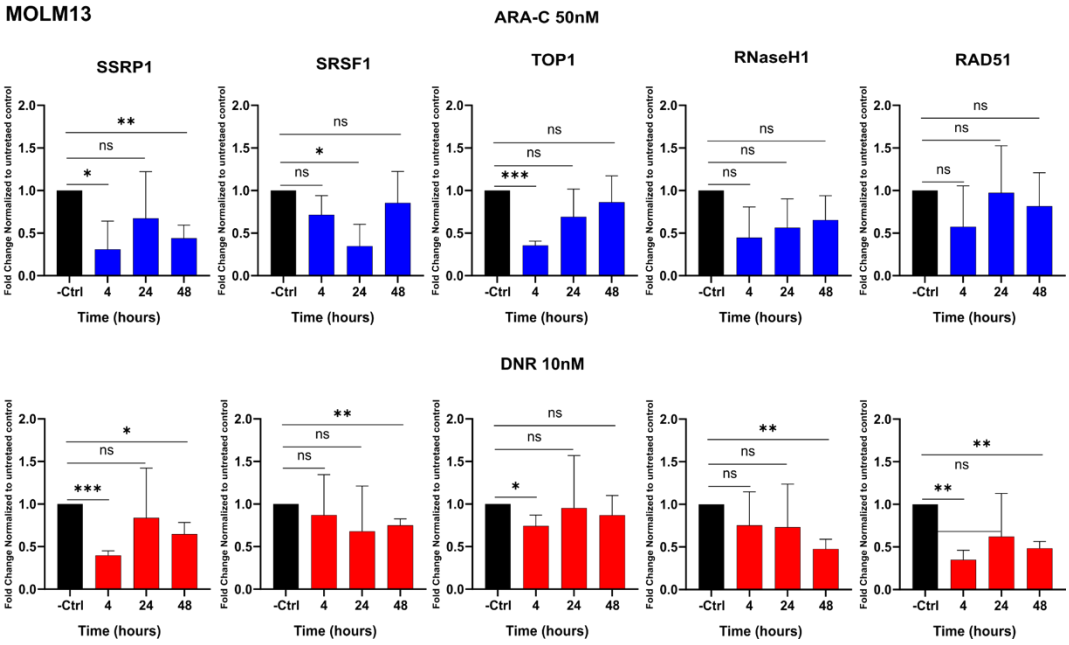


**Figure 31: Expression of Genes regulating R-loops changes upon chemotherapy in MOLM13 cell line.**

qRT-PCR analysis of gene expression of R-loop regulating genes before and after treatment with ARA-C (blue, upper panel) and DNR (red, lower panel) in HL60 cells for indicated time points and concentrations. Shown is the mean of 3 independent biological replicates. Significances were calculated using unpaired t-test *<0.05, **<0.01, ***<0.001, ns: not significant.

## 4.4 Functional analysis of role of R-loops in treatment response

### 4.4.1 Removal of R-loops by overexpression of RNaseH1

The quantification of R-loop formation upon treatment with cytotoxic drugs by dot-blot technique or immunofluorescence staining using the RNaseH1 probe suggests a possible connection between the presence of R-loops and the effects of drug-induced cell death. To explore this hypothesis further, we overexpressed RNaseH1 to remove spontaneous and drug-induced R-loops. RNaseH1 is an enzyme that specifically targets RNA-DNA hybrids and enzymatically cuts the RNA component of the hybrid by endonucleolytic cleavage [16].

We speculate that the removal of R-loops will result in resistance upon treatment with cytotoxic drugs in our AML cell lines.

In our experimental set-up, we overexpressed either i) wild-tpye (WT) RNaseH1, which is fully functional. The WT protein can catalyze reactions and effectively binds to R-loops to help resolve them; ii) a catalytically inactive variant of RNaseH1 (D210N), which cannot catalyze reactions but retains the ability to bind to R-loops; and iii) a double mutant RNaseH1 (WKKD), which is both, catalytically inactive and unable to bind to R-loops. As a result, it helps to preserve the R-loops rather than resolving or binding to them (Figure 32).

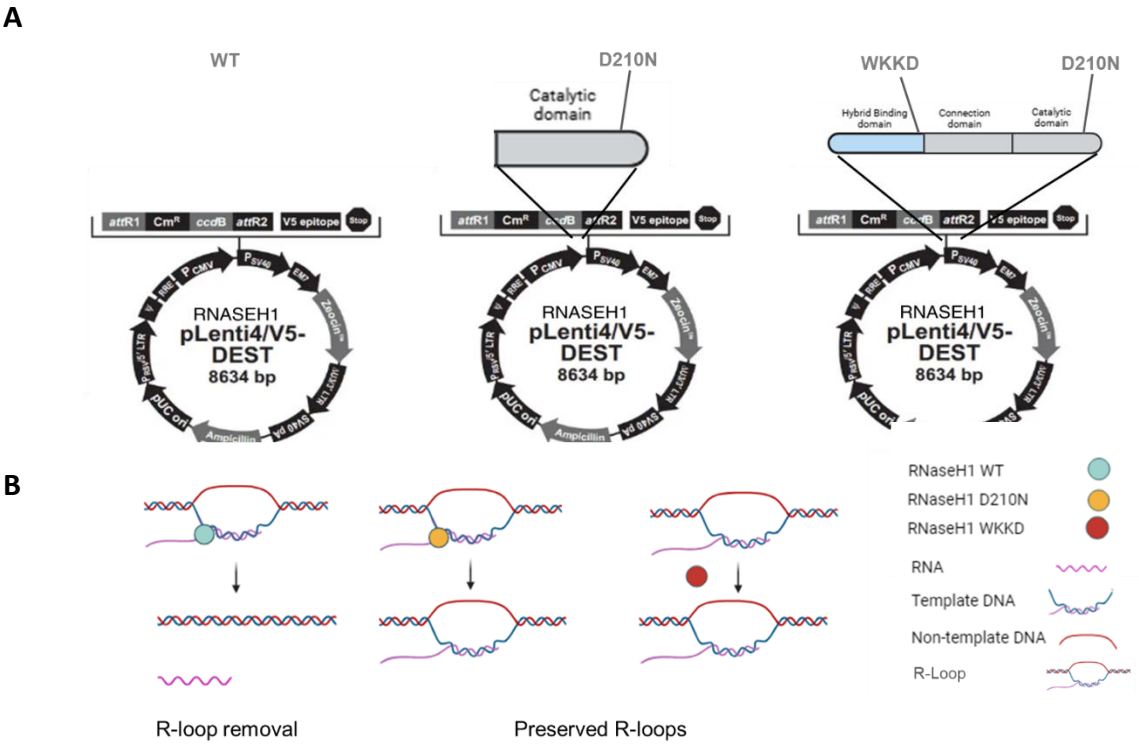


**Figure 32: Different RNaseH1 proteins overexpressed in AML cell lines and their function.**

(A) Schematic representation of the different types of RNaseH1 cloned to pLenti4/V5 DEST vector. (B) Expected outcomes upon overexpression of the different RNaseH1 proteins.

After transduction with lentivirus expressing either WT- or genetically modified RNaseH1 proteins, we performed immunoblot analysis to verify overexpression upon induction with doxycycline. The results of the Western Blot demonstrate a clearly visible overexpression of the respective proteins upon treatment with doxycycline (Figure 33).

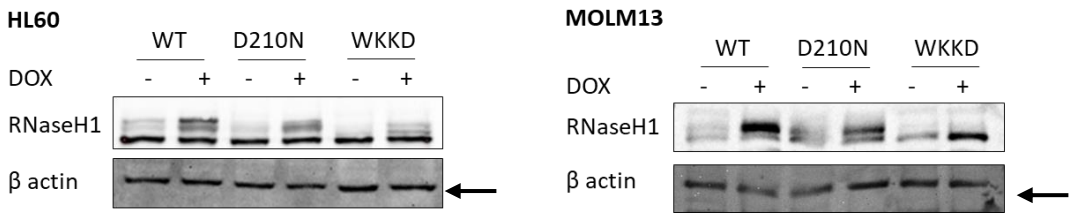


**Figure 33: RNaseH1 proteins are overexpressed upon doxycycline exposure**

Immunoblot showing expression of RNaseH1 and its inactive mutants (D210N and WKKD) in presence and absence of doxycycline (DOX). The AML cell lines were treated with 0.001 µg/µl doxycycline (DOX) for 72 hours. To ensure equal loading, blots were stripped and re-blotted with anti-ß actin antibodies. Arrows showing the band of overexpressed RNaseH1.

### 4.4.2 4.2 R-loops removal and analysis of the effect of cytotoxic drugs

#### **4.4.2.1** R-loop **removal** causes resistant to cytotoxic drugs

After stable expression of doxycycline-inducible RNaseH1 proteins, we first investigated whether the expression of each RNaseH1 protein has effects on cell growth. MTT assays did not show any significant differences in proliferation (Figure 34). Next, AML cells were treated with DNR and ARA-C with 50 nM and 1 µM, respectively, for 48 hours and 72 hours. Following the drug exposure, an Annexin V assay was performed to quantify the percentage of cells undergoing apoptotic death.

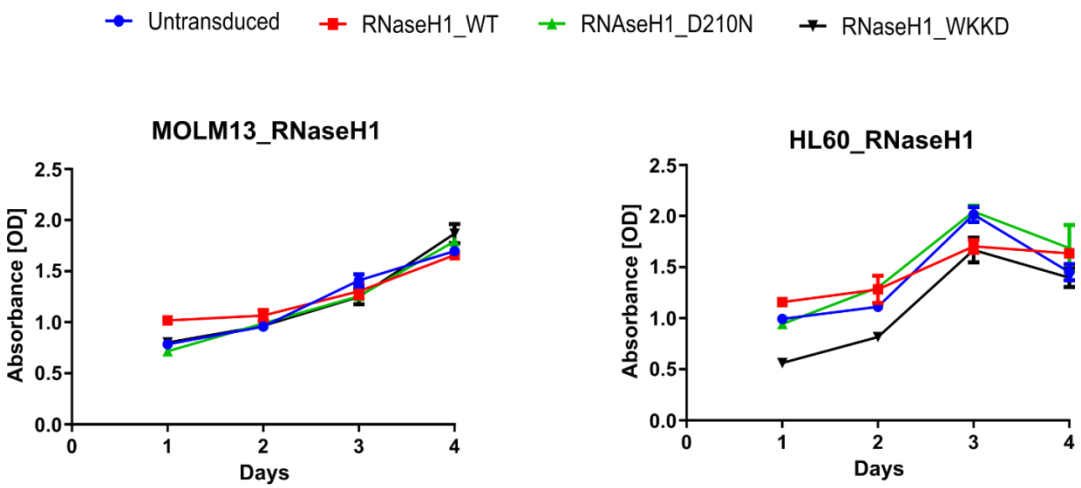


**Figure 34: Expression of RNaseH1 does not affect cell growth in AML cell lines.**

Growth curves showing the growth rate of HL60 and MOLM13 cells with and without overexpression of each RNaseH1 protein for 72 hours with 0.001µg/µl doxycycline (DOX). MTT assay was performed for cells under the following conditions: un-transduced (blue), transduced with RNaseH1 WT (red), D210N (green), WKKD (black).

Upon ARA-C treatment, HL60 cells, which overexpressed RNaseH1 WT, exhibited a markedly lower level of apoptotic cell death. Specifically, these cells showed an apoptotic cell death rate of approximately 40%. In contrast, cells without RNaseH1 WT expression (HL60 cells not treated with doxycycline) or those transduced with the RNaseH1 mutants D210N and WKKD showed a significantly higher rate of cell death, reaching nearly 80%, particularly at the 72-hour time point (Figure 35A).

Additionally, when MOLM13 cells were treated with DNR, a substantial decrease in cell death was noted in those overexpressing RNaseH1 WT. These cells had a cell death rates between 40% and 50%. In contrast, in control cells (RNaseH1 WT transduced cells, but not treated with doxycycline) or in cells with mutant, catalytic inactive RNaseH1 the level of apoptotic cell death reached around 80% (Figure 35B).

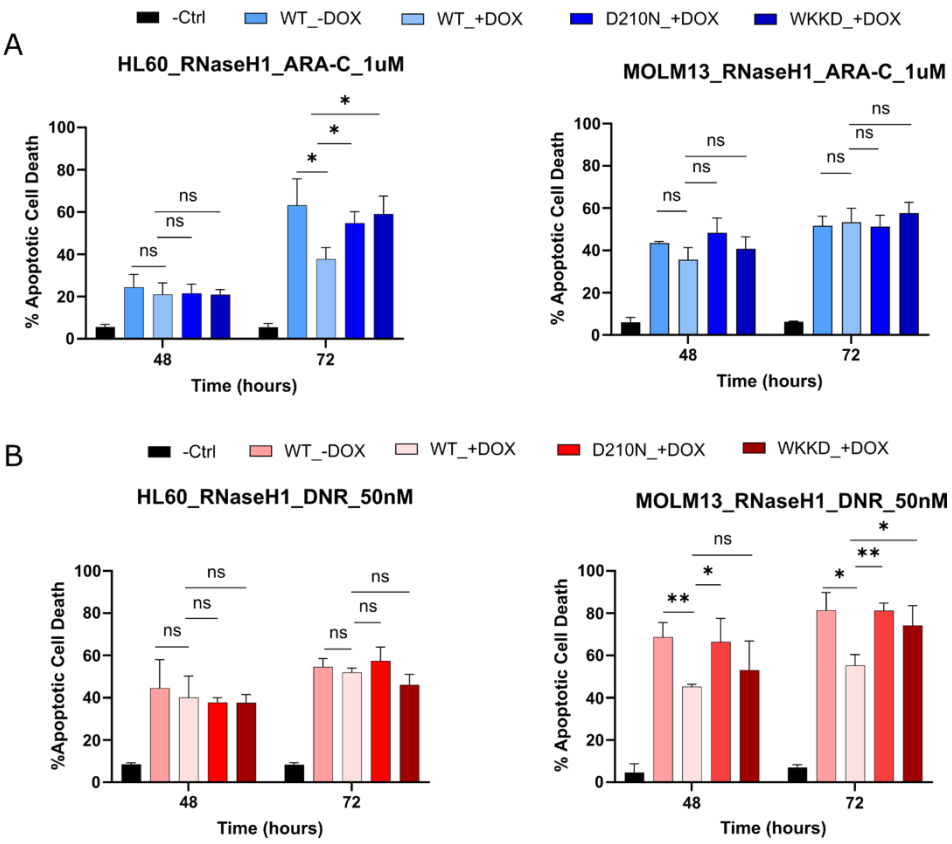


**Figure 35: R-loop removal results in chemotherapy-resistant cells**

Bar graphs representing apoptotic cell death with and without RNaseH1 overexpression and upon treatment with ARA-C and DNR. (A) and (B) data show the percentage of apoptotic cell death in HL60 and MOLM13 cells expressing either WT- or mutant RNaseH1 proteins. Cells were treated with 1 µM ARA-C or 50 nM DNR for indicated time points. Shown is the mean of 3 independent biological replicates. Significances were calculated using unpaired t-test *<0.05, **<0.01, ***<0.001, ns: not significant.

### 4.4.2.2 R-Loop removal reduces DNA damage

We next wanted to investigate whether expression of WT-RNaseH1 has any impact on DNA damage. To address this question, we performed immunofluorescent analysis using the RNaseH1 HBD probe to quantify R-loops and γH2AX staining. We observed a noticeable decrease in DNA damage upon treatment of HL60 cells with ARA-C, as indicated by a lower number of γH2AX foci in WT-RNaseH1 expression cells compared to controls (Figure 36). We further wanted to investigate whether R-loops and γH2AX are co-localized by performing immunofluorescent

analysis using γH2AX and RNaseH1 HBD probe. We did not observe a co-localization between γH2AX and R-loops, instead they are residing in neighboring locations (Figure 37).

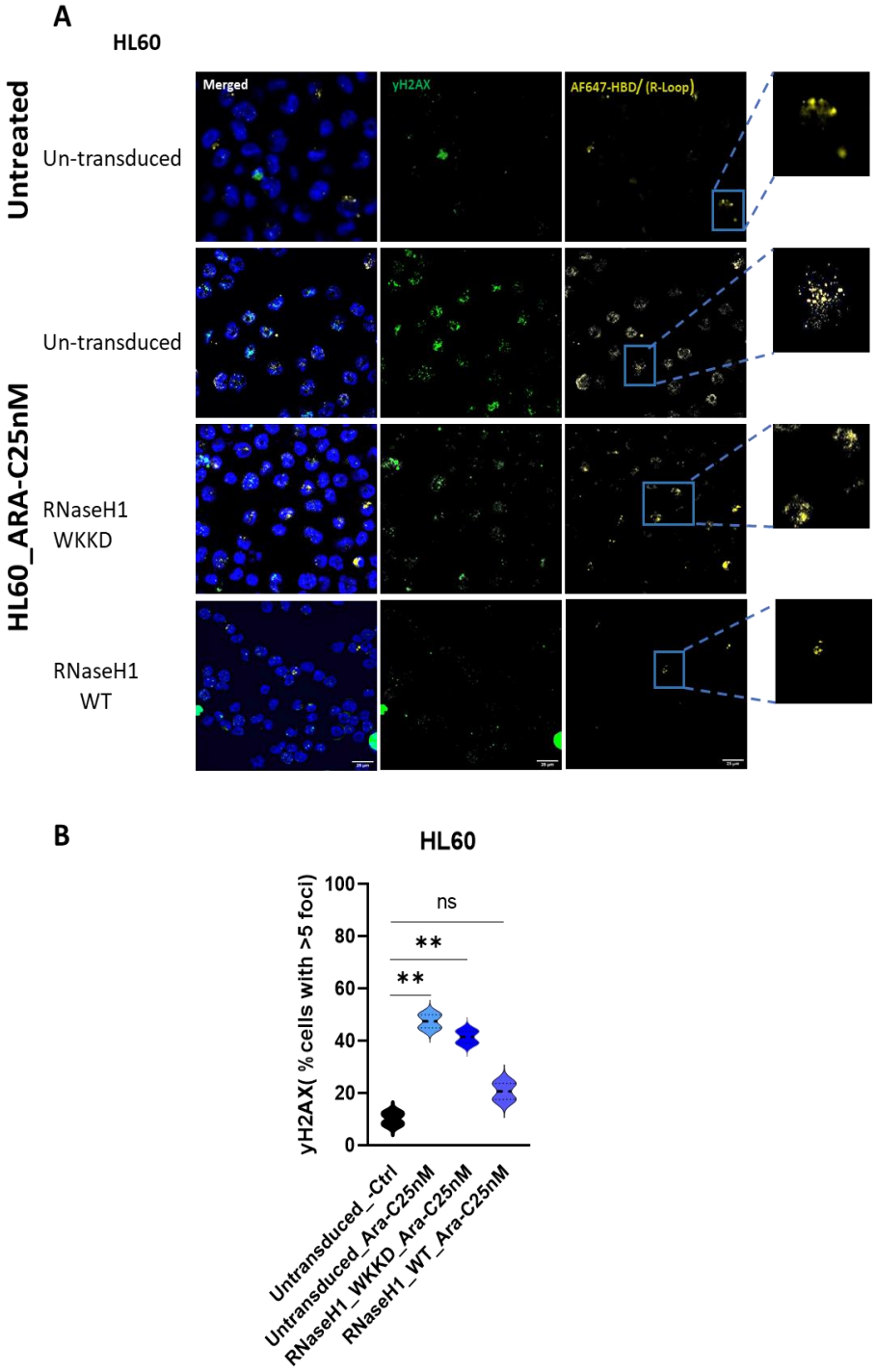


**Figure 36: R-loop removal reduces DNA damage**.

(A) Representative immunofluorescence of staining images of HL60 cells stained with DAPI (Blue), γH2AX (green) and RNaseH1 HBD probe (yellow) upon ARA-C treatment at indicated concentrations for 24 hours. (B) Violin plot

representing R-loop signal quantification before and after removal of R-loops upon treatment with ARA-C. ns: not significant, **p=0.0070, **p=0.0089. Data represent the mean of 2 independent biological replicates. Scale bar 25µm.

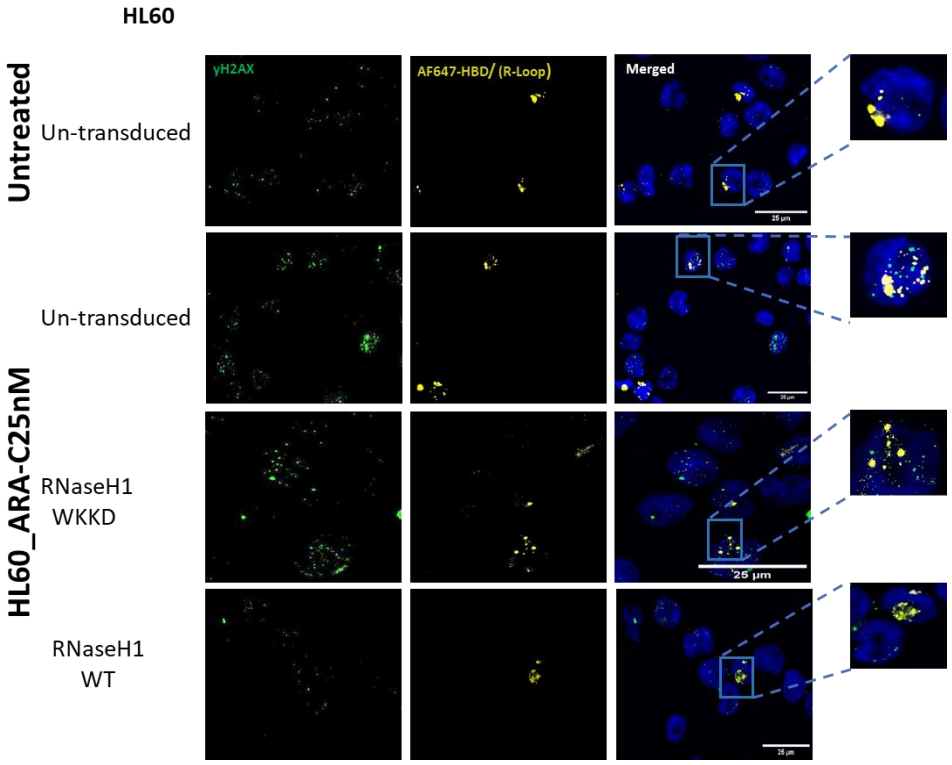


**Figure 37: co-localization between R-loops and γH2AX**

Representative immunofluorescence of staining images of HL60 cells stained with DAPI (Blue), γH2AX (green) and RNaseH1 HBD probe (yellow) upon ARA-C treatment for 24 hours demonstrating that γH2AX and R-loops are in neighboring locations rather than co-localizing with R-loops. Scale bar 25µm.

To validate this finding, an immunoblot assay was performed using an anti-γH2AX-antibody. We observed a significant reduction in the *γH2AX* signal in both HL60 and MOLM13 cell lines when RNaseH1 WT was overexpressed (Figures 38A and B). In contrast, the *γH2AX* signal remained largely unchanged in RNaseH1 mutants, regardless of the presence or absence of doxycycline (Figures 38A and B). Quantification of γH2AX signals using iBright software demonstrated a

substantial reduction in γH2AX levels, with a decrease of approximately 50% in HL60 cells overexpressing RNaseH1 (Figure 38C). A similar trend was observed in MOLM13 cells, where γH2AX levels dropped by nearly 50% (Figure 38D).

This consistent pattern across multiple analyses highlights the crucial role of R-loop removal via RNaseH1 overexpression in reducing DNA damage, as measured by the *γH2AX* response in these specific cell lines.

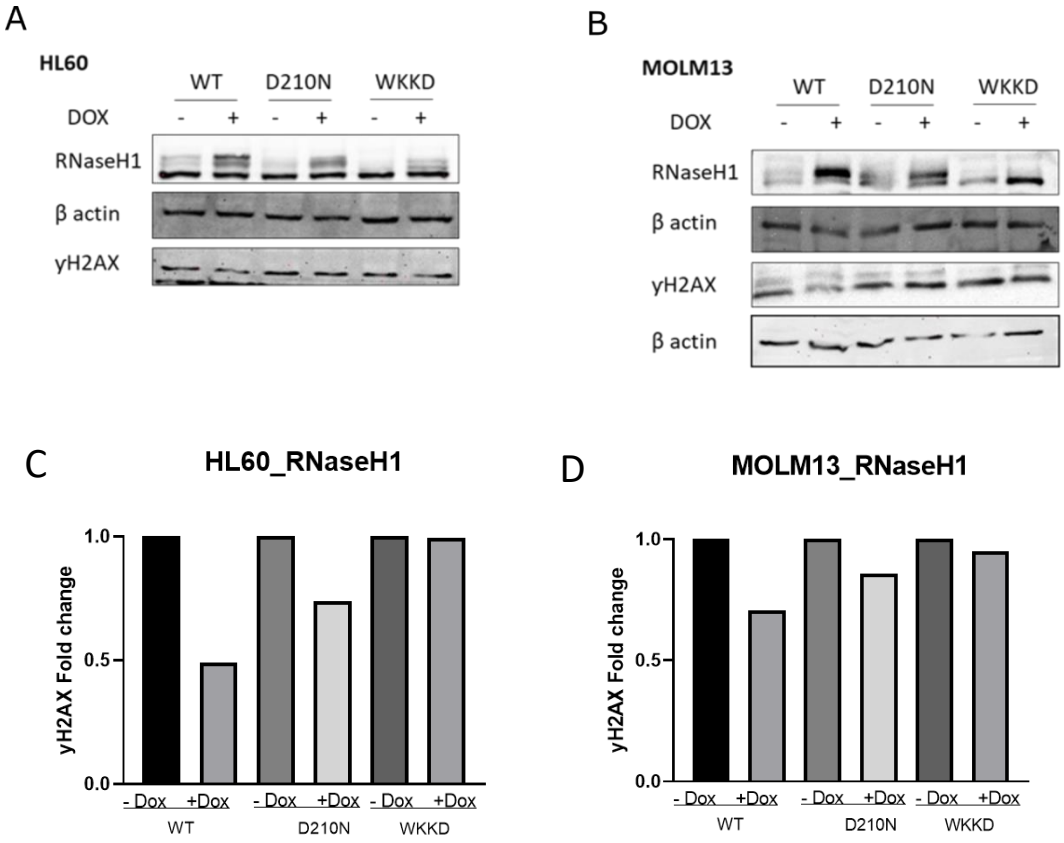


**Figure 38: R-loops resolving reduces DNA damage**.

Representative immunoblot analysis showing the expression levels of γH2AX before and after over-expression of wild-type (WT) for mutant RNaseH1 in HL60 cells (A) and Molm13 cells (B). For MOLM13 cells blots, lysates from the same sample were loaded into two different gels. (C) and (D) show graph bars representing the quantification of γH2AX of (A) and (B). Data represent one biological experiment

Taken together, our data demonstrate that AML cell lines accumulates R-loops and DNA damage upon treatment with ARA-C and DNR. These findings suggest that R-loops and DNA damage play

a key role in chemotherapy-mediated cell death in AML cells. Deeper understanding of this process could help to improve AML therapy.

# 5 Discussion

AML is a clonal malignancy originating from hematopoietic stem cells. It is characterized by recurrent gene mutations, microRNA deregulations, chromosomal abnormalities, and epigenetic modifications that alter chromatin structure and gene expression[93], [94]. AML is a highly heterogeneous disease, marked by clonal and uncontrolled proliferation of precursor cells in the bone marrow, finally disturbing its normal functions in physiologic blood cell production[93]. This study aimed to characterize the DNA damage response in AML, in particular DNA repair pathway activation in response to DNA damage induced by standard chemotherapeutics used in clinical routine. Additionally, the study aimed to explore the role of persistent R-loop formation and accumulation in genomic instability, which manifests as DNA damage. The study further investigated how R-loops contribute to drug-induced cell death and their potential as direct or indirect therapeutic targets. A deeper understanding of these mechanisms may reveal novel therapeutic strategies for AML.

## 5.1 Regulation of DSB repair pathways across the cell cycle

Exposure to genotoxic stress or DNA-damaging agents may induce DSBs. The balance between non-homologous end joining (NHEJ) and homologous recombination (HR) varies throughout the cell cycle, with recent studies providing deeper insights into the molecular mechanisms regulating this dynamic transition[95]. NHEJ, which does not require a template for repair, is predominantly active during the G1 phase of the cell cycle [4]. In contrast, HR activity is enhanced during the S and G2 phases, when sister chromatids are available as templates for repair[95], [96], [97]. However, NHEJ remains active throughout the S and G2 phases, suggesting competition between the two pathways for DSB repair, even in the presence of homologous templates[98].

To investigate this interplay, we conducted an immunofluorescence-based assay in several AML cell lines (HL60, MOLM13, and OCI-AML3) treated with ARA-C and DNR at two concentrations (25 and 50 nM for ARA-C; 5 and 10 nM for DNR) for 24 hours. We observed a higher co-localization of *yH2AX* foci with each of the DNA repair genes *53BP1* (NHEJ) and *RAD51* (HR) foci; than with RPA (miner co-localization) making it difficult to pinpoint a dominant repair pathway at this point.

This may be attributed to the dynamic switch from NHEJ to HR, which occurs during the S phase when 53BP1 is displaced to facilitate the recruitment of HR-related proteins such as BRCA1 and RAD51[99]. Previous studies have confirmed that NHEJ is predominant in G1, whereas HR becomes more active in S phase[100]. Additionally, NHEJ has been shown to function throughout the entire cell cycle, further supporting the idea that NHEJ and HR compete for DSB repair. This competition likely explains the observed co-localization of γH2AX foci with both 53BP1 and RAD51[24], [26].

However, when comparing the number of co-localized foci of either 53BP1 or RAD51 with yH2AX foci, we observed a difference between ARA-C and DNR within the same cell line. For instance, in HL60 cells treated with DNR, we observed higher co-localization of 53BP1 (almost complete co-localization) and diminished co-localization of RAD51 with yH2AX foci as compared to ARA-C. However, when treated with ARA-C the co-localization of 53BP1 and RAD51 with yH2AX was similar. According to these findings, resistance of HL60 cells to DNR might be linked to the active NHEJ repair. In contrast, MOLM13 cells showed higher co-localization of *53BP1* when treated with ARA-C which may be the cause of this cell line to be resistant to ARA-C. However, when treated with DNR, there was less co-localization of both proteins with yH2AX, which in turn may be the cause of MOLM13 being sensitive to DNR due to the lack of repair by both *53BP1* and *RAD51*. Although these findings seem promising, it remains elusive how the two DNA repair pathway are regulated in MOLM13 and HL60 with respect to ARA-C and DNR.

## 5.2 R-loops involvement in DNA damage and repair

A crucial question raised in this thesis, and also discussed in a previous study, is how R-loop hybrids can be both beneficial and detrimental to the cell simultaneously. For instance, how can regulatory R-loops activate gene expression while also having the potential to silence it? Similarly, how do R-loops contribute to DNA repair if they are also a known source of DNA damage[32]? The answer to these questions might be linked to the regulation of R-loops abundance. When R-loops are maintained at a balanced level, they function as regulatory elements that support normal cellular processes. In contrast, the loss of key regulatory factors leads to R-loop

accumulation, ultimately resulting in their conversion into unscheduled R-loops, which are detrimental to cell viability.

### 5.2.1 R-loops as source of DNA damage

The structure of R-loops presents a significant risk to genome stability, primarily due to the displaced ssDNA strand which is vulnerable to both endogenous and exogenous DNA-damaging agents[50]. Disruption of genes involved in RNA biogenesis and export demonstrated an R-loop accumulation and significantly increased DNA damage, particularly DSBs[101], [102],[103]. R-loops have also been implicated in DSB end resection. Inadequate R-loop resolution can hinder end resection at DSBs, especially in the absence of key resolution factors such as DDX5 and DHX9, leading to R-loop accumulation. Consequently, this impairs the recruitment of essential repair proteins, such as *RPA*, *RAD51*, and nucleases[104], [105],[106], resulting in further DNA damage[107], [108],[109].

Therefore, we explored and quantified R-loop levels in all three AML cell lines before and upon treatment with ARA-C and DNR. Interestingly, we observed an increase of R-loops in MOLM13 cells upon treatment with DNR in a dose and time dependent manner. In HL60 cells, we observed higher accumulation of R-loops upon ARA-C treatment in a dose and time dependent manner as well. In line with the above described findings in previous studies, the disturbed end resection can partly explain observed sensitivity of HL60 and MOLM13 cells upon treatment with ARA-C and DNR, respectively. NHEJ was less active in these settings and HR-mediated repair was prevented by disturbed end resection, which finally resulted in an increase in DSBs and eventually in apoptotic cell death.

As mentioned earlier, R-loops can form during transcription either in *cis*, at the site of transcription, or in *trans*, at distant sites, with the presence of RAD51. While trans R-loops are associated with DSB induction, certain studies suggest that only cis R-loops, in a RAD51-independent manner, cause DNA damage[63] [110]. To test this hypothesis that R-loops can be a source of DNA damage, we overexpressed RNAseH1 to resolve R-loops and treated two AML cell lines, HL60 and MOLM13, with ARA-C and DNR for 24 hours with two concentrations for each drug (25 and 50nM for ARA-C, 5 and 10nM for DNR). Immunofluorescence revealed a reduction

in γH2AX foci upon R-loop removal and chemotherapy treatment. Further validation through immunoblotting confirmed that γH2AX signal intensity decreased after overexpression of wild-type RNaseH1, but remained unchanged with RNaseH1 mutants, suggesting a direct link between R-loop resolution and DNA damage reduction.

### 5.2.2 **R-loops and DNA repair pathway choice**

Contrary to the idea that R-loops hinder DSB repair, a recent study suggested that they play an emerging role in facilitating DNA damage response (DDR) and DNA repair[111], [112]. Indeed, R-loops have been suggested to play a crucial role in both HR and NHEJ repair pathways, potentially influencing the repair pathway choice[63]. For example, it has been shown that R-loops are involved in NHEJ under certain conditions. This was proven after the KD of *SETX* gene (involved in R-loop removal) that triggered an increase in *53BP1* foci while inhibiting *RAD51* foci formation[113]. These changes were associated with an increase in translocations, indicating that the persistence of R-loops may promote error-prone DNA repair mechanisms. In line with our study, the treatment with ARA-C and DNR may regulate the transcription of specific factures that govern R-loop formation and thus leading to the accumulation of R-loops in AML cell lines. However, whether when and how R-loops regulate the DNA repair pathway choice is not fully understood. Moreover, it would be interesting to explore whether the rapid induction and the persistence of R-loops can help in predicting the response in primary AML cells and become a valuable biomarker. Other studies also showed that the loss of other R-loop resolution factors, such as *DDX1* or *EXOSC10*, favored NHEJ efficiency over HR efficiency, and the loss of *USP42/DHX9* increased *53BP1* foci[114], [115],[107]. These findings support the idea that the excessive formation of R-loops favors NHEJ in these context[63]. However, one study found that the depletion of XRN in glioblastoma cells, which also accumulate R-loops, impaired NHEJ, suggesting that not all instances of unscheduled R-loops promote NHEJ[116].

On the other hand, R-loops can also direct cells toward the HR repair pathway. It has been demonstrated that these hybrids are transiently required at DSBs to regulate resection and control the loading of RPA, essential for efficient HR[104]. Although contradictory to its role in inhibiting resection, these findings suggest that the formation and resolution of R-loops are essential for regulating the resection process[63]. Further studies support this by stating that

following 5'end resection at DSBs R-loops can form at the exposed 3' end, leading to the recruitment of several repair factors, *RAD51*, *BRCA1,* and *BRCA2*[32]. This recruitment is then followed by the removal of the RNA strand by SETX[113] or RNaseH1/H2[105], [117] resulting in *RAD51*[105], [113] recruitment and HR takes place[32]. A review by Niehrs and Luke posed an intriguing question regarding the possibility that RAD51 could be loaded onto ssDNA without the involvement of RNA-DNA hybrids. They speculated that R-loops at DSBs may enable the cell to differentiate between the exposed ssDNA during replication, where *RAD51* and HR are harmful, and the ssDNA generated at DSBs where *RAD51* is crucial for repair. They also mentioned that RNA:DNA hybrids may inhibit *RPA* from competing with *RAD51* at DSBs[32].

In this study, we link the NHEJ repair pathway to a specific drug for each cell line, i.e. NHEJ repair is more active in HL60 upon DNR treatment and MOLM13 upon ARA-C treatment, which may explain the resistance of HL60 and MOLM13 to DNR and ARA-C respectively. We hypothesize that cells initially repair DNA via NHEJ during the G1 phase, recruiting 53BP1, and then switch to HR during the S phase, when RAD51 is recruited, which might explain the co-localization of *53BP1* and *RAD51* foci with *yH2AX,* upon treatment with chemotherapy drugs. However, due to R-loop accumulation and persistence, end resection is prevented and HR is impaired. In case of diminished NHEJ activity cells accumulate DSBs and undergo apoptosis.

### 5.2.3 **R-loops in transcription-associated homologous repair**

Alternatively, DNA repair can occur as transcription-associated homologous recombination repair (TA-HR). This process takes place when R-loops are formed near break sites in actively transcribed loci[118], which are first recognized by *RAD52* that, later, will recruit *RAD51* to promote strand invasion and HR preventing the binding of *53BP1*[63]. A recent study combined two techniques to assess the formation and resolution of R-loops in real-time. Using a near-infrared (730 nm) irradiation system followed by detection of R-loops with a fluorescent-tagged HBD of RNaseH1, the study demonstrated that both the formation and resolution of R-loops are crucial for initiating TA-HR via RAD52 recruitment[118], [119].

These findings from the previously mentioned studies support the idea that R-loops are involved in TA-HR repair. In our study, RAD51, in addition to 53BP1, also promotes DNA repair via HR, as confirmed by its co-localization with yH2AX. RDA51 could be induced by R-loops whose levels increase after treatment with ARA-C and DNR for 24 hours. However, sustained accumulation of R-loops at later treatment periods, 48 and72 hours, made the cells more sensitive and prevented DNA repair from taking place. We hypothesize that R-loops may be involved in the TA-HR, forming during transcription and, once they reach a critical threshold, triggering cell death in tumor cells. We propose further experiments to investigate the specific levels of R-loops that promote TA-HR repair versus those that lead to cell death following chemotherapy treatment.

## 5.3 Resistance of AML patients to chemotherapy

AML remains challenging due to chemotherapeutic agent resistance[120]. Although induction therapy can reduce disease burden, relapse due to intrinsic or acquired drug resistance is a major treatment obstacle[121]. The main chemotherapeutic drug used in AML treatment is ARA-C, either alone[122] or in combination with antracycline [123]. For instance, the sterile alpha motif (SAM) and histidine-aspartate (HD) domain-containing protein 1 (*SAMHD1*) has been recognized to contribute to ARA-C resistance in AML patients and is considered a therapeutic target in this context[122]. This was further confirmed in other studies where they showed that *SAMHD1* is highly upregulated, leading to lower sensitivity to ARA-C treatment[124], [125]. One of the most known mutations responsible for AML are *FLT3-ITD* mutations[126], [127]. Despite their strong preclinical efficacy, *FLT3* inhibitors (*FLT3*i), such as gilteritinib, have not been able to produce long-term, durable responses in patients[128]. Resistance to *FLT3*i is characterized by a few remaining cells that persist and rely on micro-environmental secreted factors[126], [129].

In this study, we observed that the MOLM13 cell line, which harbors a *FLT3-ITD* alteration , was most sensitive to DNR treatment compared to the HL60 and OCI-AML3 cell lines, which do not harbor a *FLT3-ITD* mutation. However, MOLM13 cells were less sensitive to ARA-C treatment, suggesting that the *FLT3* mutation confers resistance to ARA-C, but not to DNR. Interestingly, when ARA-C and DNR were combined, the resistance to single-drug treatment was overcome, resulting in an additive effect for both drugs.

Mutations in tumor suppressor genes, such as *TP53* alterations, contribute to leukemogenesis by promoting the overproduction of pluripotent stem cells[10], [130]. A study by Brosh and Rotter highlighted that mutant *TP53* often acquires gain-of-function properties, which enhance metastasis, promote drug resistance, and increase tumor cell survival[131]. This acquired resistance has made *TP53*$^{mutant}$ AML a unique challenge in its treatment due to its resistance to both conventional and novel therapies[10].

In our study, we used HL60 cells with depleted *TP53*, which showed increased susceptibility to ARA-C but resistance to DNR. Resistance to DNR may be related to the lack of TP53, which appears to confer resistance to DNR, though the underlying mechanisms remain unclear. In summary, we demonstrated that AML cells, dependent on their genetic background have different sensitivities to commonly use genotoxic drugs and that sensitivity might be related to the presence of R loops. However, our data require confirmation in a larger data set.

## 5.4 R-loops in cancer

R-loops have been linked to various types of cancer through their role in inducing DNA damage, genomic instability, and altering gene expression. Abnormal accumulation of R-loops has been observed in several cancer types, including hematological malignancies, breast cancer, and other solid tumors[31], [69], [132], [133].

### 5.4.1 **Transcription-replication conflicts**

Growing evidence over the last few years has highlighted the dual role of R-loops, demonstrating both beneficial and harmful effects[133], [134], [135]. The formation and accumulation of unscheduled R-loops can result in DNA damage, particularly through transcription-replication conflicts (TRCs), which activate the ATR-mediated S-phase checkpoint. During the S phase, replication forks can collide with R-loops, causing replication stress and DNA damage[136]. While cells possess mechanisms to spatially and temporally regulate transcription and replication, conflicts between these processes can still arise due to their shared use of the same DNA template, supporting the thought that R-loops may exacerbate TRCs[29], [64], [137]. Previous

studies focused on the direction of where replication forks encounter R-loop. They can encounter them either in head-on (HO) orientation or co-directional (CO) both of which lead to replication blockade and severe genomic instability, with HO conflicts being more detrimental[63], [138]. Notably, R-loop levels are influenced by the orientation of TRCs, with HO TRCs promoting R-loop formation and co-directional TRCs reducing R-loop levels[29].

As previously mentioned in this section, TRCs are a key contributor to replication stress. To investigate this, we quantified RPA foci, a well-established biomarker for single-stranded DNA breaks and replicative stress[139]. Our findings, characterized by a very low number of co-localized and non-co-localized RPA foci with γH2AX foci, suggest that R-loop accumulation in the AML cell lines used in this study did not induce TRCs or replication stress.

### 5.4.2 **Role in tumorigenesis and resistance**

The role of R-loop deregulation in tumorigenesis is complex. On one hand, low R-loop levels may contribute to mutagenesis, while on the other, excessive R-loop accumulation can lead to severe DNA damage and cell death. Elevated DNA damage triggers immune signaling and initiates an innate immune response, resulting in chronic inflammation, which can contribute to tumorigenesis[140], [141]. The potential for R-loops to promote tumorigenesis is further supported by their capacity to induce replication stress and DNA damage, two hallmarks of cancer. Several oncogenes and proliferation factors, as well as loss-of-function mutations in tumor suppressors and other genes that suppress and resolve R-loops or TRCs, encourage the formation of R-loops and the DNA damage associated with them[63]. For instance, previous studies showed that R-loop-dependent DNA damage is driven by both estrogen and HRAS mutations in genes that form estrogen-responsive R-loops[70], [142]. R-loops are involved in telomere maintenance, which results in promoting tumorigenesis. Upregulation of the TERRA RNA and the ensuing R-loop formation encourage telomeric recombination to lengthen telomeres in cancers driven by alternative lengthening of telomeres (ALT)[63].

In our study, the accumulation of R-loops increased the sensitivity of two AML cell lines HL60 and MOLM13 to ARA-C and DNR, respectively. In contrast, the removal of R-loops conferred increased resistance to each drug, suggesting that low levels of R-loops may drive tumorigenesis in these AML cell lines. The accumulation of R-loops upon chemotherapy leads to cell death, in line with

the observations mentioned earlier in this section. Notably, R-loop resolution increased HL60 cell line resistance to ARA-C, while its resistance to DNR remained unchanged. Similarly, in MOLM13 cells, R-loops removal specifically affected DNR sensitivity, making the cell more resistant but had no impact on ARA-C resistance. This observation suggests that chemotherapy-induced cell death linked to R-loop accumulation is drug-dependent.

## 5.5 R-loops and resistance in AML

### 5.5.1 **R-loops as diagnostic biomarker**

Cells have two primary strategies to control R-loops levels: mechanisms that eliminate R-loops, including ribonucleases and RNA-DNA helicases, and mechanisms that prevent their accumulation, such as RNA-processing factors or topoisomerase 1 (TOP1)[31]. Recent reports have indicated that the accumulation of unscheduled R-loops could serve as a diagnostic tool for patient stratification[143]. For instance, a study involving 193 primary embryonal tumors with multilayered rosettes (ETMRs) showed that the loss of DICER1 function (Dicer facilitates transcription termination at sites of replication stress to preserve genome stability)[144], resulted in the accumulation of unscheduled R-loops in these tumors, which contributes to genomic instability[143], [145]. Targeting R-loops with inhibitors of topoisomerase and poly ADP ribose polymerase has shown promising potential as a treatment strategy for this lethal disease[143], [145]. Furthermore, the connections between R-loops and disease present an exciting opportunity for therapeutic manipulation of R-loop levels. Studies have shown that small molecules can target R-loops to mitigate molecular phenotypes linked to disease[29], [146], [147].

To explore the potential for indirectly targeting R-loops, we examined the expression of key R-loop-regulating genes using qRT-PCR and RNA sequencing analysis. Both approaches revealed the downregulation of several genes involved in either R-loop prevention or removal, including TOP1, SRSF1, SSRP1, and DDX9 upon treatment with cytotoxic drugs. This suggests that one of these genes may be responsible for R-loop accumulation. To validate this, KD experiments of these genes should be conducted, followed by treating the three AML cell lines with chemotherapeutic agents to determine which gene contributes to hybrid accumulation. Notably, R-loop

accumulation in the case of the AML cell lines used in this study has a beneficial outcome as it rendered the cells sensitive to the treatment and ultimately caused cell death.

### 5.5.2 R-loops in AML resistance to chemotherapy

While the role of R-loops in cancer has been of growing interest for the last two decades, unfortunately, less is known about their role in AML. Recent studies have suggested that RNA modifications, such as $m^6A$ facilitate transcription termination by promoting R-loop formation[32], [148] and maintaining R-loop stability[149], [150]. Modifications in $m^6A$, however, have been linked to several types of cancers including AML and resistance to antineoplastic therapy[150], [151]. Dysregulation of R-loop resolving proteins or those involved in recognizing DNA damage contributes to cancer progression and resistance to therapy. However, R-loop accumulation has been linked to genome instability and causing senescence in cancer cells[152].

To gain a deeper understanding on R-loop formation in AML cell lines with different genetic backgrounds, we analyzed R-loop levels in both untreated cells and after treatment with DNR and ARA-C.

Using the S9.6 antibody, which specifically targets RNA:DNA hybrids, we performed a dot blot assay. HL60 and MOLM13 cells exhibited contrasting R-loop levels when treated with ARA-C and DNR. HL60 cells showed higher levels of R-loops when treated with ARA-C than with DNR, with a constant increase over time. In contrast, MOLM13 cells exhibited opposite trends under the same conditions. This constant formation of R-loops may help explain why HL60 and MOLM13 cells are highly sensitive to ARA-C and DNR treatment, respectively.

This finding raises significant questions about the relationship between R-loop formation and cellular responses to chemotherapeutic agents. Further investigation is needed to clarify how R-loops influence therapeutic outcomes. This suggests that R-loop induction could be a key factor influencing chemotherapy efficacy in different leukemia cell lines, including those used in this study.

Further analysis has been conducted, to further investigate the implication of R-loops in chemotherapy-induced cell death by overexpressing RNaseH1 to resolve R-loops. Indeed, the

removal of R-loops resulted in increased resistant cells to chemotherapeutic agents, suggesting that R-loops may play a role in senescence in AML, as noted in the previous study[152].

As mentioned, KD of the genes regulating R-loops is required to identify the specific gene responsible for R-loop accumulation.

# 6 Conclusion

Based on our findings, we were unable to identify one DNA repair pathway that AML cell lines use when treated with both drugs due to the co-localization of *yH2AX* with both *53BP1* and *RAD51* with quit high number. However, we observe that NHEJ repair pathway was mainly active in HL60 and MOLM13 cells when treated with ARA-C and DNR respectively. This may explain the resistance of HL60 to DNR and MOLM13 to ARA-C. Moreover, we confirm a link between R-loop accumulation and chemotherapy-induced cell death, suggesting that R-loops could serve as therapeutic targets, either directly or indirectly, through genes responsible for their regulation.

# 7 References


[1] A. Pelcovits and R. Niroula, 'Acute Myeloid Leukemia: A Review'. [Online]. Available: https://seer.cancer.gov/statfacts/

[2] Y. Ishikawa, 'Recent progress in AML with recurrent genetic abnormalities', *Int J Hematol*, Nov. 2024, doi: 10.1007/s12185-024-03848-3.

[3] J. S. Welch *et al.*, 'The origin and evolution of mutations in acute myeloid leukemia', *Cell*, vol. 150, no. 2, 2012, doi: 10.1016/j.cell.2012.06.023.

[4] I. De Kouchkovsky and M. Abdul-Hay, '"Acute myeloid leukemia: A comprehensive review and 2016 update"', 2016. doi: 10.1038/bcj.2016.50.

[5] H. Döhner *et al.*, 'Diagnosis and management of AML in adults: 2017 ELN recommendations from an international expert panel', 2017. doi: 10.1182/blood-2016-08-733196.

[6] S. Li, N. Li, Y. Chen, Z. Zheng, and Y. Guo, 'FLT3-TKD in the prognosis of patients with acute myeloid leukemia: A meta-analysis', 2023. doi: 10.3389/fonc.2023.1086846.

[7] M. Yanada, K. Matsuo, T. Suzuki, H. Kiyoi, and T. Naoe, 'Prognostic significance of FLT3 internal tandem duplication and tyrosine kinase domain mutations for acute myeloid leukemia: A meta-analysis', *Leukemia*, vol. 19, no. 8, 2005, doi: 10.1038/sj.leu.2403838.

[8] N. Sharma and J. L. Liesveld, 'NPM 1 Mutations in AML—The Landscape in 2023', 2023. doi: 10.3390/cancers15041177.

[9] R. Ranieri *et al.*, 'Current status and future perspectives in targeted therapy of NPM1-mutated AML', 2022. doi: 10.1038/s41375-022-01666-2.

[10] M. Shahzad *et al.*, 'What have we learned about TP53-mutated acute myeloid leukemia?', Dec. 01, 2024, *Springer Nature*. doi: 10.1038/s41408-024-01186-5.

[11] D. Wolf and V. Rotter, 'Major deletions in the gene encoding the p53 tumor antigen cause lack of p53 expression in HL-60 cells', *Proc Natl Acad Sci U S A*, vol. 82, no. 3, 1985, doi: 10.1073/pnas.82.3.790.

[12] A. M. Ali and G. F. Salih, 'Molecular and clinical significance of FLT3, NPM1, DNMT3A and TP53 mutations in acute myeloid leukemia patients', *Mol Biol Rep*, vol. 50, no. 10, 2023, doi: 10.1007/s11033-023-08680-2.

[13] H. Kantarjian *et al.*, 'Acute myeloid leukemia: current progress and future directions', 2021. doi: 10.1038/s41408-021-00425-3.

[14] H. Kantarjian, 'Acute myeloid leukemia-Major progress over four decades and glimpses into the future', *Am J Hematol*, vol. 91, no. 1, 2016, doi: 10.1002/ajh.24246.

[15] T. M. Kadia, F. Ravandi, J. Cortes, and H. Kantarjian, 'Toward individualized therapy in acute myeloid leukemia a contemporary review', 2015. doi: 10.1001/jamaoncol.2015.0617.

[16] D. S. Krause and R. A. Van Etten, 'Right on target: eradicating leukemic stem cells', 2007. doi: 10.1016/j.molmed.2007.09.003.

[17] B. Lowenberg and J. M. Rowe, 'Introduction to the review series on advances in acute myeloid leukemia (AML)', 2016. doi: 10.1182/blood-2015-10-662684.

[18] Q. Gong, L. Zhou, S. Xu, X. Li, Y. Zou, and J. Chen, 'High doses of daunorubicin during induction therapy of newly diagnosed acute myeloid leukemia: A systematic review and meta-analysis of prospective clinical trials', 2015. doi: 10.1371/journal.pone.0125612.

[19] B. Tomic *et al.*, 'Cytarabine-induced differentiation of AML cells depends on Chk1 activation and shares the mechanism with inhibitors of DHODH and pyrimidine synthesis', *Sci Rep*, vol. 12, no. 1, 2022, doi: 10.1038/s41598-022-15520-z.

[20] E. Firouzi Niaki *et al.*, 'Interactions of Cisplatin and Daunorubicin at the Chromatin Level', *Sci Rep*, vol. 10, no. 1, 2020, doi: 10.1038/s41598-020-57702-7.

[21] M. Gachechiladze, J. Škarda, A. Soltermann, and M. Joerger, 'RAD51 as a potential surrogate marker for DNA repair capacity in solid malignancies', 2017. doi: 10.1002/ijc.30764.

[22] S. Panier and S. J. Boulton, 'Double-strand break repair: 53BP1 comes into focus', 2014. doi: 10.1038/nrm3719.

[23] A. Maréchal and L. Zou, 'RPA-coated single-stranded DNA as a platform for post-translational modifications in the DNA damage response', 2015. doi: 10.1038/cr.2014.147.

[24] R. Ceccaldi, B. Rondinelli, and A. D. D'Andrea, 'Repair Pathway Choices and Consequences at the Double-Strand Break', 2016. doi: 10.1016/j.tcb.2015.07.009.

[25] T. Aparicio, R. Baer, and J. Gautier, 'DNA double-strand break repair pathway choice and cancer', *DNA Repair (Amst)*, vol. 19, 2014, doi: 10.1016/j.dnarep.2014.03.014.

[26] K. Karanam, R. Kafri, A. Loewer, and G. Lahav, 'Quantitative Live Cell Imaging Reveals a Gradual Shift between DNA Repair Mechanisms and a Maximal Use of HR in Mid S Phase', *Mol Cell*, vol. 47, no. 2, 2012, doi: 10.1016/j.molcel.2012.05.052.

[27] K. K. Chiruvella, Z. Liang, and T. E. Wilson, 'Repair of double-strand breaks by end joining', *Cold Spring Harb Perspect Biol*, vol. 5, no. 5, 2013, doi: 10.1101/cshperspect.a012757.

[28] W. D. Heyer, K. T. Ehmsen, and J. Liu, 'Regulation of homologous recombination in eukaryotes', 2010. doi: 10.1146/annurev-genet-051710-150955.

[29] M. P. Crossley, M. Bocek, and K. A. Cimprich, 'R-Loops as Cellular Regulators and Genomic Threats', 2019. doi: 10.1016/j.molcel.2019.01.024.

[30] A. Aguilera and T. García-Muse, 'R Loops: From Transcription Byproducts to Threats to Genome Stability', 2012. doi: 10.1016/j.molcel.2012.04.009.

[31] J. M. Santos-Pereira and A. Aguilera, 'R loops: New modulators of genome dynamics and function', 2015. doi: 10.1038/nrg3961.

[32] C. Niehrs and B. Luke, 'Regulatory R-loops as facilitators of gene expression and genome stability', 2020. doi: 10.1038/s41580-019-0206-3.

[33] L. Chen *et al.*, 'R-ChIP Using Inactive RNase H Reveals Dynamic Coupling of R-loops with Transcriptional Pausing at Gene Promoters', *Mol Cell*, vol. 68, no. 4, 2017, doi: 10.1016/j.molcel.2017.10.008.

[34] R. W. Roberts and D. M. Crothers, 'Stability and properties of double and triple helices: Dramatic effects of RNA or DNA backbone composition', *Science (1979)*, vol. 258, no. 5087, 1992, doi: 10.1126/science.1279808.

[35] 'ratmeyer-et-al-2002-sequence-specific-thermodynamic-and-structural-properties-for-dna-cntdot-rna-duplexes'.

[36] R. W. Roberts and D. M. Crothers, 'Stability and Properties of Double and Triple Helices: Dramatic Effects of RNA or DNA Backbone Composition', 2025. [Online]. Available: https://www.science.org

[37] N. N. Shaw and D. P. Arya, 'Recognition of the unique structure of DNA:RNA hybrids', 2008. doi: 10.1016/j.biochi.2008.04.011.

[38] L. Wahba, S. K. Gore, and D. Koshland, 'The homologous recombination machinery modulates the formation of RNA-DNA hybrids and associated chromosome instability', *Elife*, vol. 2013, no. 2, 2013, doi: 10.7554/eLife.00505.

[39] P. A. Ginno, Y. W. Lim, P. L. Lott, I. Korf, and F. Chédin, 'GC skew at the 59 and 39 ends of human genes links R-loop formation to epigenetic regulation and transcription termination', *Genome Res*, vol. 23, no. 10, pp. 1590–1600, Oct. 2013, doi: 10.1101/gr.158436.113.

[40] P. A. Ginno, P. L. Lott, H. C. Christensen, I. Korf, and F. Chédin, 'R-Loop Formation Is a Distinctive Characteristic of Unmethylated Human CpG Island Promoters', *Mol Cell*, vol. 45, no. 6, 2012, doi: 10.1016/j.molcel.2012.01.017.

[41] L. Wahba, J. D. Amon, D. Koshland, and M. Vuica-Ross, 'RNase H and Multiple RNA Biogenesis Factors Cooperate to Prevent RNA:DNA Hybrids from Generating Genome Instability', *Mol Cell*, vol. 44, no. 6, 2011, doi: 10.1016/j.molcel.2011.10.017.

[42] I. J. Holt, 'Survey and summary: The mitochondrial R-loop', *Nucleic Acids Res*, vol. 47, no. 11, 2019, doi: 10.1093/nar/gkz277.

[43] E. Petermann, L. Lan, and L. Zou, 'Sources, resolution and physiological relevance of R-loops and RNA–DNA hybrids', 2022. doi: 10.1038/s41580-022-00474-x.

[44] S. Silva, L. P. Camino, and A. Aguilera, 'Human mitochondrial degradosome prevents harmful mitochondrial R loops and mitochondrial genome instability', *Proc Natl Acad Sci U S A*, vol. 115, no. 43, 2018, doi: 10.1073/pnas.1807258115.

[45] M. P. Crossley *et al.*, 'R-loop-derived cytoplasmic RNA–DNA hybrids activate an immune response', *Nature*, vol. 613, no. 7942, 2023, doi: 10.1038/s41586-022-05545-9.

[46] M. P. Crossley *et al.*, 'Catalytically inactive, purified rnase h1: A specific and sensitive probe for rna–dna hybrid imaging', *Journal of Cell Biology*, vol. 220, no. 9, 2021, doi: 10.1083/jcb.202101092.

[47] Q. Sun, T. Csorba, K. Skourti-Stathaki, N. J. Proudfoot, and C. Dean, 'R-loop stabilization represses antisense transcription at the arabidopsis FLC locus', *Science (1979)*, vol. 340, no. 6132, 2013, doi: 10.1126/science.1234848.

[48] L. A. Sanz *et al.*, 'Prevalent, Dynamic, and Conserved R-Loop Structures Associate with Specific Epigenomic Signatures in Mammals', *Mol Cell*, vol. 63, no. 1, 2016, doi: 10.1016/j.molcel.2016.05.032.

[49] K. Skourti-Stathaki, N. J. Proudfoot, and N. Gromak, 'Human Senataxin Resolves RNA/DNA Hybrids Formed at Transcriptional Pause Sites to Promote Xrn2-Dependent Termination', *Mol Cell*, vol. 42, no. 6, 2011, doi: 10.1016/j.molcel.2011.04.026.

[50] K. Stratigi, A. Siametis, and G. A. Garinis, 'Looping forward: exploring R-loop processing and therapeutic potential', Jan. 01, 2024, *John Wiley and Sons Inc*. doi: 10.1002/1873-3468.14947.

[51] J. Sollier and K. A. Cimprich, 'Breaking bad: R-loops and genome integrity', 2015. doi: 10.1016/j.tcb.2015.05.003.

[52] L. Chen *et al.*, 'The Augmented R-Loop Is a Unifying Mechanism for Myelodysplastic Syndromes Induced by High-Risk Splicing Factor Mutations', *Mol Cell*, vol. 69, no. 3, 2018, doi: 10.1016/j.molcel.2017.12.029.

[53] M. Tresini *et al.*, 'The core spliceosome as target and effector of non-canonical ATM signalling', *Nature*, vol. 523, no. 7558, 2015, doi: 10.1038/nature14512.

[54] Y. Teng *et al.*, 'ROS-induced R loops trigger a transcription-coupled but BRCA1/2-independent homologous recombination pathway through CSB', *Nat Commun*, vol. 9, no. 1, 2018, doi: 10.1038/s41467-018-06586-3.

[55] L. H. Wong *et al.*, 'Centromere RNA is a key component for the assembly of nucleoproteins at the nucleolus and centromere', *Genome Res*, vol. 17, no. 8, 2007, doi: 10.1101/gr.6022807.

[56] F. Ferri, H. Bouzinba-Segard, G. Velasco, F. Hubé, and C. Francastel, 'Non-coding murine centromeric transcripts associate with and potentiate Aurora B kinase', *Nucleic Acids Res*, vol. 37, no. 15, 2009, doi: 10.1093/nar/gkp529.

[57] Q. Liu *et al.*, 'Emerging roles of centromeric RNAs in centromere formation and function', 2021. doi: 10.1007/s13258-021-01041-y.

[58] M. Castellano-Pozo *et al.*, 'R loops are linked to histone H3 S10 phosphorylation and chromatin condensation', *Mol Cell*, vol. 52, no. 4, 2013, doi: 10.1016/j.molcel.2013.10.006.

[59] P. K. Mishra, A. Chakraborty, E. Yeh, W. Feng, K. S. Bloom, and M. A. Basrai, 'R-loops at centromeric chromatin contribute to defects in kinetochore integrity and chromosomal instability in budding yeast', *Mol Biol Cell*, vol. 32, no. 1, 2021, doi: 10.1091/MBC.E20-06-0379.

[60] L. Kabeche, H. D. Nguyen, R. Buisson, and L. Zou, 'A mitosis-specific and R loop-driven ATR pathway promotes faithful chromosome segregation', *Science (1979)*, vol. 359, no. 6371, 2018, doi: 10.1126/science.aan6490.

[61] T. García-Muse and A. Aguilera, 'R Loops: From Physiological to Pathological Roles', 2019. doi: 10.1016/j.cell.2019.08.055.

[62] S. Hamperl and K. A. Cimprich, 'Conflict Resolution in the Genome: How Transcription and Replication Make It Work', 2016. doi: 10.1016/j.cell.2016.09.053.

[63] J. R. Brickner, J. L. Garzon, and K. A. Cimprich, 'Walking a tightrope: The complex balancing act of R-loops in genome stability', 2022. doi: 10.1016/j.molcel.2022.04.014.

[64] M. Lalonde, M. Trauner, M. Werner, and S. Hamperl, 'Consequences and resolution of transcription–replication conflicts', 2021. doi: 10.3390/life11070637.

[65] C. Rinaldi, P. Pizzul, M. P. Longhese, and D. Bonetti, 'Sensing R-Loop-Associated DNA Damage to Safeguard Genome Stability', 2021. doi: 10.3389/fcell.2020.618157.

[66] N. Saini, S. A. Roberts, J. F. Sterling, E. P. Malc, P. A. Mieczkowski, and D. A. Gordenin, 'APOBEC3B cytidine deaminase targets the non-transcribed strand of tRNA genes in yeast', *DNA Repair (Amst)*, vol. 53, 2017, doi: 10.1016/j.dnarep.2017.03.003.

[67] Y. Zheng, C. Lorenzo, and P. A. Beal, 'DNA editing in DNA/RNA hybrids by adenosine deaminases that act on RNA', *Nucleic Acids Res*, vol. 45, no. 6, 2017, doi: 10.1093/nar/gkx050.

[68] F. Li *et al.*, 'R-Loops in Genome Instability and Cancer', 2023. doi: 10.3390/cancers15204986.

[69] J. P. Wells, J. White, and P. C. Stirling, 'R Loops and Their Composite Cancer Connections', 2019. doi: 10.1016/j.trecan.2019.08.006.

[70] P. Kotsantis *et al.*, 'Increased global transcription activity as a mechanism of replication stress in cancer', *Nat Commun*, vol. 7, 2016, doi: 10.1038/ncomms13087.

[71] S. J. Collins, R. C. Gallo, and R. E. Gallagher, 'Continuous growth and differentiation of human myeloid leukaemic cells in suspension culture', *Nature*, vol. 270, no. 5635, 1977, doi: 10.1038/270347a0.

[72] Y. Matsuo *et al.*, 'Two acute monocytic leukemia (AML-M5a) cell lines (MOLM-13 and MOLM-14) with interclonal phenotypic heterogeneity showing MLL-AF9 fusion resulting from an occult chromosome insertion, ins(11;9)(q23;p22p23)', *Leukemia*, vol. 11, no. 9, 1997, doi: 10.1038/sj.leu.2400768.

[73] H. Quentmeier *et al.*, 'Cell line OCI/AML3 bears exon-12 NPM gene mutation-A and cytoplasmic expression of nucleophosmin', *Leukemia*, vol. 19, no. 10, 2005, doi: 10.1038/sj.leu.2403899.

[74] H. Quentmeier, J. Reinhardt, M. Zaborski, and H. G. Drexler, 'FLT3 mutations in acute myeloid leukemia cell lines', *Leukemia*, vol. 17, no. 1, 2003, doi: 10.1038/sj.leu.2402740.

[75] A. Ianevski, A. K. Giri, and T. Aittokallio, 'SynergyFinder 3.0: an interactive analysis and consensus interpretation of multi-drug synergies across multiple samples', *Nucleic Acids Res*, vol. 50, no. W1, 2022, doi: 10.1093/nar/gkac382.

[76] A. Ianevski, A. K. Giri, and T. Aittokallio, 'SynergyFinder 2.0: Visual analytics of multi-drug combination synergies', *Nucleic Acids Res*, vol. 48, no. 1, 2021, doi: 10.1093/NAR/GKAA216.

[77] J. T. Chiou, C. C. Hsu, Y. C. Hong, Y. C. Lee, and L. Sen Chang, 'Cytarabine-induced destabilization of MCL1 mRNA and protein triggers apoptosis in leukemia cells', *Biochem Pharmacol*, vol. 211, 2023, doi: 10.1016/j.bcp.2023.115494.

[78] 'Cytoplasmic R-loop Processing-Derived RNA-DNA Hybrids Are Immunogenic', *Cancer Discov*, vol. 13, no. 3, 2023, doi: 10.1158/2159-8290.CD-RW2023-006.

[79] P. Ramirez, R. J. Crouch, V. G. Cheung, and C. Grunseich, 'R-loop analysis by dot-blot', *Journal of Visualized Experiments*, vol. 2021, no. 167, 2021, doi: 10.3791/62069.

[80] H. D. VanGuilder, K. E. Vrana, and W. M. Freeman, 'Twenty-five years of quantitative PCR for gene expression analysis', 2008. doi: 10.2144/000112776.

[81] A. Lockhart *et al.*, 'RNase H1 and H2 Are Differentially Regulated to Process RNA-DNA Hybrids', *Cell Rep*, vol. 29, no. 9, 2019, doi: 10.1016/j.celrep.2019.10.108.

[82] A. T. Das, L. Tenenbaum, and B. Berkhout, 'Tet-On Systems For Doxycycline-inducible Gene Expression', *Curr Gene Ther*, vol. 16, no. 3, 2016, doi: 10.2174/1566523216666160524144041.

[83] J. Renart, J. Reiser, and G. R. Stark, 'Transfer of proteins from gels to diazobenzyloxymethyl-paper and detection with antisera: A method for studying antibody specificity and antigen structure', 1979. [Online]. Available: https://www.pnas.org

[84] W. N. Burnette', '"Western Blotting": Electrophoretic Transfer of Proteins from Sodium Dodecyl Sulfate-Polyacrylamide Gels to Unmodified Nitrocellulose and Radiographic Detection with Antibody and Radioiodinated Protein A', 1981.

[85] U. K. Laemmli, 'Cleavage of structural proteins during the assembly of the head of bacteriophage T4', *Nature*, vol. 227, no. 5259, 1970, doi: 10.1038/227680a0.

[86] J. E. Lancet *et al.*, 'CPX-351 versus 7+3 cytarabine and daunorubicin chemotherapy in older adults with newly diagnosed high-risk or secondary acute myeloid leukaemia: 5-year results of a randomised, open-label, multicentre, phase 3 trial', *Lancet Haematol*, vol. 8, no. 7, 2021, doi: 10.1016/S2352-3026(21)00134-4.

[87] B. Yadav, K. Wennerberg, T. Aittokallio, and J. Tang, 'Searching for Drug Synergy in Complex Dose-Response Landscapes Using an Interaction Potency Model', *Comput Struct Biotechnol J*, vol. 13, 2015, doi: 10.1016/j.csbj.2015.09.001.

[88] H. Imai, H. Dansako, Y. Ueda, S. Satoh, and N. Kato, 'Daunorubicin, a topoisomerase II poison, suppresses viral production of hepatitis B virus by inducing cGAS-dependent innate immune response', *Biochem Biophys Res Commun*, vol. 504, no. 4, 2018, doi: 10.1016/j.bbrc.2018.08.195.

[89] L. J. Mah, A. El-Osta, and T. C. Karagiannis, 'γh2AX: A sensitive molecular marker of DNA damage and repair', 2010. doi: 10.1038/leu.2010.6.

[90] K. S. Prabhu *et al.*, 'H2AX: A key player in DNA damage response and a promising target for cancer therapy', *Biomedicine & Pharmacotherapy*, vol. 175, p. 116663, Jun. 2024, doi: 10.1016/J.BIOPHA.2024.116663.

[91] S. Tashiro, N. Kotomura, A. Shinohara, K. Tanaka, K. Ueda, and N. Kamada, 'S phase specific formation of the human Rad51 protein nuclear foci in lymphocytes', *Oncogene*, vol. 12, no. 10, 1996.

[92] D. F. Allison and G. G. Wang, 'R-loops: Formation, function, and relevance to cell stress', 2019. doi: 10.15698/cst2019.02.175.

[93] H. Singh, M. Kumar, and H. Kanungo, 'Role of Gene Mutations in Acute Myeloid Leukemia: A Review Article', *Glob Med Genet*, vol. 10, no. 02, 2023, doi: 10.1055/s-0043-1770768.

[94] J. Chen, O. Odenike, and J. D. Rowley, 'Leukaemogenesis: More than mutant genes', 2010. doi: 10.1038/nrc2765.

[95] M. Shrivastav, L. P. De Haro, and J. A. Nickoloff, 'Regulation of DNA double-strand break repair pathway choice', *Cell Res*, vol. 18, no. 1, 2008, doi: 10.1038/cr.2007.111.

[96] M. L. G. Dronkert, H. B. Beverloo, R. D. Johnson, J. H. J. Hoeijmakers, M. Jasin, and R. Kanaar, ' Mouse RAD54 Affects DNA Double-Strand Break Repair and Sister Chromatid Exchange ', *Mol Cell Biol*, vol. 20, no. 9, 2000, doi: 10.1128/mcb.20.9.3147-3156.2000.

[97] L. C. Kadyk and L. H. Hartwell, 'Sister chromatids are preferred over homologs as substrates for recombinational repair in Saccharomyces cerevisiae', *Genetics*, vol. 132, no. 2, 1992, doi: 10.1093/genetics/132.2.387.

[98] M. Takata *et al.*, 'Homologous recombination and non-homologous end-joining pathways of DNA double-strand break repair have overlapping roles in the maintenance of chromosomal integrity in vertebrate cells', *EMBO Journal*, vol. 17, no. 18, 1998, doi: 10.1093/emboj/17.18.5497.

[99] M. L. Swift, K. Beishline, S. Flashner, and J. Azizkhan-Clifford, 'DSB repair pathway choice is regulated by recruitment of 53BP1 through cell cycle-dependent regulation of Sp1', *Cell Rep*, vol. 34, no. 11, 2021, doi: 10.1016/j.celrep.2021.108840.

[100] M. L. Swift and J. Azizkhan-Clifford, 'DNA damage-induced sumoylation of Sp1 induces its interaction with RNF4 and degradation in S phase to remove 53BP1 from DSBs and permit HR', *DNA Repair (Amst)*, vol. 111, 2022, doi: 10.1016/j.dnarep.2022.103289.

[101] P. Huertas and A. Aguilera, 'Cotranscriptionally formed DNA:RNA hybrids mediate transcription elongation impairment and transcription-associated recombination', *Mol Cell*, vol. 12, no. 3, 2003, doi: 10.1016/j.molcel.2003.08.010.

[102] X. Li and J. L. Manley, 'Inactivation of the SR protein splicing factor ASF/SF2 results in genomic instability', *Cell*, vol. 122, no. 3, 2005, doi: 10.1016/j.cell.2005.06.008.

[103] R. D. Paulsen *et al.*, 'A Genome-wide siRNA Screen Reveals Diverse Cellular Processes and Pathways that Mediate Genome Stability', *Mol Cell*, vol. 35, no. 2, 2009, doi: 10.1016/j.molcel.2009.06.021.

[104] C. Ohle, R. Tesorero, G. Schermann, N. Dobrev, I. Sinning, and T. Fischer, 'Transient RNA-DNA Hybrids Are Required for Efficient Double-Strand Break Repair', *Cell*, vol. 167, no. 4, 2016, doi: 10.1016/j.cell.2016.10.001.

[105] G. D'Alessandro *et al.*, 'BRCA2 controls DNA:RNA hybrid level at DSBs by mediating RNase H2 recruitment', *Nat Commun*, vol. 9, no. 1, 2018, doi: 10.1038/s41467-018-07799-2.

[106] J. M. Daley *et al.*, 'Specificity of end resection pathways for double-strand break regions containing ribonucleotides and base lesions', *Nat Commun*, vol. 11, no. 1, 2020, doi: 10.1038/s41467-020-16903-4.

[107] M. Matsui *et al.*, 'USP42 enhances homologous recombination repair by promoting R-loop resolution with a DNA–RNA helicase DHX9', *Oncogenesis*, vol. 9, no. 6, 2020, doi: 10.1038/s41389-020-00244-4.

[108] Z. Yu *et al.*, 'DDX5 resolves R-loops at DNA double-strand breaks to promote DNA repair and avoid chromosomal deletions', *NAR Cancer*, vol. 2, no. 3, 2020, doi: 10.1093/narcan/zcaa028.

[109] L. Alfano *et al.*, 'Depletion of the RNA binding protein HNRNPD impairs homologous recombination by inhibiting DNA-end resection and inducing R-loop accumulation', *Nucleic Acids Res*, vol. 47, no. 8, 2019, doi: 10.1093/nar/gkz076.

[110] J. Lafuente-Barquero, M. L. García-Rubio, M. S. Martin-Alonso, B. Gómez-González, and A. Aguilera, 'Harmful DNA:Rna hybrids are formed in cis and in a rad51-independent manner', *Elife*, vol. 9, 2020, doi: 10.7554/ELIFE.56674.

[111] A. Marnef and G. Legube, 'R-loops as Janus-faced modulators of DNA repair', 2021. doi: 10.1038/s41556-021-00663-4.

[112] T. T. Paull, 'RNA–DNA hybrids and the convergence with DNA repair', 2019. doi: 10.1080/10409238.2019.1670131.

[113] S. Cohen *et al.*, 'Senataxin resolves RNA:DNA hybrids forming at DNA double-strand breaks to prevent translocations', *Nat Commun*, vol. 9, no. 1, 2018, doi: 10.1038/s41467-018-02894-w.

[114] J. Domingo-Prim *et al.*, 'EXOSC10 is required for RPA assembly and controlled DNA end resection at DNA double-strand breaks', *Nat Commun*, vol. 10, no. 1, 2019, doi: 10.1038/s41467-019-10153-9.

[115] L. Li *et al.*, 'DEAD Box 1 Facilitates Removal of RNA and Homologous Recombination at DNA Double-Strand Breaks', *Mol Cell Biol*, vol. 36, no. 22, 2016, doi: 10.1128/mcb.00415-16.

[116] T. T. Dang and J. C. Morales, 'Xrn2 links RNA: Dna hybrid resolution to double strand break repair pathway choice', *Cancers (Basel)*, vol. 12, no. 7, pp. 1–15, Jul. 2020, doi: 10.3390/cancers12071821.

[117] S. Britton *et al.*, 'DNA damage triggers SAF-A and RNA biogenesis factors exclusion from chromatin coupled to R-loops removal', *Nucleic Acids Res*, vol. 42, no. 14, 2014, doi: 10.1093/nar/gku601.

[118] T. Yasuhara *et al.*, 'Human Rad52 Promotes XPG-Mediated R-loop Processing to Initiate Transcription-Associated Homologous Recombination Repair', *Cell*, vol. 175, no. 2, 2018, doi: 10.1016/j.cell.2018.08.056.

[119] R. Kato, K. Miyagawa, and T. Yasuhara, 'The role of R-loops in transcription-associated DNA double-strand break repair', *Mol Cell Oncol*, vol. 6, no. 1, 2019, doi: 10.1080/23723556.2018.1542244.

[120] J. Ge, X. Yin, X. Sun, L. Kou, X. Xue, and J. Ma, 'Chemotherapy resistance in acute myeloid leukemia is associated with decreased anti-tumor immune response through MHC molecule and B7 family members', *Discover Oncology*, vol. 15, no. 1, Dec. 2024, doi: 10.1007/s12672-024-01072-3.

[121] S. M. Stief *et al.*, 'Loss of KDM6A confers drug resistance in acute myeloid leukemia', *Leukemia*, vol. 34, no. 1, 2020, doi: 10.1038/s41375-019-0497-6.

[122] F. Zhang *et al.*, 'Stabilization of SAMHD1 by NONO is crucial for Ara-C resistance in AML', *Cell Death Dis*, vol. 13, no. 7, 2022, doi: 10.1038/s41419-022-05023-0.

[123] R. Di Francia *et al.*, 'Response and toxicity to cytarabine therapy in leukemia and lymphoma: From dose puzzle to pharmacogenomic biomarkers', 2021. doi: 10.3390/cancers13050966.

[124] C. Schneider *et al.*, 'SAMHD1 is a biomarker for cytarabine response and a therapeutic target in acute myeloid leukemia', *Nat Med*, vol. 23, no. 2, 2017, doi: 10.1038/nm.4255.

[125] N. Herold *et al.*, 'Targeting SAMHD1 with the Vpx protein to improve cytarabine therapy for hematological malignancies', *Nat Med*, vol. 23, no. 2, 2017, doi: 10.1038/nm.4265.

[126] P. Gui and T. G. Bivona, 'Stepwise evolution of therapy resistance in AML', *Cancer Cell*, vol. 39, no. 7, 2021, doi: 10.1016/j.ccell.2021.06.004.

[127] L. Fletcher, S. K. Joshi, and E. Traer, 'Profile of quizartinib for the treatment of adult patients with relapsed/refractory FLT3-ITD-positive acute myeloid leukemia: Evidence to date', 2020. doi: 10.2147/CMAR.S196568.

[128] A. E. Perl *et al.*, ' Gilteritinib or Chemotherapy for Relapsed or Refractory FLT3 -Mutated AML ', *New England Journal of Medicine*, vol. 381, no. 18, 2019, doi: 10.1056/nejmoa1902688.

[129] E. Weisberg *et al.*, 'Using combination therapy to override stromal-mediated chemoresistance in mutant FLT3-positive AML: Synergism between FLT3 inhibitors, dasatinib/multi-targeted inhibitors and JAK inhibitors', *Leukemia*, vol. 26, no. 10, 2012, doi: 10.1038/leu.2012.96.

[130] K. T. Bieging, S. S. Mello, and L. D. Attardi, 'Unravelling mechanisms of p53-mediated tumour suppression', 2014. doi: 10.1038/nrc3711.

[131] R. Brosh and V. Rotter, 'When mutants gain new powers: News from the mutant p53 field', 2009. doi: 10.1038/nrc2693.

[132] P. B. Chen, H. V. Chen, D. Acharya, O. J. Rando, and T. G. Fazzio, 'R loops regulate promoter-proximal chromatin architecture and cellular differentiation', *Nat Struct Mol Biol*, vol. 22, no. 12, 2015, doi: 10.1038/nsmb.3122.

[133] R. P. MacKay, Q. Xu, and P. M. Weinberger, 'R-Loop Physiology and Pathology: A Brief Review', 2020. doi: 10.1089/dna.2020.5906.

[134] M. Groh and N. Gromak, 'Out of Balance: R-loops in Human Disease', 2014. doi: 10.1371/journal.pgen.1004630.

[135] K. Skourti-Stathaki and N. J. Proudfoot, 'A double-edged sword: R loops as threats to genome integrity and powerful regulators of gene expression', 2014. doi: 10.1101/gad.242990.114.

[136] A. M. Friedel, B. L. Pike, and S. M. Gasser, 'ATR/Mec1: coordinating fork stability and repair', 2009. doi: 10.1016/j.ceb.2009.01.017.

[137] W. Gan *et al.*, 'R-loop-mediated genomic instability is caused by impairment of replication fork progression', *Genes Dev*, vol. 25, no. 19, 2011, doi: 10.1101/gad.17010011.

[138] S. Hamperl, M. J. Bocek, J. C. Saldivar, T. Swigut, and K. A. Cimprich, 'Transcription-Replication Conflict Orientation Modulates R-Loop Levels and Activates Distinct DNA Damage Responses', *Cell*, vol. 170, no. 4, 2017, doi: 10.1016/j.cell.2017.07.043.

[139] S. B. Dreyer *et al.*, 'Targeting DNA Damage Response and Replication Stress in Pancreatic Cancer', *Gastroenterology*, vol. 160, no. 1, 2021, doi: 10.1053/j.gastro.2020.09.043.

[140] F. Coquel *et al.*, 'SAMHD1 acts at stalled replication forks to prevent interferon induction', *Nature*, vol. 557, no. 7703, 2018, doi: 10.1038/s41586-018-0050-1.

[141] S. M. Harding, J. L. Benci, J. Irianto, D. E. Discher, A. J. Minn, and R. A. Greenberg, 'Mitotic progression following DNA damage enables pattern recognition within micronuclei', *Nature*, vol. 548, no. 7668, 2017, doi: 10.1038/nature23470.

[142] C. T. Stork *et al.*, 'Co-transcriptional R-loops are the main cause of estrogen-induced DNA damage', *Elife*, vol. 5, no. AUGUST, 2016, doi: 10.7554/eLife.17548.

[143] E. S. Khan and S. Danckwardt, 'Pathophysiological Role and Diagnostic Potential of R-Loops in Cancer and Beyond', 2022. doi: 10.3390/genes13122181.

[144] S. E. Castel *et al.*, 'Dicer promotes transcription termination at sites of replication stress to maintain genome stability', *Cell*, vol. 159, no. 3, 2014, doi: 10.1016/j.cell.2014.09.031.

[145] S. Lambo *et al.*, 'The molecular landscape of ETMR at diagnosis and relapse', *Nature*, vol. 576, no. 7786, 2019, doi: 10.1038/s41586-019-1815-x.

[146] W. T. Powell *et al.*, 'R-loop formation at Snord116 mediates topotecan inhibition of Ube3a-antisense and allele-specific chromatin decondensation', *Proc Natl Acad Sci U S A*, vol. 110, no. 34, 2013, doi: 10.1073/pnas.1305426110.

[147] D. Colak *et al.*, 'Promoter-bound trinucleotide repeat mRNA drives epigenetic silencing in fragile X syndrome', *Science (1979)*, vol. 343, no. 6174, 2014, doi: 10.1126/science.1245831.

[148] X. Yang *et al.*, 'm6A promotes R-loop formation to facilitate transcription termination', 2019. doi: 10.1038/s41422-019-0235-7.

[149] A. Abakir *et al.*, 'N 6-methyladenosine regulates the stability of RNA:DNA hybrids in human cells', 2020. doi: 10.1038/s41588-019-0549-x.

[150] Y. Qiu *et al.*, 'R-loops' m6A modification and its roles in cancers.', *Mol Cancer*, vol. 23, no. 1, p. 232, Oct. 2024, doi: 10.1186/s12943-024-02148-y.

[151] J. Paris *et al.*, 'Targeting the RNA m6A Reader YTHDF2 Selectively Compromises Cancer Stem Cells in Acute Myeloid Leukemia', *Cell Stem Cell*, vol. 25, no. 1, 2019, doi: 10.1016/j.stem.2019.03.021.

[152] N. Elsakrmy and H. Cui, 'R-Loops and R-Loop-Binding Proteins in Cancer Progression and Drug Resistance', 2023. doi: 10.3390/ijms24087064.

# 8 Appendix

## 8.1 Supplementary figures

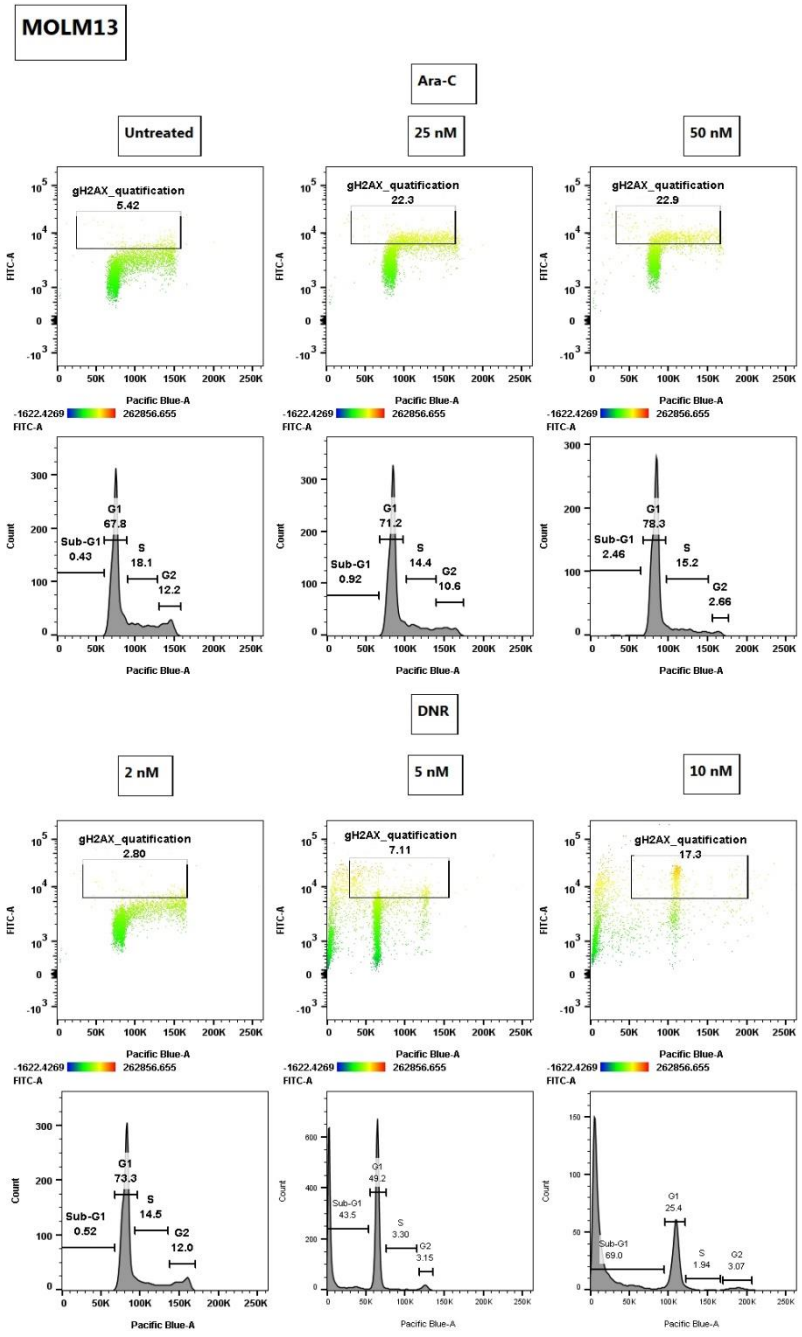


**Supplementary figure 39: DNA damage increases in dose dependent manner in MOLM13**

Flow cytometry analysis of γH2AX and cell cycle in MOLM13 cells, upon treatment for 48hr with ARA-C and DNR with different concentrations as indicated. Bivariate dot plots (upper panel for ARA-C and DNR) representing the changes in percentage of γH2AX before and upon treatment. Histogram plots (DAPI, lower panels for ARA-C and DNR) showing the distribution of cells in the phases (G1, S, G2) of the cell cycle.

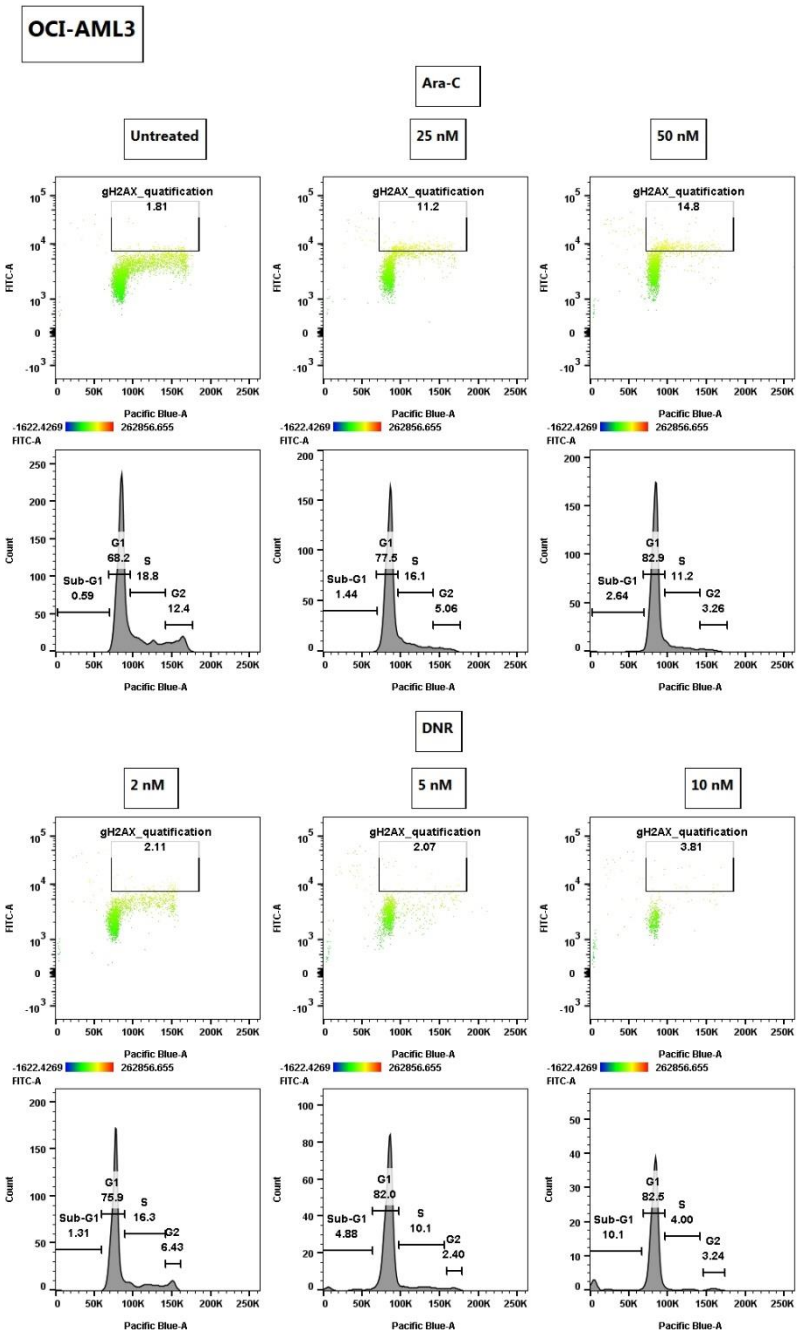


**Supplementary figure 40: DNA damage increases in dose dependent manner in OCI-AML3 cells**

Flow cytometry analysis of yH2AX and cell cycle in HL60 cells, upon treatment for 48hr with ARA-C and DNR with different concentrations as indicated. Bivariate dot plots (upper panel for ARA-C and DNR) representing the changes in percentage of yH2AX before and upon treatment. Histogram plots (DAPI, lower panels for ARA-C and DNR) showing the distribution of cells in the phases (G1, S, G2) of the cell cycle.

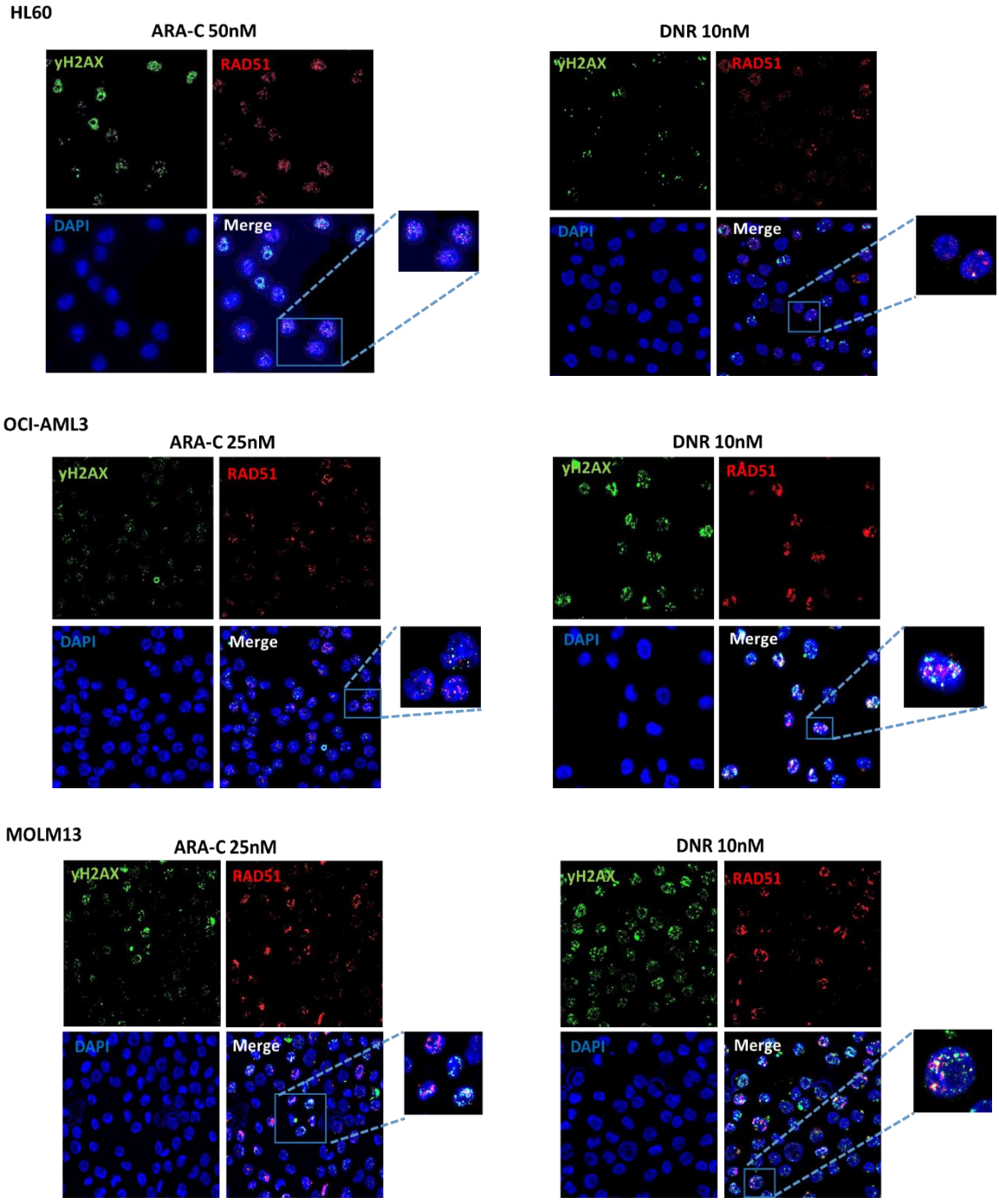


**Supplementary figure 41: RAD51 co-localizes with yH2AX.**

Representative immunofluorescence images of HL60, MOLM13 and OCI-AML3 cells stained with DAPI (blue), yH2AX (green) and RAD51 (red) upon treatment with ARA-C and DNR.

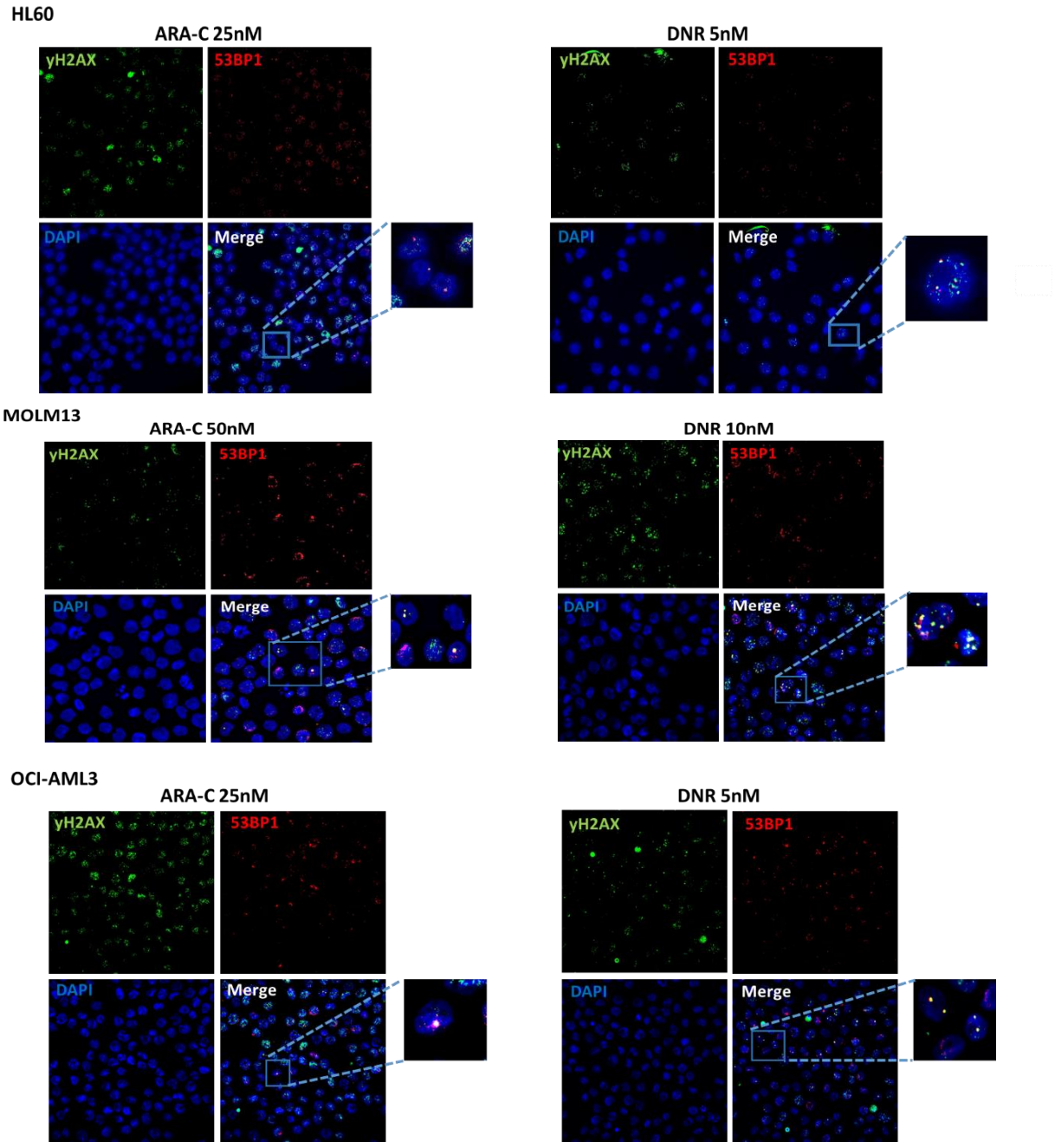


**Supplementary figure 42: 53BP1 co-localizes with yH2AX.**

Representative immunofluorescence images of HL60, MOLM13 and OCI-AML3 cells stained with DAPI (blue), yH2AX (green) and RAD51 (red) upon treatment with ARA-C and DNR.

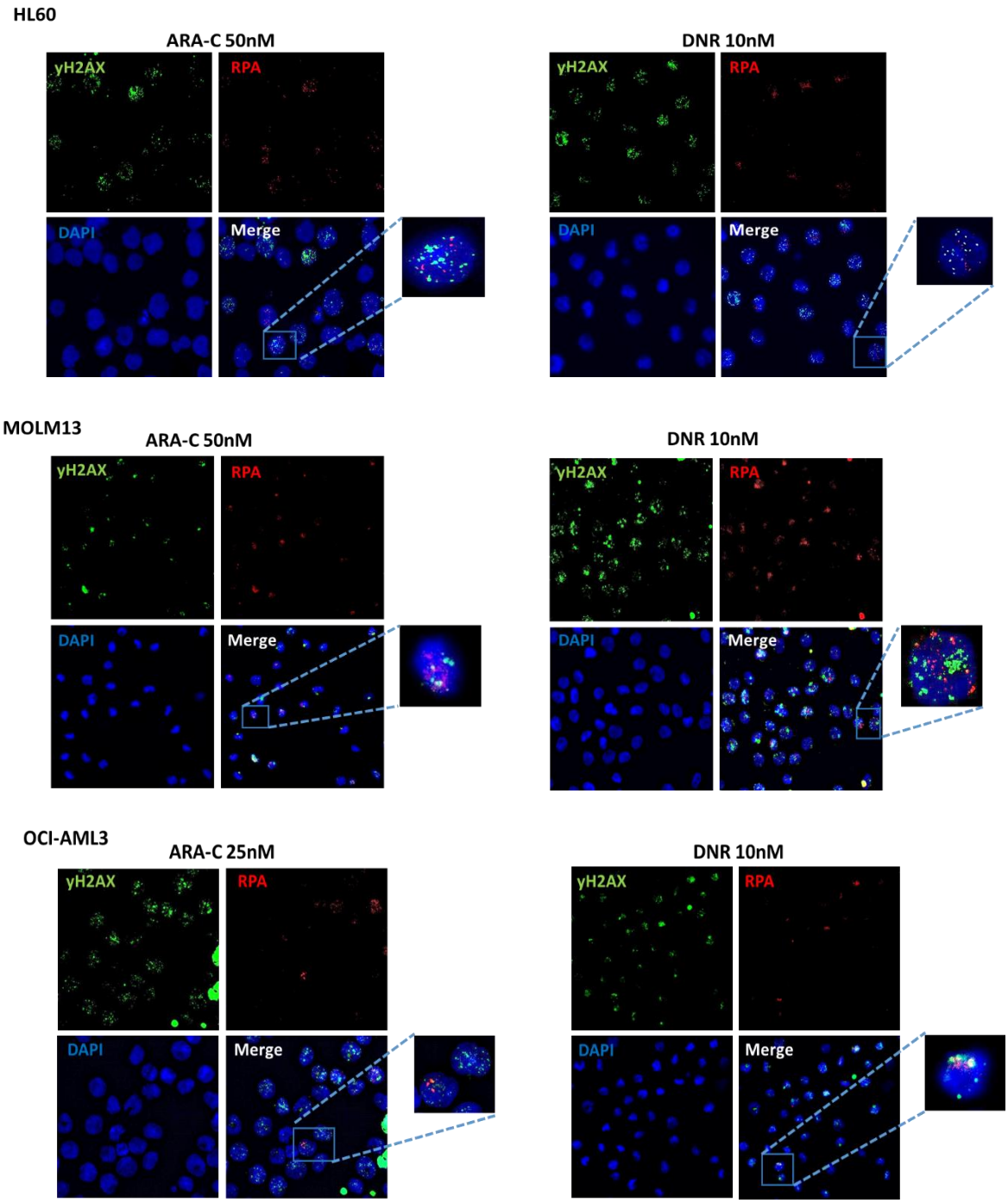


**Supplementary figure 43: RPA does not co-localize with yH2AX.**

Representative immunofluorescence images of HL60, MOLM13 and OCI-AML3 cells stained with DAPI (blue), yH2AX (green) and RPA (red) upon treatment with ARA-C and DNR.

## 8.2 List of tables

## 8.3 List of figures

# Acknowledgements

# Eidesstaatliche Erklärung

Hiermit versichere ich, Moufida Taileb, geboren am 02.05.1989 in Annaba, Algerien, dass ich die vorliegende Dissertation mit dem Titel „Role of R-loops in chemotherapy-induced cell death in acute myeloid leukemia-“ selbständig verfasst und keine anderen als die angegebenen Quellen und Hilfsmittel verwendet habe. Alle wörtlichen und sinngemäßen Zitate sind als solche gekennzeichnet. Ich versichere außerdem, dass meine Dissertation bei keiner anderen Stelle veröffentlicht oder in anderer Form als Prüfungsleistung vorgelegt wurde.

Mainz, den 31.03.2025

(Moufida Taileb)